

UNCLASSIFIED

AD NUMBER

AD885643

LIMITATION CHANGES

TO:

Approved for public release; distribution is unlimited.

FROM:

Distribution authorized to U.S. Gov't. agencies only; Test and Evaluation; JUL 1971. Other requests shall be referred to Armament Development and Test Center, Attn: DLDG, Eglin AFB, FL 32542.

AUTHORITY

AFATL ltr, 24 Jun 1974

THIS PAGE IS UNCLASSIFIED

AEDC-TR-71-141
AFATL-TR-71-73

ARCHIVE COPY
DO NOT LOAN

Copy.



RESULTS OF AN AIR FORCE ADVANCED TACTICAL ROCKET DEVELOPMENT PROGRAM

James C. Uselton
ARO, Inc.

July 1971

This document has been approved for public release
its distribution is unlimited. *Per TAB 74/6
DIA 2 Aug 74*

~~Distribution limited to U.S. Government agencies only;
this report contains information on test and evaluation of
military hardware; July 1971; other requests for this
document must be referred to Armament Development
and Test Center (DLDG), Eglin AFB, Florida 32542.~~

VON KÁRMÁN GAS DYNAMICS FACILITY
ARNOLD ENGINEERING DEVELOPMENT CENTER
AIR FORCE SYSTEMS COMMAND
ARNOLD AIR FORCE STATION, TENNESSEE

AEDC TECHNICAL LIBRARY



PROPERTY OF U.S. AIR FORCE
AEDC LIBRARY
F40600-72-C-0003

NOTICES

When U. S. Government drawings specifications, or other data are used for any purpose other than a definitely related Government procurement operation, the Government thereby incurs no responsibility nor any obligation whatsoever, and the fact that the Government may have formulated, furnished, or in any way supplied the said drawings, specifications, or other data, is not to be regarded by implication or otherwise, or in any manner licensing the holder or any other person or corporation, or conveying any rights or permission to manufacture, use, or sell any patented invention that may in any way be related thereto.

Qualified users may obtain copies of this report from the Defense Documentation Center.

References to named commercial products in this report are not to be considered in any sense as an endorsement of the product by the United States Air Force or the Government.

RESULTS OF AN AIR FORCE ADVANCED TACTICAL
ROCKET DEVELOPMENT PROGRAM

James C. Uselton
ARO, Inc.

Distribution limited to U.S. Government agencies only;
this report contains information on test and evaluation of
military hardware July 1971; other requests for this
document must be referred to Armament Development
and Test Center (DDTC), Eglin AFB, Florida 32542.

This document has been approved for public release
and its distribution is unlimited. Ref ID: AEDC-TR-71-141
D/C 2 August, 1974

FOREWORD

The work reported herein was done at the request of the Armament Development and Test Center (Air Force Armament Laboratory), Air Force Systems Command (AFSC) under Program Element 63716F, System 670A.

The results of the tests presented were obtained by ARO, Inc. (a subsidiary of Sverdrup & Parcel and Associates, Inc.), contract operator of the Arnold Engineering Development Center (AEDC), (AFSC), Arnold Air Force Station, Tennessee, under Contract F40600-72-C-0003. The tests were conducted from April 17 to 25, 1970, September 18 to 25, 1970, October 23 to 26, 1970, and on March 10, 1971, under ARO Projects No. VT0975 and PC0003. The manuscript was submitted for publication on April 2, 1971.

This technical report has been reviewed and is approved.

Emmett A. Niblack, Jr.
Lt Colonel, USAF
AF Representative, VKF
Directorate of Test

Joseph R. Henry
Colonel, USAF
Director of Test

ABSTRACT

Currently the Air Force Armament Laboratory (AFATL) is developing an Advanced Tactical Rocket (ATR). The ATR aerodynamic configuration is being designed by the von Kármán Gas Dynamics Facility of the Arnold Engineering Development Center for AFATL. The details of the development of the aerodynamic configuration are presented in this report. It contains the results of wind-tunnel tests, a trajectory analysis, and a dispersion analysis. The wind-tunnel tests provided essential data necessary for the trajectory and dispersion investigations. Static-force and moment tests were conducted over a broad range of Mach numbers (0.3 to 4.5), Reynolds number (1.4×10^6 to 17.1×10^6), and angle of attack (-3 to 10 deg). These test data were used in a six-degree-of-freedom trajectory program to obtain the basic trajectory and dispersion results. Included in the dispersion study are the effects of thrust misalignment, fin misalignment, initial angular disturbances, and cross-winds. This study indicates that both a 2.5- and a 3.0-caliber tangent ogive nose are acceptable and that a 2.0-caliber tail fin with an 11-deg leading-edge sweep angle is most advantageous. The tail fin should either be canted to 0.5 deg or have 10-deg (0.36 sq in., area) roll tabs to provide the required roll characteristics. An initial spin rate of 500 rpm is necessary for low dispersion of the rocket.

Distribution limited to U.S. Government agencies only; this report contains information on test and evaluation of military hardware; July 1971; other requests for this document must be referred to Armament Development and Test Center (DLDG), Eglin AFB, Florida 32542.

This document has been approved for public release
... its distribution is unlimited. *Per TAB 74-16,
dtd 2 August, 74*

CONTENTS

	<u>Page</u>
ABSTRACT	iii
NOMENCLATURE	ix
I. INTRODUCTION	1
II. DESIGN CONSIDERATIONS	
2.1 General	1
2.2 Nose Shape	2
2.3 Tail Fins	2
III. EXPERIMENTAL APPARATUS AND PROCEDURE	
3.1 ATR Test Models	3
3.2 Instrumentation and Procedure	4
3.3 Test Facilities	5
IV. TEST CONDITIONS AND PRECISION OF DATA	
4.1 Test Conditions	6
4.2 Precision of Data	7
V. PRESENTATION AND DISCUSSION OF EXPERIMENTAL RESULTS	8
VI. COMPUTER INVESTIGATION OF THE ATR PERFORMANCE	
6.1 General	11
6.2 Required Input Data	11
6.3 Basic Trajectory Data	12
6.4 Dispersion	13
VII. CONCLUDING REMARKS	
7.1 Summary of Results	18
7.2 Configuration Selection	20
REFERENCES	21

APPENDIXES

I. ILLUSTRATIONS

Figure

1. Phase 1 Model Details	
a. Basic Model and Fins	25
b. Modified Fins	26
c. Model Disassembled	27
2. Phase 2 Model Details	
a. Basic Configuration	28
b. Fin Geometry	29
c. Rocket Nozzle Simulation	30
d. Plume Simulation	30

<u>Figure</u>	<u>Page</u>
3. Model Photographs	
a. Phase 1 Model Installed in Tunnel 4T	31
b. Phase 1 Model Installed in Tunnel A	31
4. Typical Variation of the Static Stability, Roll, and Axial-Force Coefficients with Angle of Attack, Configuration N ₂ T ₃	32
5. Effect of Fin Configuration on the Stability Derivatives, Static Margin, and Axial Force at $\alpha = 0$	
a. C _{Nα} versus M _{∞}	33
b. C _{mα} versus M _{∞}	34
c. dC _m /dC _N versus M _{∞}	35
d. C _A versus M _{∞} (Phase 1 Fins)	36
e. C _A versus M _{∞} (T ₃ and Phase 2 Fins)	37
6. Effect of Nose Configuration on the Stability Derivatives, Static Margin, and Axial Force at $\alpha = 0$	
a. C _{Nα} versus M _{∞}	38
b. C _{mα} versus M _{∞}	39
c. dC _m /dC _N versus M _{∞}	40
d. C _A versus M _{∞}	41
7. Variation of the Stability Derivatives, Static Margin, and Axial Force with Reynolds Number at $\alpha = 0$, Configuration N ₂ T ₃	42
8. Variation of the Roll-Moment Coefficient with Fin Configuration at $\alpha = 0$, Phase 1 Fins	43
9. Variation of the Roll-Moment Coefficient with Reynolds Number at $\alpha = 0$	44
10. Variation of the Roll-Moment Coefficient at $\alpha = 0$ with Fin Configuration	
a. C _{ℓ} versus M _{∞}	45
b. C _{ℓ_p} versus M _{∞}	46
c. P _{SS} versus M _{∞}	47
11. C _{Nα} and C _{mα} versus M _{∞}	
a. N ₂ T ₄	48
b. N ₂ T ₂	49
c. N ₂ T ₃	50
d. N ₂ T ₈	51

<u>Figure</u>	<u>Page</u>
12. C_{N_q} and C_{m_q} versus M_∞	
a. N ₂ T ₄	52
b. N ₂ T ₂	53
c. N ₂ T ₃ and N ₂ T ₈	54
13. $\partial C_{m_q} / \partial (\Delta x_{cg})$ versus M_∞	
a. N ₂ T ₄	55
b. N ₂ T ₂	56
c. N ₂ T ₃	57
14. $(C_{A_t}) \alpha = 0$ versus M_∞	
a. N ₂ T ₄	58
b. N ₂ T ₂	59
c. N ₂ T ₃ , N ₂ T ₅ , and N ₂ T ₈	60
15. Variation of h , q_∞ , and M_∞ with Time for the ATR Configuration N ₂ T ₃ Trajectory	
a. $h_i = 7000$ ft, $V_i = 844$ ft/sec	61
b. $h_i = 7000$ ft, $V_i = 506$ ft/sec	62
c. $h_i = 7000$ ft, $V_i = 169$ ft/sec	63
d. $h_i = 7000$ ft, $V_i = 0$	64
e. $h_i = 5000$ ft, $V_i = 844$ ft/sec	65
f. $h_i = 5000$ ft, $V_i = 506$ ft/sec	66
g. $h_i = 5000$ ft, $V_i = 169$ ft/sec	67
h. $h_i = 5000$ ft, $V_i = 0$	68
16. Altitude versus Downrange Distance for the ATR Configuration N ₂ T ₃ Trajectory	
a. $h_i = 7000$ ft, $V_i = 844$ ft/sec	69
b. $h_i = 7000$ ft, $V_i = 506$ ft/sec	70
c. $h_i = 7000$ ft, $V_i = 169$ ft/sec	71
d. $h_i = 7000$ ft, $V_i = 0$	72
e. $h_i = 5000$ ft, $V_i = 844$ ft/sec	73
f. $h_i = 5000$ ft, $V_i = 506$ ft/sec	74
g. $h_i = 5000$ ft, $V_i = 169$ ft/sec	75
h. $h_i = 5000$ ft, $V_i = 0$	76
17. Variation of Impact M_∞ , Time, and Horizontal Range with Initial Velocity	77
18. Variation of Slant Range with Initial Velocity	78
19. Variation of Spin Rate with Flight Time for N ₂ T ₅ , N ₂ T ₈ , N ₂ T ₉ and N ₂ T ₁₀ with $h_i = 7000$ ft and $V_i = 844$ ft/sec	79

<u>Figure</u>	<u>Page</u>
20. Effects of Initial Angle of Attack on Missile Dispersion	80
21. Effects of Initial Pitch Rate on Missile Dispersion	81
22. Illustration of Wind Effects	82
23. Illustration of the Thrust and Body Coordinate Nomenclature	83
24. Variation of the Vehicle Lateral Displacement with Down-range Distance for a 10-ft/sec Crosswind	84
25. Variation of Dispersion with Crosswind Velocity	85
26. Variation of Vehicle Static Margin with Flight Time	86
27. Effect of Static Margin on the Vehicle Lateral Displacement Caused by Crosswinds	87
28. Comparison of the Effects of Wind and Launch Error on Dispersion when Reducing the Static Margin of the Vehicle	88
29. Variation of Dispersion with Starting Time for a Wind Gust Lasting for One Second	89
30. Variation of the Vehicle Roll Rate and Total Angle of Attack with Flight Time	90
31. Effect of Linear Thrust Misalignment on Missile Dispersion	91
32. Effect of Angular Thrust Misalignment on Missile Dispersion	92
33. Effects of Fin Misalignment on Missile Dispersion	93
34. Variation of Dispersion with Initial Spin Rate	94
35. Effects of Fin Opening Time on Dispersion	95

II. TABLES

I. Test Summary	
a. Phase 1	96
b. Phase 2	96

II. TABLES (Continued)

	<u>Page</u>
II. Tabulated Data ($\alpha = 0$)	
a. Configuration N ₂ T ₄	97
b. Configuration N ₂ T ₂	98
c. Configuration N ₂ T ₃ and all Phase 2 Fins	99
d. Roll and Axial-Force Data	100

NOMENCLATURE

A	Reference area, full-scale base area = 9.618 sq in.
C _A	Forebody axial-force coefficient, C _{A_t} - C _{A_B} , forebody axial force/q _∞ A
C _{A_B}	Base pressure axial-force coefficient, (p _∞ - p _b)/q _∞ A
C _{A_t}	Total axial-force coefficient, axial force/q _∞ A
C _ℓ	Rolling-moment coefficient, rolling moment/q _∞ A
C _{ℓ_p}	Roll-damping derivative coefficient, ∂C _ℓ /∂(pd/2V _∞)
C _m	Pitching-moment coefficient, pitching moment/q _∞ Ad (reference at 0.421ℓ from nose)
C _{m_q}	∂C _m /∂(qd/2V _∞), per radian
C _{m_α}	∂C _m /∂α, per deg
C _N	Normal-force coefficient, normal force/q _∞ A
C _{N_α}	∂C _N /∂α, per deg
C _{N_q}	∂C _N /∂(qd/2V _∞), per radian
C _{n_r}	∂C _n /∂(rd/2V _∞), per radian
C _{n_β}	∂C _n /∂β, per deg
C _{Y_r}	∂C _Y /∂(rd/2V _∞), per radian
C _{Y_β}	∂C _Y /∂β, per deg
d	Reference length, full-scale diameter = 3.50 in.
d _T	Linear thrust displacement along z _B axis, ft.
$\frac{dC_m}{dC_N}$	Static margin, $\frac{X_{cg} - X_{cp}}{d}$

$\frac{\partial C_{m_q}}{\partial(\Delta x_{cg})}$	Derivative of C_{m_q} with respect to movement of center of gravity, (radian-ft.) ⁻¹
h	Altitude, ft
I_x	Roll moment of inertia, slug-sq ft
I_y	Pitch moment of inertia, slug-sq ft
ℓ	Vehicle length, full scale, 66 in.
M_∞	Free-stream Mach number
p	Vehicle spin rate, radians/sec or rpm
p_b	Base pressure, psia
p_o	Stagnation pressure, psia
p_∞	Free-stream static pressure, psia
$pd/2V_\infty$	Spin parameter, radians
q	Vehicle pitch rate, radians/sec
q_∞	Free-stream dynamic pressure, psia
Re_ℓ	Reynolds number based on vehicle length
R_s	Slant range of vehicle, ft
R_x	Horizontal downrange displacement
r	Vehicle yaw rate, radians/sec
\bar{r}	Distance (measured in the plane perpendicular to the initial flight path angle) between the impact points of a trajectory with dispersion producing factors and a zero-error trajectory, ft.
T_o	Stagnation temperature, °R
t	Flight time, sec
t_{w_i}	Initial time for a one-second duration wind gust, sec
V	Vehicle velocity, ft/sec
V_w	Wind velocity, ft/sec
X	Axial distance along vehicle centerline measured from nose, ft
x, y, z	Position of projectile referenced to earth-fixed inertia coordinate system (see Fig. 23)
x_B, y_B, z_B	Body coordinate axis, (see Fig. 23)

α	Angle of attack, deg
β	Angle of sideslip, deg
Δ	Dispersion in mils, $\Delta = \bar{r}/R_s \times 1000$
γ	Elevation flight path angle, deg
σ	Angle between thrust vector and vehicle centerline, deg
δ	Fin cant angle, deg (see Fig. 2b)
λ	Fin misalignment error, deg
θ_w, θ_c	Fin wedge tab angle and cone tab angle (see Fig. 2b), deg

SUBSCRIPTS

B	Body alone
BT	Complete configuration (body plus tail)
BT-B	Body-tail minus body
cg	Center of gravity
cp	Center of pressure
i	Initial conditions
ss	Steady-state condition
T	Tail fins
$(\cdot)_{\alpha=0}$	Indicates value of term in parenthesis taken at $\alpha = 0$
∞	Free-stream condition

SECTION I INTRODUCTION

Currently the Air Force Armament Laboratory of Eglin Air Force Base is developing an Advanced Tactical Rocket (ATR) and an associated launcher. Basically, the ATR is to be an unguided, fin-stabilized, air-launched missile. The ATR aerodynamic configuration is being designed by the von Kármán Gas Dynamics Facility (VKF) of the Arnold Engineering Development Center (AEDC) for the AFATL. The ATR launcher is being investigated by the Propulsion Wind Tunnel Facility (PWT) and will be reported in a separate report.

Two series of wind-tunnel tests (designated Phase 1 and Phase 2 tests) have been conducted on ATR configurations. The Phase 1 tests were conducted to investigate basic nose and tail-fin effects on the static stability, drag, and static rolling-moment characteristics. The Phase 2 tests were conducted to obtain the roll-damping characteristics and to obtain data on other tail-fin configurations. The data from the wind-tunnel tests were used in a six-degree-of-freedom (6-DOF) computer program to obtain trajectory and dispersion information. This report contains design considerations, the results of the wind-tunnel test program, and an analysis of the trajectory and dispersion study.

The static-force and roll tests on the ATR configuration models were conducted in the AEDC Aerodynamic Wind Tunnel (4T) of the PWT and the Supersonic Wind Tunnel (A) of the VKF. Data were obtained at Mach numbers from 0.3 to 4.5 at free-stream Reynolds numbers, based on model length, between 1.4×10^6 and 17.1×10^6 . Angle of attack was varied from -3 to 10 deg.

SECTION II DESIGN CONSIDERATIONS

2.1 GENERAL

The ATR configuration length (66 in.) and diameter (3.5 in.) were specified by AFATL. Also, the ATR is to be tube-launched so that the fins must be contained within the 3.5-in. diam at launch and then pop out to their extended position. It was preferable that the fins have a hinge line running along the chord of the fin parallel to the model center-line; this limits the span of the fin (see Fig. 1, Appendix I). Therefore, with these limitations, the aerodynamic design problem develops into one of defining an acceptable nose shape and tail-fin configuration.

2.2 NOSE SHAPE

The drag and volume are the two prime considerations in selecting the nose shape for the ATR. If exotic low-drag nose shapes are excluded because of manufacturing difficulty and the wide ATR Mach number range, the primary shapes to be considered are the cone, secant ogive, and tangent ogive. For any given nose length, the secant ogive has a lower drag than the cone or the tangent ogive (Ref. 1), both of which have essentially the same drag. The nose volume, of course, is minimum for the cone and maximum for the tangent ogive. For the initial study, the small decrease in the drag by going to the secant ogive was not felt to be necessary since warhead volume would be decreased. If a drag reduction is deemed necessary after considering the rocket motor performance, then a secant ogive shape will be considered. Therefore, tangent ogive noses of 2.5 and 3.0 calibers in length were selected for the preliminary configurations.

2.3 TAIL FINS

As explained earlier, the maximum tail-fin span is fixed by the folding arrangement selected by AFATL. Also, a tail chord length of 2 calibers is the maximum allowable length because of the nozzle and propellant volume considerations as specified by AFATL.

Thus, the primary parameters for the fin design are fin span, chord, sweep angle, and thickness. Since the maximum allowable fin span and chord are known, the only consideration is whether they should be reduced. The static margin increases approximately linearly with fin span (Ref. 2). Therefore, the maximum allowable fin span was selected for the preliminary configurations.

For similar configurations (Ref. 2), the static margin had been found to increase for increasing fin chord length up to approximately 1.5 to 2 calibers and then start leveling off. Therefore, fin chord lengths of 1.5 and 2.0 calibers were selected for the preliminary investigation.

As is widely known (Refs. 3 and 4), fins can be made more effective in producing lift at certain Mach numbers by sweeping the leading edge. If the fin planform area can be kept constant, the fins can be optimized for a particular Mach number by the fin sweep angle. However, for the ATR there is a wide range of flight Mach numbers, and sweeping the fin reduces the fin area since the trailing edge cannot extend beyond the model base. Therefore, it is believed that considering

the full range of flight Mach numbers, the best performance would be obtained from the maximum area fin (zero-sweep angle). However, other considerations suggest that some sweep of the fins is necessary for the best mechanical operation of the fins during their unfolding sequence. Therefore, fins of 0- and 45-deg sweep angle were investigated in the Phase 1 tests, and 11-deg swept fins were tested during the Phase 2 tests.

To minimize the error from thrust and fin misalignments, it is necessary to spin the vehicle. AFATL personnel requested that the fin leading edges be beveled to produce a rolling torque large enough to spin the vehicle at a rate of 1200 rpm. The bevel was selected over canting the fins because of the ease of manufacturing. However, as will be shown later, the beveled fins produced undesirable roll characteristics, so fins with roll tabs and cant angle were tested. Also, fins with conical protrusions at their base to produce roll and to allow for a larger rocket exit area were investigated along with a tail section with a simulated rocket nozzle extending from the flat section of the aft tail portion (Fig. 2c).

The fin thickness must be large enough for strength considerations and allowance of adequate bevel angle, but excessive thickness gives a drag penalty. For the ATR, the thickness also controls to some extent the allowable span because the fin must fold within the cylinder outside diameter. A fin thickness of 0.2 in. was selected and represents a reasonable compromise.

Since the possibility exists that the rocket plume could change the vehicle aerodynamic characteristics and possibly cause flight problems, the effects of a simulated plume (Fig. 2d) were investigated. The size of the plume was selected by personnel of the Air Force Rocket Propulsion Laboratory (RPL) at Edwards Air Force Base. According to the RPL personnel, the selected plume size is probably larger than could be expected in the ATR trajectory and therefore can be considered conservative in judging its effect.

SECTION III EXPERIMENTAL APPARATUS AND PROCEDURE

3.1 ATR TEST MODELS

Details of the 0.5-scale Phase 1 model and of the 0.57-scale Phase 2 model are shown in Figs. 1 and 2, respectively. Photographs of the

Phase 1 model are shown in Fig. 3. Basically, the ATR model is a tangent ogive cylinder with cruciform fins mounted to a square section at the base. The square section is necessary for the fins to fold down on the actual vehicle such that it may be tube launched. Throughout this report the configurations will be designated by $N_a T_b$ where the N_a designates either the N_1 or N_2 nose and T_b designates one of the tail-fin configurations. Two tangent ogive noses of 2.5 calibers (N_1) and 3.0 calibers (N_2) in length were tested. The initial series of the Phase 1 tests was conducted on the model with no fins and with the three sets of 11-deg bevel fins (T_1 , T_2 , and T_3) (Fig. 1a). The smaller 45-deg swept fins (T_1) were then modified to make the fin cross section symmetrical (Fin T_4 , Fig. 1b). Three sets of tabs (Fig. 1b) were then attached to the T_4 fin to provide rolling-moment capability. The tabs were designed to give adequate tube clearance with the fins in the folded position.

The Phase 2 model, which was tested to determine the roll characteristics of the ATR and to obtain the static aerodynamic data for different tail fins, had fins with a 11-deg leading-edge sweep angle. This sweep angle was chosen to allow for easier fin opening. The Phase 2 model (Fig. 2b) was tested with fins of three different roll tabs, with fins of cant angles of 0.5 and 1.0 deg, and with fins with three different conical protrusions at the trailing edge. Details of the nozzle simulator and the plume simulator are shown in Figs. 2c and 2d, respectively.

3.2 INSTRUMENTATION AND PROCEDURE

Model static forces and moments were measured with a six-component, moment-type, strain-gage balance supplied by VKF. In the VKF, base pressures were measured with 1- and 15-psid transducers referenced to a near vacuum. In the PWT, base pressures were measured with 5-psid transducers, referenced to free-stream pressure.

For the roll-damping tests, the model was mounted on ball bearings and allowed to spin at its steady-state spin rate. The spin rate was monitored using a photocell diode-type tachometer. Knowing the static rolling moment and the steady-state spin rate the roll-damping derivative coefficient was found by:

$$C_{\ell p} = (C_{\ell}/p_{ss}) d / 2 V_{\infty}$$

The bearing damping for the higher spin rates is estimated from other tests to be approximately two percent of the present aerodynamic damping. This is within the expected accuracy of the dynamic data, and therefore, no corrections were made for the bearing damping.

3.3 TEST FACILITIES

The Aerodynamic Wind Tunnel (4T) is a closed-circuit, continuous flow, variable density wind tunnel that can be operated at Mach numbers from 0.10 to 1.40. At all Mach numbers, the stagnation pressure can be varied from about 2 to 26 psia. The test section is 48 in. square and 150 in. long with perforated, variable porosity (0.5 to 6.0 percent) walls. It is completely enclosed in a plenum chamber from which the air can be evacuated, allowing part of the tunnel airflow to be removed through the perforated walls of the test section. The wall perforations are 0.50-in.-diam holes inclined 60 deg from the normal to the wall surface. This design allows control of wave attenuation and blockage effects. Further control of wall interference effects can be accomplished by converging or diverging the top and bottom test section walls by as much as 0.5 deg.

The Supersonic Wind Tunnel (A) is a continuous, closed-circuit, variable density wind tunnel with an automatically driven flexible-plate-type nozzle and a 40- by 40-in. test section. The tunnel can be operated at Mach numbers from 1.5 to 6 at maximum stagnation pressures from 29 to 200 psia, respectively, and at stagnation temperatures up to 750°R. Minimum stagnation pressures range from about one-tenth to one-twentieth of the maximum pressure at each Mach number. Mach number changes may be made without stopping the tunnel in most instances. The model can be injected into the tunnel for a test run and then retracted for model changes without interrupting the tunnel flow. For more information on Tunnels 4T and A, see Ref. 5.

SECTION IV
TEST CONDITIONS AND PRECISION OF DATA

4.1 TEST CONDITIONS

A test summary is given in Table I, Appendix II. The nominal tunnel conditions at which the tests were conducted are given below.

Phase 1 Model					
<u>Nominal</u> <u>M_∞</u>	<u>P_{∞},</u> <u>psia</u>	<u>T_{∞},</u> <u>°R</u>	<u>P_∞,</u> <u>psia</u>	<u>q_∞,</u> <u>psia</u>	<u>$Re_\ell \times 10^{-6}$</u>
0.3	23.8	560	22.3	1.41	8.25
0.6	22.2		17.4	4.39	13.8
	16.1		12.6	3.18	10.5
	12.0		9.4	2.37	7.43
	7.1		5.57	1.41	4.40
0.8	18.7		12.3	5.50	13.8
0.9	17.7		10.5	5.94	13.8
1.0	17.1		9.04	6.33	13.8
1.1	20.8		9.74	8.25	17.1
	16.8		7.86	6.65	13.8
	12.8		5.97	5.06	10.5
	9.1		4.24	3.59	7.43
1.3	16.7		6.03	7.13	13.8
1.5	17.3		4.70	7.39	13.8
2.0	20.5		2.62	7.34	13.8
	15.6		1.99	5.58	10.5
	11.1		1.42	3.96	7.43
	6.6		0.839	2.35	4.40
	2.1		0.262	0.734	1.38
2.5	26.1		1.53	6.69	13.8
3.0	34.8	570	0.948	5.97	13.8
3.5	45.3		0.594	5.09	13.8
4.0	58.8		0.387	4.33	13.8
	44.6		0.294	3.29	10.5
	31.7		0.209	2.34	7.43
	18.8		0.124	1.39	4.40
	5.9		0.0387	0.433	1.38
4.5	75.6		0.261	3.70	13.8

Phase 2 Model

<u>Nominal M_∞</u>	<u>P_o, psia</u>	<u>T_o, °R</u>	<u>P_∞, psia</u>	<u>q_∞, psia</u>	<u>V_∞, ft/sec</u>	<u>$Re \times 10^{-6}$</u>
0.3	20.9	560	19.6	1.24	345	8.25
0.6	19.6		15.3	3.86	672	13.8
0.8	16.5		10.8	4.84	873	
1.0	15.1		7.95	5.57	1060	
1.1	14.8		6.91	5.86	1150	
1.3	14.7		5.30	6.27	1300	
1.5	15.2		4.13	6.50	1440	
2.5	23.0	570	1.35	5.89	1930	
3.5	39.9	570	0.523	4.48	2200	
4.5	66.5	570	0.230	3.26	2340	

4.2 PRECISION OF DATA

Before the tests, balance static loadings were applied which simulated the model loading range anticipated during the tests. The uncertainties listed below correspond to the differences between the applied loads and the values calculated by the final data reduction balance equations.

<u>Balance Components</u>	<u>Design Load</u>	<u>Maximum Static Loads</u>	<u>Uncertainties</u>
Normal force, lb	150	75	±0.20
Pitching moment, in.-lb	510	265	±1.52
Rolling moment, in.-lb	100	48	±0.11
Axial force, lb	25	15	±0.11

The uncertainties for the basic tunnel parameters p_o , T_o , and M_∞ were estimated from calibration of the p_o and T_o instruments and examination of tunnel-flow uniformity and repeatability. These uncertainties, along with the estimated balance uncertainties, were then used to compute the uncertainties in the force coefficients listed below, assuming a random combination of the uncertainties (Ref. 6).

Estimated Uncertainty*

<u>Nominal M_∞</u>	<u>q_α, percent</u>	<u>C_N</u>	<u>C_m</u>	<u>C_ℓ</u>	<u>C_A</u>
0.3	± 3.3	± 0.059	± 0.26	± 0.019	± 0.032
0.6	± 1.7	± 0.019	± 0.082	± 0.006	± 0.010
0.8	± 1.7	± 0.015	± 0.066	± 0.005	± 0.032
0.9	± 1.1	± 0.014	± 0.061	± 0.004	± 0.008
1.0	± 1.1	± 0.013	± 0.057	± 0.004	± 0.007
1.1	± 1.6	± 0.010	± 0.044	± 0.003	± 0.006
1.3	± 3.3	± 0.012	± 0.051	± 0.004	± 0.006
1.5	± 2.8	± 0.011	± 0.049	± 0.004	± 0.010
2.0	± 1.6	± 0.011	± 0.049	± 0.004	± 0.007
2.5	± 2.3	± 0.012	± 0.054	± 0.004	± 0.007
3.0	± 1.3	± 0.014	± 0.060	± 0.004	± 0.008
3.5	± 2.3	± 0.016	± 0.071	± 0.005	± 0.009
4.0	± 1.6	± 0.019	± 0.083	± 0.006	± 0.011
4.5	± 1.9	± 0.022	± 0.098	± 0.012	± 0.012

$$*Re_\ell = 13.8 \times 10^6$$

SECTION V

PRESENTATION AND DISCUSSION OF EXPERIMENTAL RESULTS

Figure 4 presents the typical variation of the static stability, rolling-moment, and axial-force coefficients with angle of attack. These curves are for the N₂T₃ configuration at $M_\infty = 0.3, 1.0, 2.5$, and 4.5. The variations of C_N and C_m with α were essentially linear up to 3 or 4 deg, and C_A and C_ℓ were practically constant for the lower angles of attack.* Thus, these data indicate that C_{N_α} , C_{m_α} , C_A , and C_ℓ evaluated at $\alpha = 0$ can be used in trajectory calculations without any loss of accuracy as long as the vehicle does not reach angles of attack greater than 4 deg. The data are typical of the results of the other finned configurations in that there was no indication of any anomalies that would be detrimental to the rocket flight if sufficient disturbances were introduced to cause high angles of attack.

*The moment data are referenced to the burnout center of gravity (0.421 ℓ) unless otherwise stated.

The effect of fin configuration on the stability derivatives, static margin, and axial force at $\alpha = 0$ is illustrated in Fig. 5. The stability data exhibit the normal trend of high static stability at the subsonic and transonic Mach numbers and the decrease of stability in the supersonic region. The finned configurations were all statically stable throughout the Mach number range. At Mach numbers below 1.5, the static margin was essentially the same for each fin configuration; however, in the critical supersonic regime the static margin increased with fin plan area, with T₃ and T₈ having the higher and essentially the same stability indicating no significant loss from the 11-deg swept leading edge. There was no notable effect of the roll tabs (T_{4B}) on the stability. The body-alone data are also presented and are necessary in calculating the dynamic coefficients as will be shown later. The method of Ref. 7 adequately estimates the stability margin and is sufficient for a preliminary analysis. This method (Ref. 7) utilizes empirical correlations and because of this is limited to $0.6 < M_\infty < 3.0$. Therefore, another theoretical estimate using the method of Ref. 8 and shock-expansion theory is included for $M_\infty = 1.5$ to 4.5 and compares well with the data.

The axial-force coefficient for the Phase 1 model (Fig. 5d) also increased with fin planform area and with the T₃ fins the vehicle axial force was 1.3 times the body-alone axial force. The data show that the addition of the roll tabs increased the axial-force coefficient slightly over 10 percent. The method of Ref. 7 proved to be inadequate for predicting C_A. Therefore, the method of Ref. 9 was used and, as shown in Fig. 5d, the results compare quite well with the present experimental data. For the analytical estimate, the model was assumed to have a straight cylindrical afterbody; thus, the effect of the square aft section was not considered. The axial-force coefficient variation for the Phase 2 model is presented in Fig. 5e. The fins with the conical protrusions and nozzle simulator, which as stated earlier would allow the actual vehicle to have a larger rocket exit area, had a substantially higher drag.

The effect of nose shape on the stability and axial-force coefficients of the ATR model is shown in Fig. 6. The model with the slender (3.0-caliber) nose, N₂, was only slightly more statically stable but had a notably lower drag at Mach numbers greater than 1.3.

The variation of the stability derivatives, static margin, and axial force with Reynolds number is shown in Fig. 7 for the N₂T₃ configuration. The data, which are typical of the other configurations, show some slight variations at the lower Mach numbers, but the values are essentially constant for the higher Reynolds numbers and Mach numbers to be encountered during the flight.

The variation of the rolling-moment coefficient at $\alpha = 0$ with Mach number for the Phase 1 fin configurations is shown in Fig. 8. The data show that the fins with the 11-deg beveled leading edge (T₁, T₂, T₃) had a rolling moment which was near zero for $M_\infty = 1$ and reversed direction in the supersonic Mach number range. Theoretically and experimentally (Refs. 10, 11, and 12) considering each fin separately, the reversed rolling moment would not occur until possibly at low subsonic Mach numbers. The strange roll reversal characteristics were attributed to the shock from the bevel interacting with the flow over the square base and creating a high pressure on the aft portion of the adjacent fin. This pressure evidently counteracted the bevel pressure at the lower Mach numbers. Obviously, this type of roll reversal characteristic can lead to higher missile dispersion since any manufacturing asymmetries would not be averaged over a roll cycle. Therefore, the bevel was taken off the T₁ fin and roll tabs added to the aft portion (Fig. 1b). The tab fin data show the desirable constant direction rolling moment, and the values agree quite well with the theoretical estimate (Ref. 10). For the Phase 1 tabs tested, the data show only small variations in the rolling-moment coefficient with length and span. As is shown in Fig. 9, there were no notable effects of Reynolds number on C_l .

A more extensive study of the roll characteristics of the ATR for various fins was made in the Phase 2 tests; the data are shown in Fig. 10. The rolling-moment coefficient variations with Mach number, shown in Fig. 10a, indicate that all of the conical protrusion fins had a much larger rolling moment than one would expect from using simple cone theory for the protrusion pressure. The tab fins and the canted fins of 0.5 and 1.0 deg have the lower level and more expected rolling-moment coefficients. The roll-damping-derivative coefficients for all the 11-deg swept leading-edge fins were essentially equal, and the variation with Mach number is presented in Fig. 10b. The actual criteria for comparing the roll characteristics of the different fins are the roll rates. The steady-state spin rate for the wind-tunnel conditions is shown in Fig. 10c. For the ATR flight purposes a spin rate high enough to adequately average any asymmetries, but less than 2000 rpm to avoid large Magnus effects, is desirable. Of course, judgement must be made on the trajectory spin rate history, but the wind-tunnel steady-state spin rates certainly indicate that T₅, T₈, and T₉ have the most promising roll characteristics. Certainly, even the smallest conical protrusion fin leads to roll rates much too high.

Data were also obtained on fin T_{5A} (same dimensions as T₅ but with the tab made by bending out the fin) which has obvious production advantages. As the data in Fig. 10a show, the void behind the roll tab increased the rolling moment substantially and would lead to too high a

roll rate. Therefore, if on the production projectile the tab is produced by a pressing operation, the tab size must be decreased.

As was discussed earlier, tests were conducted with a simulated plume cone mounted on the sting behind the model. There was no notable effect of the plume except on the rolling-moment coefficient of N₂T₅ and N₂T₉ at Mach numbers < 1.0 where, as shown in Fig. 10a, the rolling-moment coefficient was reduced approximately 20 percent. No effect of the plume was found on the static stability at any condition. As stated by RPL personnel, the plume shape used in the tests was conservative; therefore, the wind-tunnel results indicate that the plume would have no notable effect on the ATR flight performance.

SECTION VI COMPUTER INVESTIGATION OF THE ATR PERFORMANCE

6.1 GENERAL

A comparison of the various ATR configurations cannot be made on wind-tunnel aerodynamic data alone. The effect of the aerodynamic differences on the ATR trajectory and dispersion must be assessed to fully judge the different configurations. The measured static and roll-damping data, calculated dynamic coefficients, and estimated ATR physical and thrust characteristics were used in a six-degree-of-freedom (6-DOF) flight path study computer program (Ref. 13) to investigate the vehicle trajectory.

6.2 REQUIRED INPUT DATA

The required aerodynamic input data are presented in Figs. 10 through 14 and in more complete tabulated form in Table II, Appendix II. The static data and the roll-damping data are, of course, the experimentally determined data. The aerodynamic pitch-damping coefficients were calculated using the static data in the following equations (Refs. 14, 15, and 16):

$$(C_{m_q})_B = -2(C_{N_\alpha})_B \left(\frac{l - X_{cg}}{d} \right)^2$$

$$(C_{m_q})_T = -2(C_{N_\alpha})_{BT-B} \left(\frac{X_{cpT} - X_{cg}}{d} \right)^2$$

$$C_{mq} = (C_{mq})_B + (C_{mq})_T$$

$$(C_{Nq})_B = 2(C_{N\alpha})_B \left(\frac{l - X_{cg}}{d} \right)$$

$$(C_{Nq})_T = 2(C_{N\alpha})_{BT-B} \left(\frac{X_{cpT} - X_{cg}}{d} \right)$$

$$C_{Nq} = (C_{Nq})_B + (C_{Nq})_T$$

The total axial-force coefficient (C_{A_t}) was used for the entire trajectory. Of course, this is not correct for the thrust phase of the trajectory, but the error introduced (by the additional base drag) was calculated to be 0.15 percent of the thrust and is considered negligible.

The vehicle characteristics as estimated by AFATL personnel and used in the trajectory analysis are:

Time from Launch, sec	Mass, slugs	X_{cg} , ft	I_x , slug-sq ft	I_y , slug-sq ft	Vacuum Thrust, lb
0	1.465	2.695	0.0174	3.65	2200
0.5	1.325	2.650	0.0160	3.36	
1.0	1.182	2.581	0.0146	3.06	
1.5	1.042	2.500	0.0132	2.77	
2.0	0.897	2.419	0.0128	2.48	
2.25	0.839	2.318	0.0108	2.32	
>2.25	0.839	2.318	0.0108	2.32	0

6.3 BASIC TRAJECTORY DATA

The basic trajectory data for configuration N₂T₃ are presented in Figs. 15 and 16. The variations of Mach number (M_∞), altitude (h), and dynamic pressure (q_∞) with vehicle flight time and h versus down-range displacement (R_x) are presented for initial altitudes of 7000 and 5000 ft with various initial launcher velocities ranging from 0 to 844 ft/sec. An initial flight elevation angle of -30 deg and an initial angle of attack and pitch rate of zero were used for these trajectories. The trajectory data show that a maximum Mach number of 4.4 and a peak q_∞ of 2.45×10^4 psf are obtained at motor burnout.

The impact flight time, Mach number, and horizontal range are presented in Fig. 17 as a function of initial velocity for configurations N₂T₄, N₂T₂, N₂T₅, N₂T₈, N₂T_{9(N)}, and N₂T₃. Also, the slant range versus initial velocity is shown in Fig. 18. The data show the expected trends of decreasing flight time and increasing Mach number and range with increasing initial velocity. The computed trajectory data show less than three-percent variation of these parameters between these different configurations. For clarity, since the small differences are not distinguishable on the plots, the impact values of M_∞, t, R_X for configurations N₂T₅, N₂T₈, and N₂T_{9(N)} are listed below for V_i = 844 ft/sec and h_i = 7000 ft.

At Impact (V_i = 884 ft/sec, h_i = 7000 ft)

Configuration	M _∞	t, sec	R _X , ft
N ₂ T ₃	3.59	3.91	11,383
N ₂ T ₅	3.53	3.94	11,380
N ₂ T ₈	3.57	3.92	11,382
N ₂ T _{9(N)}	3.34	4.01	11,370

The values indicate the actual small effect that the different drag values (see Fig. 5e) have on the actual trajectory of the ATR with its predicted thrust capability. Therefore, the drag is not of major concern when comparing the various configurations.

The variation of spin rate with flight time for configurations N₂T₅, N₂T₈, N₂T₉, and N₂T₁₀ is shown in Fig. 19. The trajectory results are computed with an initial spin rate of 500 rpm which, as will be shown later, is required for low dispersion. The computed results indicate that configurations with rolling-moment coefficients higher than those of N₂T₅ (see Fig. 10) would spin the vehicle to a roll rate higher than desired for the ATR flight. The roll rate is to be kept below 2000 rpm to reduce any possible Magnus effects causing larger dispersion and also to avoid any stress problems associated with high spin rates. Therefore, from roll considerations tab T₅ or the 0.5-deg canted fin (T₉) produce acceptable results.

6.4 DISPERSION

Dispersion of a rocket from the intended flight path can be caused by launch errors, thrust misalignments, fin misalignments, and wind effects. The effect of these various factors was examined independently by the use of the 6-DOF computer program to compute the trajectory of the ATR configurations with a known misalignment, launch error,

or wind effect. The deviation of this trajectory from the trajectory with no dispersion-producing factors was calculated and the dispersion in mils obtained. The dispersion of a given trajectory, Δ , is defined as the distance between its impact point and that from the zero-error trajectory in a plane perpendicular to the initial flight path angle and non-dimensionalized by the slant range, that is,

$$\Delta = \frac{\bar{r}}{R_s} \times 1000, \text{ mils}$$

6.4.1 Launch Error Effects

Dispersion can arise from errors induced at launch. Launch errors that effectively give the rocket initial angle of attack or an initial pitch rate were investigated, and the dispersions are shown in Figs. 20 and 21. The data obtained from the computer 6-DOF trajectories show that all the configurations have similar dispersions for initial angles of attack up through 1 deg. However, for an initial angle of attack of 2 deg, the least statically stable configuration N₂T₄ has a dispersion of 2.5 mils, approximately 40 percent more than N₂T₂, N₂T₅, and N₂T₃. For initial pitch rates up to 0.15 radians/sec, the dispersion of all the configurations is similar and less than 2 mils. It should be noted that the initial disturbance values used are only assumed values and do not necessarily represent maximum values. Detail measurements of the forces and moments induced on the rocket vehicle as it leaves the launcher would be necessary to make any absolute calculations. However, the trends do indicate, as one would suspect, that the configurations with higher static stability will be affected less by launch error.

6.4.2 Wind Effects

Winds can cause dispersion of rockets not only in the conventional drift manner but can also cause the rocket to "weathercock." When the rocket weathercocks into the wind, the thrust vector is turned, thus the rocket can be driven upwind and large dispersions can result. For aircraft firings it might be assumed that the plane will be drifting with the wind, thus the rocket will have a velocity of zero relative to the crosswind and therefore will not weathercock. These two different firing conditions are illustrated in Fig. 22, and the coordinate systems are illustrated in Fig. 23. Dispersions caused by firing under each condition were investigated. The variations of the lateral displacement with downrange distance are shown in Fig. 24 for both types of firings. The computed trajectory data show the large distances that the rocket is

thrust laterally when it is fired without a lateral velocity equal to that of the wind. The data show for configuration N₂T₃ or N₂T₅ (both have such similar static margins that there is no notable difference) that the rocket goes laterally upwind 115 ft when it weathercocks compared to only a 40-ft drift when it is fired with a lateral velocity equal to that of the wind. Similar behavior of rockets fired into a crosswind have been noted in Ref. 17.

Obviously, rockets should be fired from aircraft drifting with the wind; however, normally there will be some differences in the velocities and also some wind gusts. Therefore, for a comparison of the wind effects on the different configurations and an investigation of the effects of static margin, it will be considered that the rocket with no lateral velocity is fired into a constant velocity crosswind that does not vary with altitude or time.

The variations of the dispersion with crosswind velocity are shown in Fig. 25. The computed dispersion increases linearly with crosswind velocity and shows no notable difference with configuration. In Fig. 26, the variation of vehicle static margin $(dC_m/dC_N)_{\alpha=0}$ with flight time, taking into account the shift in center of gravity, is presented. The data show that in the flight time period the rocket would weathercock into the wind. All the configurations have similar static margins and therefore would turn equally fast into the wind.

Vehicle static margin controls, to some extent, how rapidly the vehicle responds to the crosswind. Since the rocket is thrusting and therefore gaining velocity, the slower the rocket responds to the crosswind the smaller the actual angle it will end up turning into the wind. Therefore, the static margin should have some control over how much the rocket is affected by the crosswind, and many designers use a low static margin to minimize the effect of the wind. To investigate this phenomenon, trajectories were computed for the vehicle with constant static margin with respect to flight time. That is, the pitching moment was calculated and input into the 6-DOF program such that $(dC_m/dC_N)_{\alpha=0}$ remained constant with flight time. Values of $(dC_m/dC_N)_{\alpha=0} = -0.1$ and -1.0 were used with the vehicle fired into a 10-ft/sec crosswind. The results are presented in Fig. 27 as the lateral displacement variation with distance downrange. The computed results show that the wind effects can indeed be reduced, but the sacrifice in static margin must be very large to make any sizable reductions. Before reducing the static margin to reduce wind effects, the corresponding increase in launch effects caused by the reduction of static margin must be considered. A comparison of the dispersion caused by launch error to that

caused by wind effects as the static margin is decreased is shown in Fig. 28. As was noted earlier, a drastic reduction must be made in the static margin to substantially reduce the wind effects. The computed results show that with this reduction in static margin the dispersion caused by the nominal launch error magnifies greatly and completely overshadows any reduction in wind dispersion. Therefore, it must be concluded that it is not advisable to reduce the static margin in an attempt to lower dispersion unless one is sure that there are essentially no launch errors.

Actually, what would normally be encountered by the ATR in its flight would be changes in the relative wind or wind gusts. Therefore, the dispersion caused by a wind gust lasting for one second and beginning at different flight times, t_{w_i} , was computed and is presented in Fig. 29. The results indicate that the effect of the gusts reduces quickly with increasing wind gust starting time. Of course, this is expected since the ATR accelerates rapidly, thus the wind component relative to the rocket velocity would be lower and thereby reduce the turning angle of the rocket. These results point out that wind gusts after the first second of flight would not be too detrimental but do indicate the possible problem that might arise from aircraft and/or launcher flow-field effects.

6.4.3 Thrust and Fin Misalignment Effects

Dispersion can arise from thrust and/or fin misalignments. Tolerances on the rocket motor assembly can cause the thrust vector to act along a line offset both linearly and angularly from the aerodynamic centerline of the rocket (see Fig. 23). Thus, the thrust force will produce a moment. Similarly, fin misalignments from manufacturing tolerances can cause slight asymmetric forces and moments which can result in dispersion.

Since the thrust and fin misalignment forces and moments are body-fixed, their dispersion effects are dependent on the spin history of the vehicle. Trajectories were computed for the vehicle with misalignments using the rolling moments produced by the beveled edges (N_2T_3) and the rolling moment of N_2T_5 . Also, a trajectory was computed with an initial roll rate of 1000 rpm for the N_2T_5 configuration. The spin-rate histories are presented as a function of flight time in Fig. 30. The computed data show that the beveled fins produced an undesirable roll history as the spin rate reverses twice during the flight and crosses the model pitch-rate curve three times. Both these factors would tend to produce large dispersions. The N_2T_5 roll velocity doesn't change direction, and after the initial launch the spin rate stays above the pitch frequency.

Also shown in Fig. 30 are the variations of the total angle of attack with flight time for the vehicle with a linear thrust misalignment of 0.1 in. for the various roll-rate histories. The computed data show that the total angle of attack remains quite low for the prespun vehicle. For N₂T₅ ($p_i = 0$) the total angle of attack goes rapidly to 1.75 deg and damps to less than 0.1 deg after 1.25 sec of flight time. For the bevel fins, alpha total goes through perturbations as the roll rate passes through the pitch frequency.

The effects of linear thrust, angular thrust, and fin misalignments on the missile dispersion are presented in Figs. 31, 32, and 33, respectively. The thrust misalignment data show the large effect of spin history on dispersion. The beveled fin rolling moment leads to dispersions as high as 2.5 times those of the fins with the tab B and T₅ rolling moments. Also, the data show the very favorable results from prespinning the vehicle. Without prespin, the missile dispersion reaches 2 mils at a linear thrust misalignment of 0.05 in. (Fig. 31), at an angular misalignment of 0.1 deg (Fig. 32), and at a fin misalignment of 0.55 deg (Fig. 33). By prespinning the missile to 1000 rpm, the dispersion from a linear thrust misalignment of 0.05 in. was only 0.24 mils, a reduction of 88 percent. The reductions in dispersions caused by angular thrust and fin misalignments were 93 and 89 percent, respectively, when the vehicle was initially spun to 1000 rpm.

For the thrust misalignments (Figs. 31 and 32), the dispersion results are essentially independent of configuration. Since the misalignment of the fins for the different configurations will produce different forces and moments, the data (Fig. 33) show that the dispersion is slightly higher for the N₂T₅ configuration.

6.4.4 Effects of Combined Launch and Misalignment Error

The variation of dispersion caused by launch and misalignment error with initial spin rate is shown in Fig. 34. The dispersion, of course, depends on what combination of errors is assumed. However, for the separate cases shown in Figure 34 the computed data indicate that an initial spin rate of 500 rpm would always be sufficient as the rate of decline of dispersion decreases substantially in this area. The errors used for the combined effects study are considered to be near the maximum levels, and with these errors the maximum dispersion for the cases considered is 2.5 mils with an initial spin rate of 500 rpm.

Also, for one set of combined errors the effect of fin opening time was investigated, and the results are shown in Fig. 35. The effects of fin opening time were investigated by assuming that the body-alone

aerodynamic characteristics applied until the designated fin opening time, and after this time the aerodynamic characteristics for the body with fins fully extended applied. Although this type of assumption would obviously be invalid, since the fins would begin to open immediately and aerodynamic characteristics other than the body-alone characteristics would be applicable until the fins were fully extended, the computed data do indicate that the dispersion caused by the combined errors will definitely rise quite rapidly as the time required for the fins to open increases. It should be noted here that dispersion produced by the aircraft flow field and launcher effects would probably decrease as the fin opening time increased, since there would be less stability to turn the vehicle to the flow and less fin surface to receive the high-pressure gradients produced by the launcher. Regardless of the relative merits, it is evident that if there are tipoff effects at launch a fast fin opening time will be necessary to hold the dispersion to an acceptable level.

SECTION VII CONCLUDING REMARKS

7.1 SUMMARY OF RESULTS

A development program for the aerodynamic shape of an Advanced Tactical Rocket (ATR) was conducted at Arnold Engineering Development Center. The results of wind-tunnel tests and computer-calculated trajectory analyses indicate the following conclusions:

1. All ATR configurations tested were statically stable throughout the flight Mach number regime..
2. The static margin was essentially the same for each of the configurations in the subsonic and transonic Mach number regime but increased with fin planform area in the critical supersonic Mach number regime.
3. The addition of roll tabs, cant angle, and conical protrusions to the fins increased the axial force but had no notable effect on the static stability.
4. The slender nose (3-caliber) configurations had only slightly higher static margins, but had a notably lower drag at Mach numbers greater than 1.3 when compared to the more blunt 2.5-caliber nose.
5. The axial-force coefficient increased with fin planform area.

6. The fins with the beveled leading edges produced undesirable rolling moments which changed direction with increasing Mach number.
7. The rolling moment produced by the roll tabs, canted fins, and conical protrusions remained in the same direction at all Mach numbers.
8. The roll tab made by a pressing operation, thus leaving a void behind the tab, had a higher rolling moment than the conventional roll tab. Therefore, if on the production projectile the tab is produced by a pressing operation the tab size must be reduced.
9. The test data with the simulated jet plume indicate that the ATR should experience no notable effect of the plume during its flight.
10. Reynolds number effects were slight, and constant aerodynamic coefficients can be assumed for the high Reynolds number to be encountered during the ATR flight.
11. The trajectory data indicate that a maximum Mach number of 4.4 and a peak q_∞ of 2.45×10^4 psf are obtained at motor burnout.
12. The maximum slant range obtained was 13,360 ft for $h_i = 7000$ ft, $\gamma_i = -30$ deg, $V_i = 844$ ft/sec.
13. The flight times ($\gamma_i = -30$ deg) were approximately 3.9 sec and 3.1 sec for $h_i = 7000$ ft and 5000 ft, respectively.
14. Trajectory computations show that the drag is not of major concern when comparing the different ATR configurations since an increase of approximately 20 percent in drag increases the flight time by only 0.10 sec and decreases the horizontal range by only 13 ft.
15. The dispersion for a launch error producing initial angles of attack up to 2 deg or initial pitch rates up to 0.15 rad/sec is less than 2 mils.
16. Large dispersions upwind result when the rocket is fired without a lateral velocity equal to that of the wind.
17. The dispersion produced by the crosswind increases in a near linear fashion with crosswind velocity.

18. Reducing the static margin to reduce dispersion caused by wind effects is not advisable because of the resulting rapid growth in dispersion caused by the launch effects.
19. Wind gusts create large dispersions if they are encountered early in the flight of the rocket; however wind gusts occurring late in the flight of the rocket - after it has substantial velocity - have little effect on dispersion.
20. The roll-rate history has a significant effect on the dispersion produced by body-fixed moments such as thrust and fin misalignments.
21. The roll-rate history produced by the bevel fins causes large intolerable dispersion.
22. Only the T₅ (tab fins) and the T₉ (1/2-deg canted fin) fins produced acceptable rolling moments.
23. A dispersion of 4 mils is obtained for a linear thrust misalignment of 0.10 in. for the fin configurations with roll tabs and no initial spin rate. This dispersion is reduced to 0.5 mils by pre-spinning the vehicle to 1000 rpm.
24. A dispersion of 3 mils is obtained for an angular thrust misalignment of 0.15 deg for the fin configurations with roll tabs and no initial spin rate. This dispersion is reduced to 0.2 mils by pre-spinning the vehicle to 1000 rpm.
25. A dispersion of almost 4.0 mils is obtained for a fin misalignment of 1.0 deg with the roll tabs and no initial spin rate. This dispersion is reduced to 0.38 mils by prespinning the vehicle to 1000 rpm.
26. The major reduction in dispersion is accomplished by an initial spin rate of 500 rpm.
27. Various combined launch and misalignment errors produced a maximum dispersion of 2.5 mils with an initial spin rate of 500 rpm.
28. Dispersion increased with fin opening time.

7.2 CONFIGURATION SELECTION

The experimental, trajectory, and dispersion analyses of the ATR configurations indicate that both the 2.5- and 3.0-caliber tangent ogive

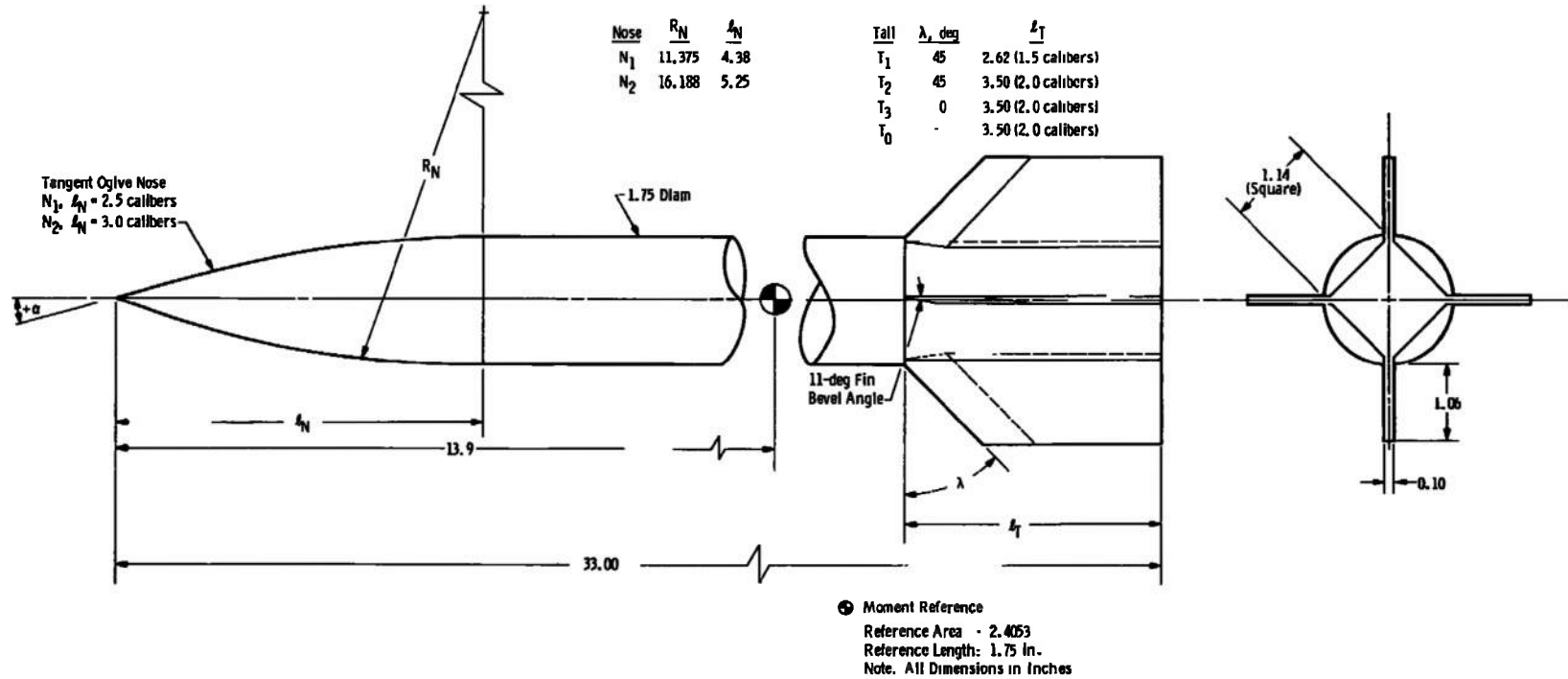
noses will be acceptable since there are only slight effects of drag on the ATR performance. There are no notable aerodynamic disadvantages to using the maximum chord length and most statically stable fins, and since an 11-deg sweep angle is desired for ease in mechanically opening the fins, the Phase 2 fins are the most adequate. Only the T₅ and T₉ tail fins have an acceptable roll-rate history. Therefore, the T₅ tab fin and the 1/2-deg canted fin, T₉, are the most desirable tail fins, and they may be used either with N₁ or N₂ with no notable change in performance. An initial spin rate of 500 rpm is necessary for low dispersion.

REFERENCES

1. Handbook of Supersonic Aerodynamics, Section 8 Bodies of Revolution. NAVWEPS Report 1488, Volume 3, pp. 222-239.
2. Davis, Levere, Jr., Follin, James W., Jr., and Blitzer, Leon. Exterior Ballistics of Rockets. New Jersey, D. Van Nostrand Company, 1958. p. 57.
3. Shapiro, Ascher H. The Dynamics and Thermodynamics of Compressible Fluid Flow, Volume II, The Ronald Press Company, New York, 1954, pp. 709-714.
4. Jones, Robert T. and Cohen, Doris. High Speed Wing Theory. Princeton University Press, Princeton, N.J., 1960, pp. 213-215.
5. Test Facilities Handbook (Eighth Edition). "Von Kármán Gas Dynamics Facility, Vol. 4." Arnold Engineering Development Center, December 1969 (AD863646).
6. Scarborough, James B. Numerical Mathematical Analysis. Johns Hopkins Press, Baltimore, Maryland (1962), pp. 504-507.
7. Eaton, Peter. T. "A Method for Predicting the Static Aerodynamic Characteristics of Low-Aspect-Ratio Configurations." David Taylor Model Basin Aero Report 1112, (AD647234).
8. Allen, H. Julian, and Perkins, Edward W. "Characteristics of Flow over Inclined Bodies of Revolution." NACA RMA50L07, March 1951.
9. USAF Stability and Control Datcom. Air Force Flight Dynamics Laboratory Report, Contract AF 33(616)-6460, October 1960, revised November 1965.
10. Kuethe, A. M. and Schetzer, J. D. Foundations of Aerodynamics. New York, John Wiley and Sons, Inc., 1959.

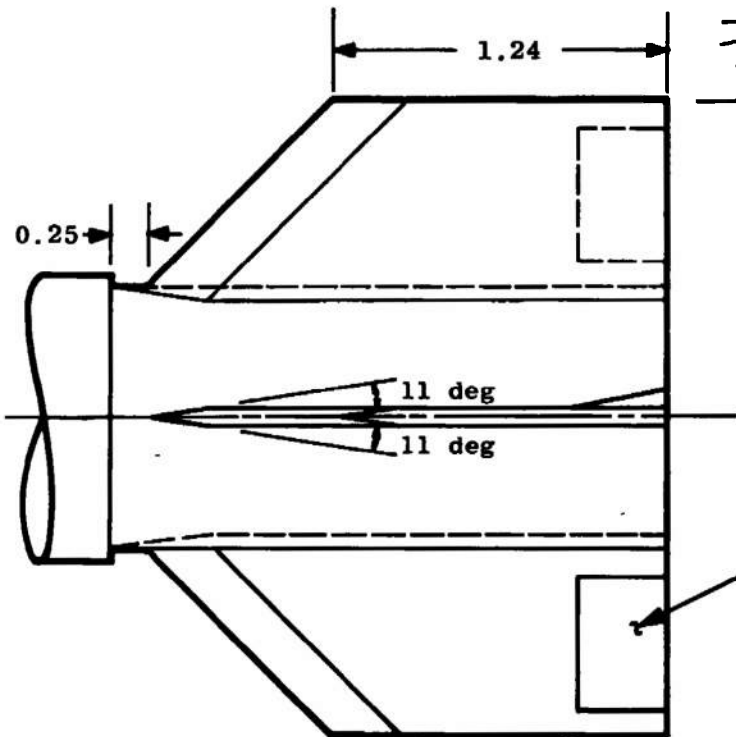
11. Bryson, Arthur E., Jr. "An Experimental Investigation of Transonic Flow Past Two-Dimensional Wedge and Circular-Arc Sections Using a Mach-Zehnder Interferometer." NACA TN 2560.
12. Vincenti, Walter G. and Wagoner, Cleo B. "Transonic Flow Past a Wedge Profile with Detached Bow Wave-General Analytical Method and Final Calculated Results." NACA TN 2339.
13. Vorwald, R. F. "Six-Degree-of-Freedom Flight Path Study Generalized Computer Program." FDL-TDR-64-1, Part II, Volume I.
14. Nielsen, Jack N. Missile Aerodynamics. New York, McGraw-Hill, 1960, pp. 409-416.
15. Chin, S. S. Missile Configuration Design. New York, McGraw-Hill, 1961, pp. 260-262.
16. Hatalsky, W., Arnold, R. P. and Turner, S. W. "Improved 2.75; FFAT." Stability and Control Report, Volume I, January 1968, Aerojet General.
17. Molitz, H. "Perturbation Effects on Rockets." AGARD Conference Proceedings No. 10, pp. 167-180, September 1966.

APPENDIXES
I. ILLUSTRATIONS
II. TABLES

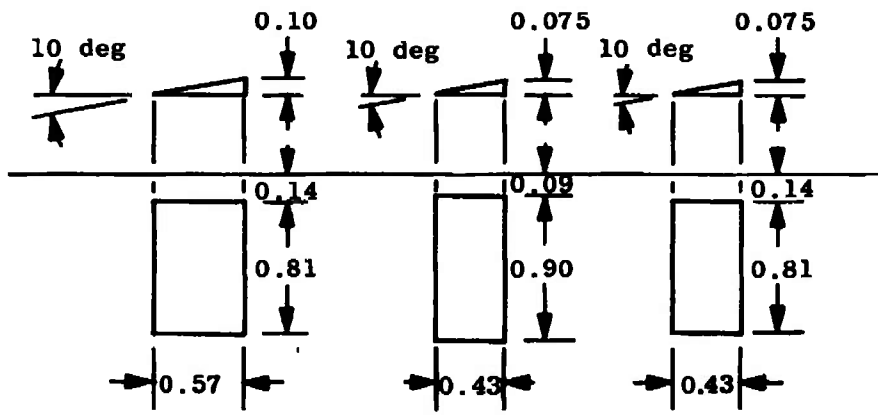


a. Basic Model and Fins
Fig. 1 Phase 1 Model Details

Note: Dimensions on Fin T_4 are the same as on T_1 except where noted.



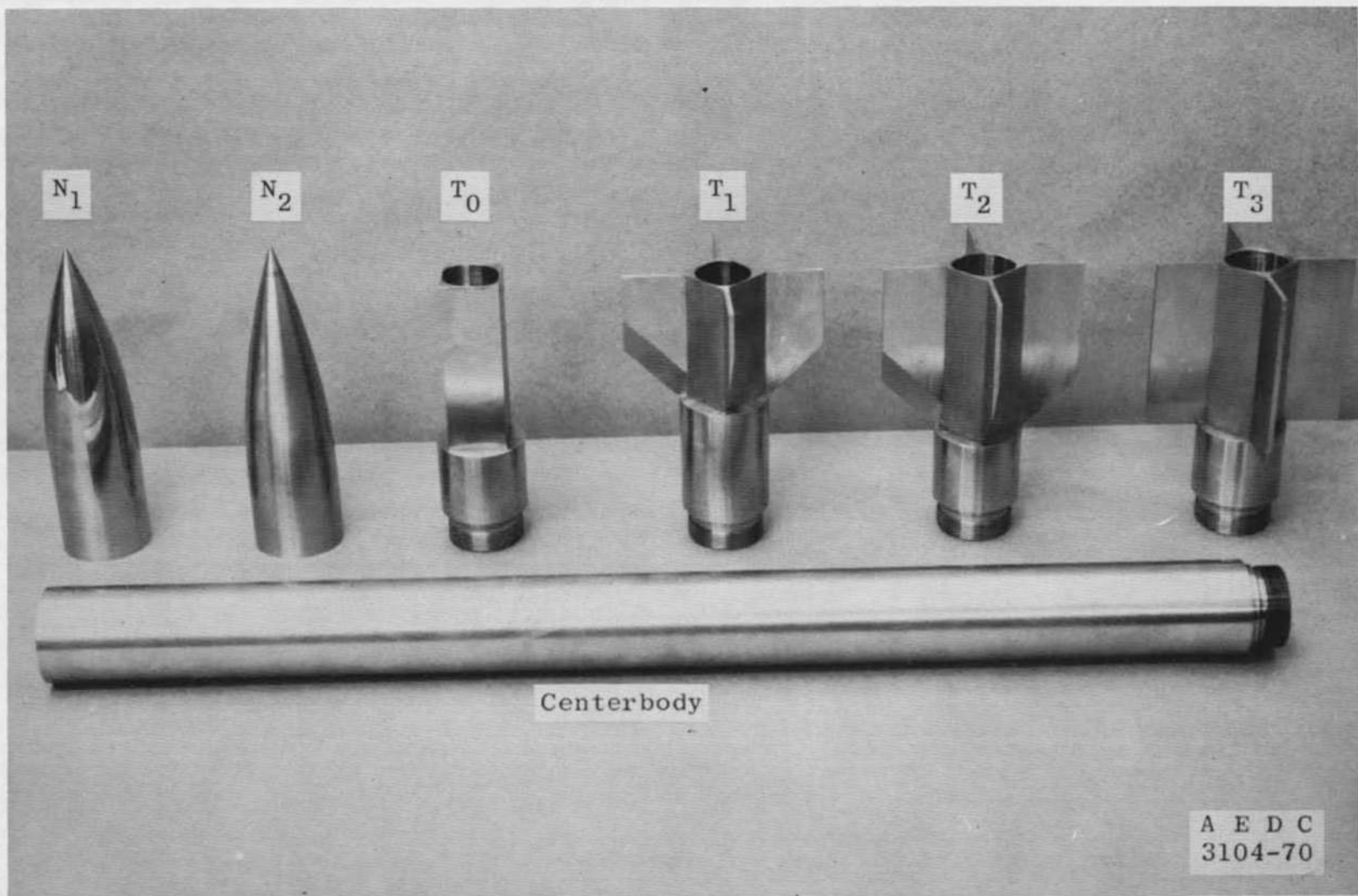
Tail T_4 with Tab B



Tab B Tab C Tab D

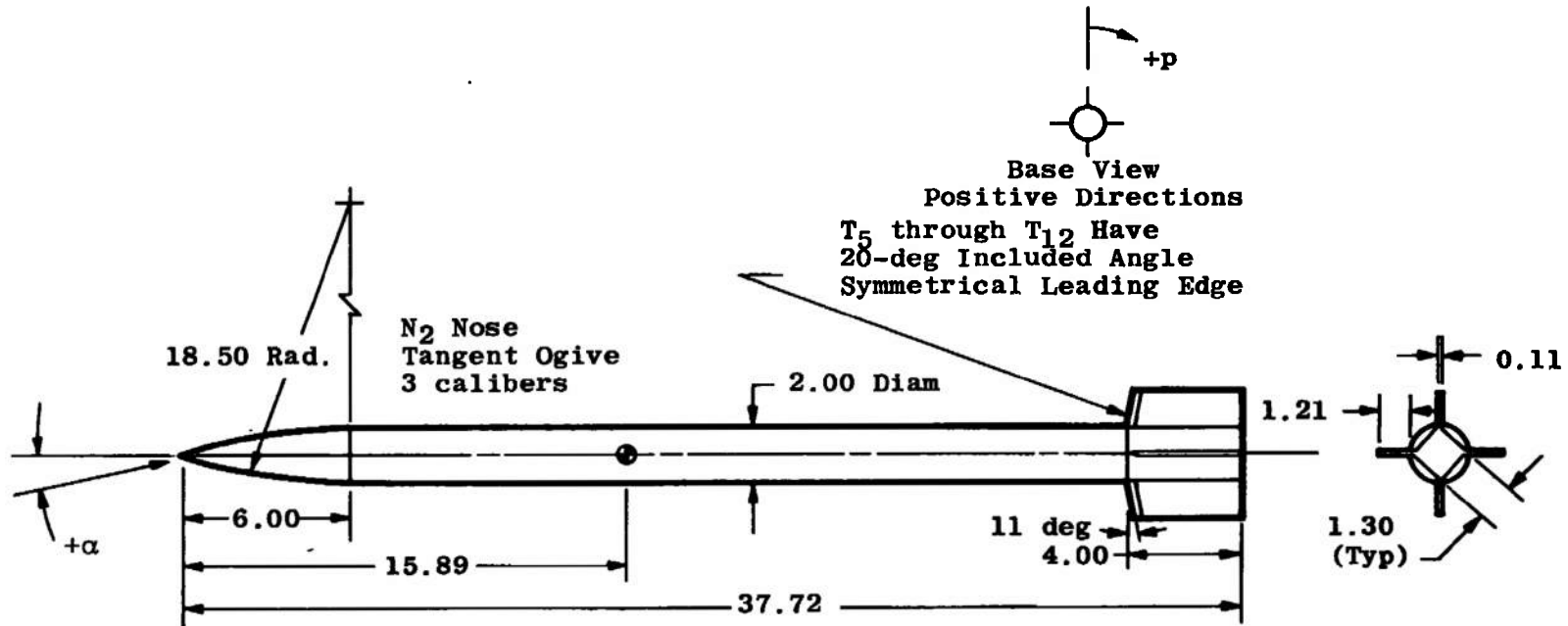
All Dimensions in Inches

b. Modified Fins
Fig. 1 Continued



c. Model Disassembled
Fig. 1 Concluded

28



Moment Reference

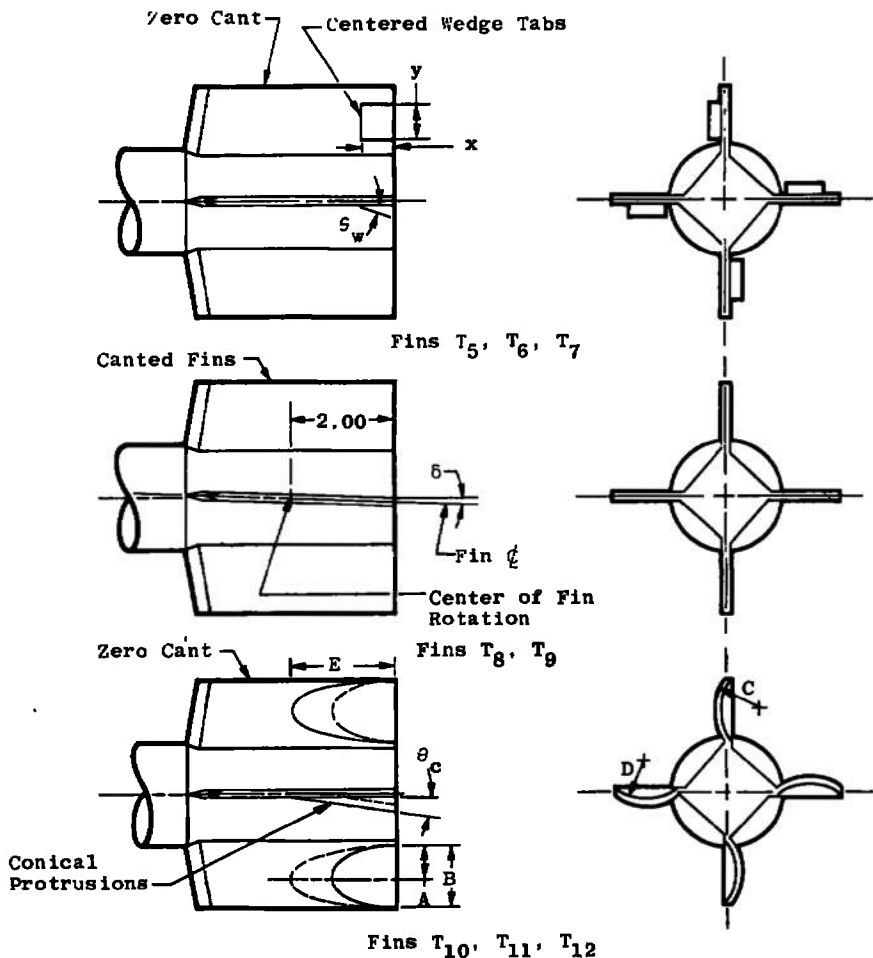
Reference Area = 3.1416 sq in.

Reference Length = 2.00 in.

All Dimensions in Inches

a. Basic Configuration

Fig. 2 Phase 2 Model Details



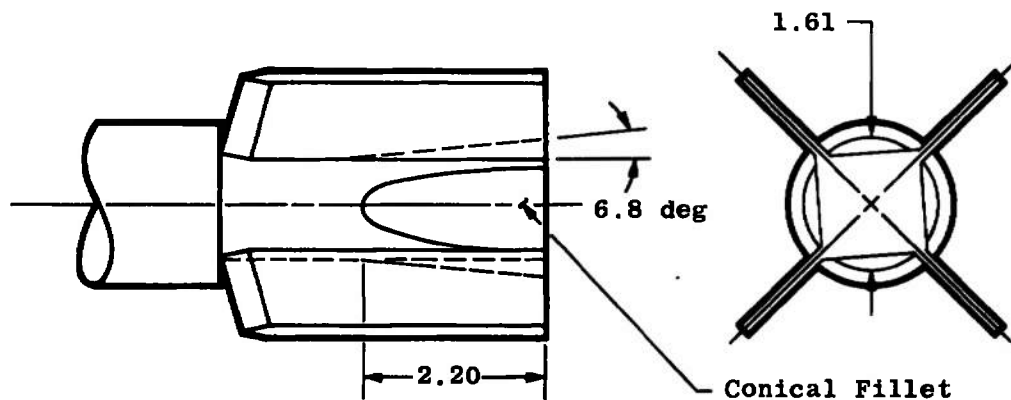
All Dimensions in Inches

Fins	δ , deg	θ_w , deg	x, in.	y, in.
T ₅ *	0	6	0.6	0.97
T ₆	0	10	0.6	0.60
T ₇	0	10	0.6	0.97
T ₈	1.0	0	0	0
T ₉	0.5	0	0	0

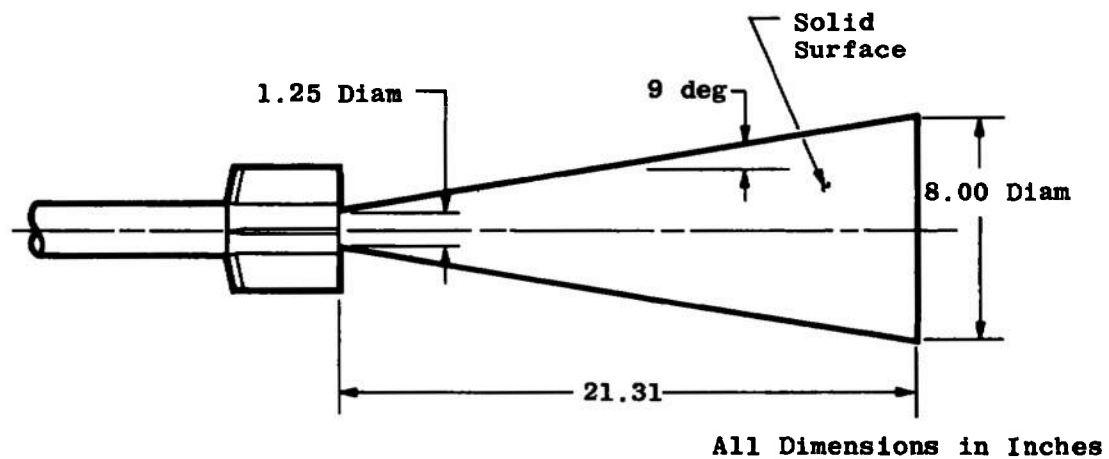
*Another fin designated T_{5A} has the same dimensions as T₅ except the tab was made by bending out the fin leaving a void behind the tab, thus simulating a possible production piece.

Fins	A, in.	B, in.	C, in.	D, in.	E, in.	θ_c' , deg
T ₁₀	0.60	1.21	0.90	0.81	2.00	6.7
T ₁₁	0.60	1.21	0.90	0.81	1.00	13.2
T ₁₂	0.36	0.73	0.40	0.31	0.85	15.5

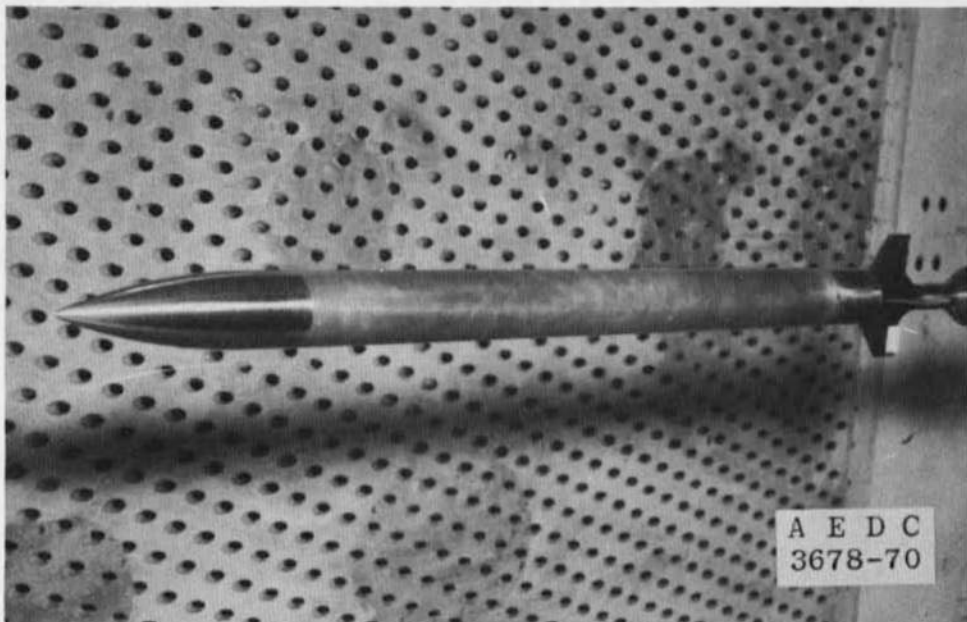
b. Fin Geometry
Fig. 2 Continued



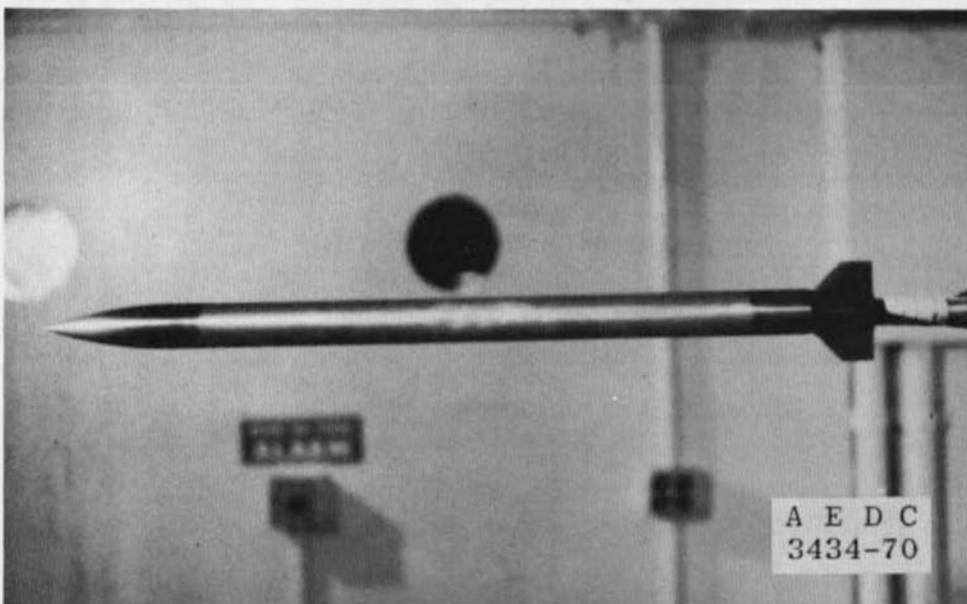
c. Rocket Nozzle Simulation



d. Plume Simulation
Fig. 2 Concluded



a. Phase 1 Model Installed in Tunnel 4T



b. Phase 1 Model Installed in Tunnel A
Fig. 3 Model Photographs

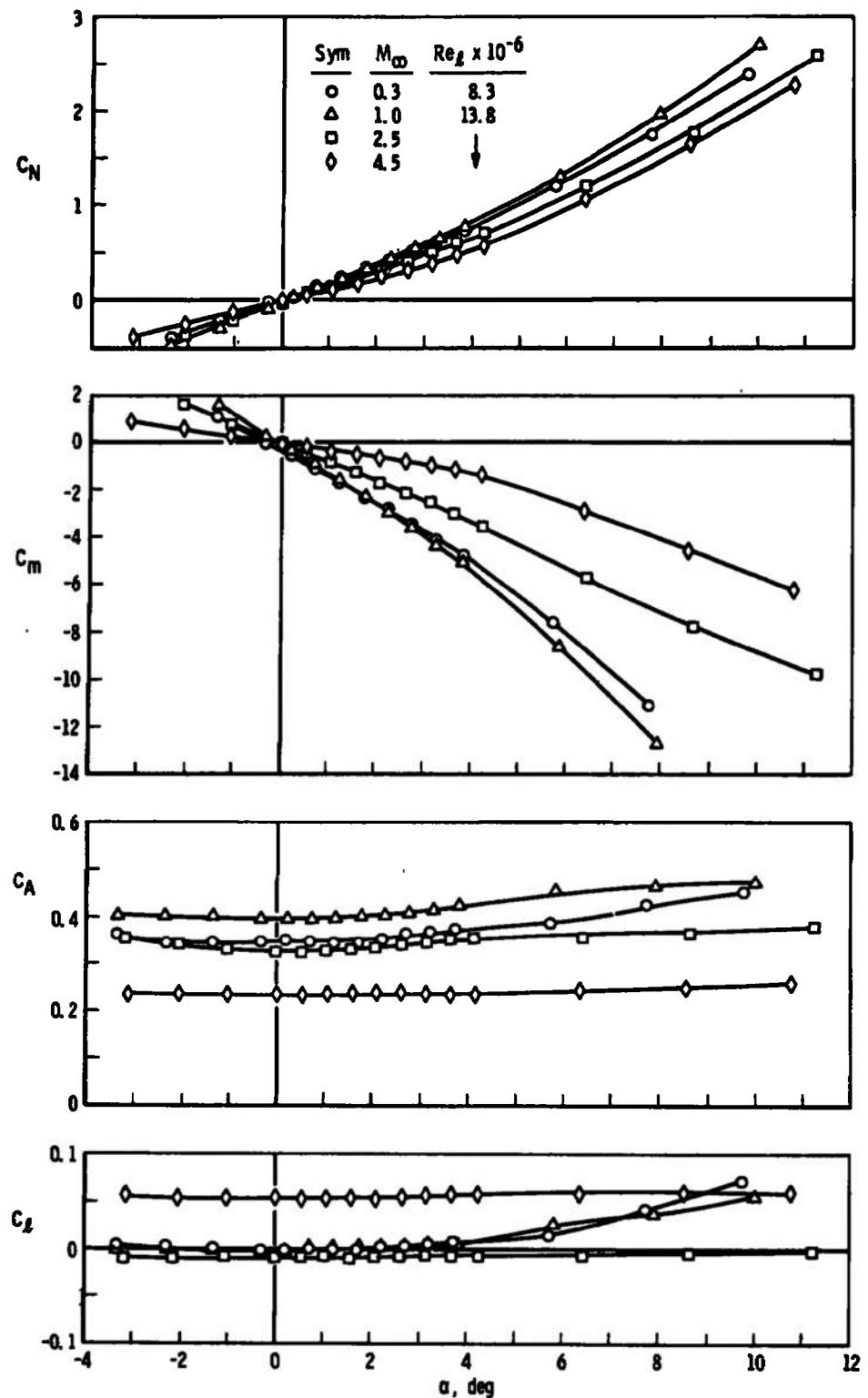
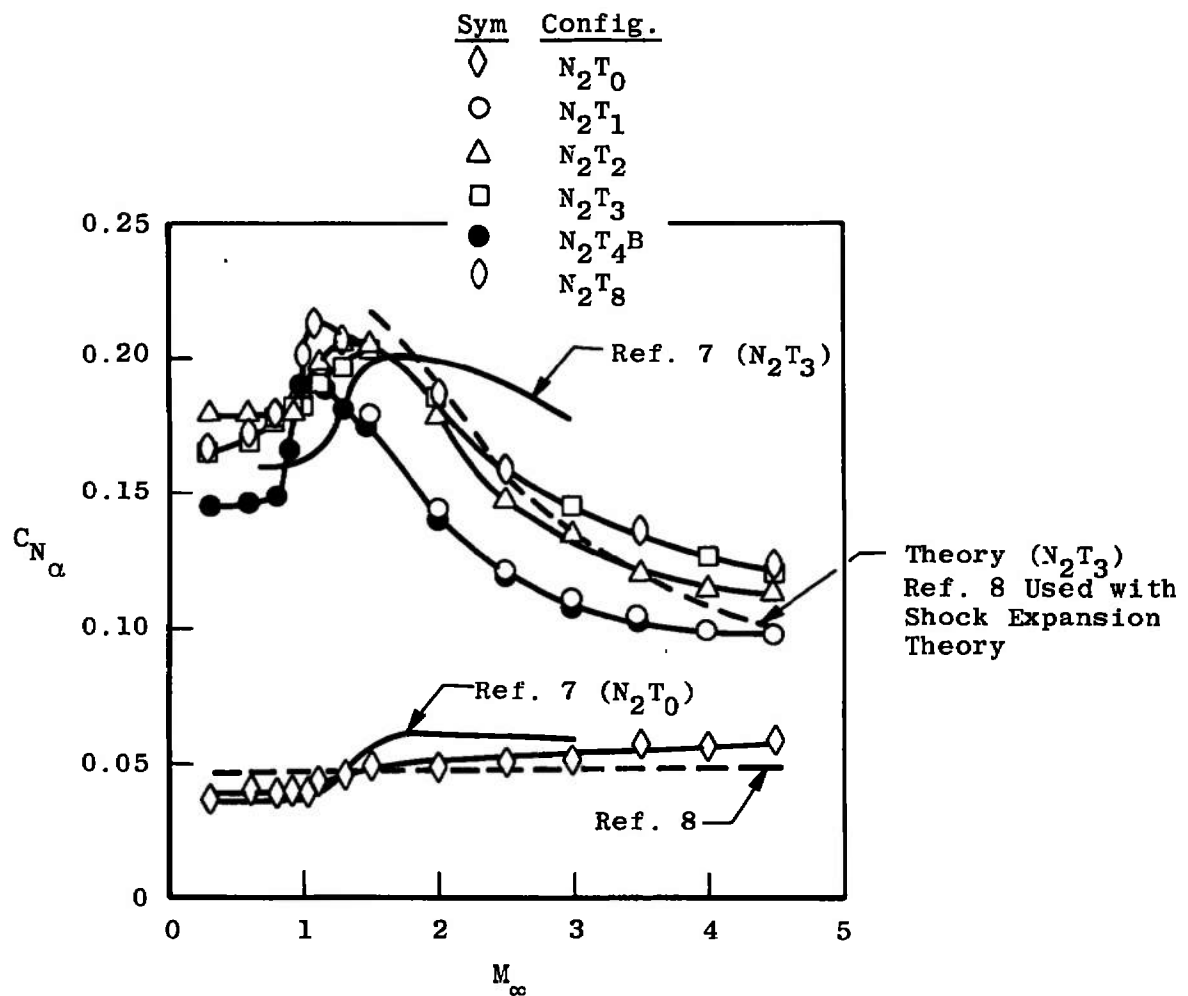
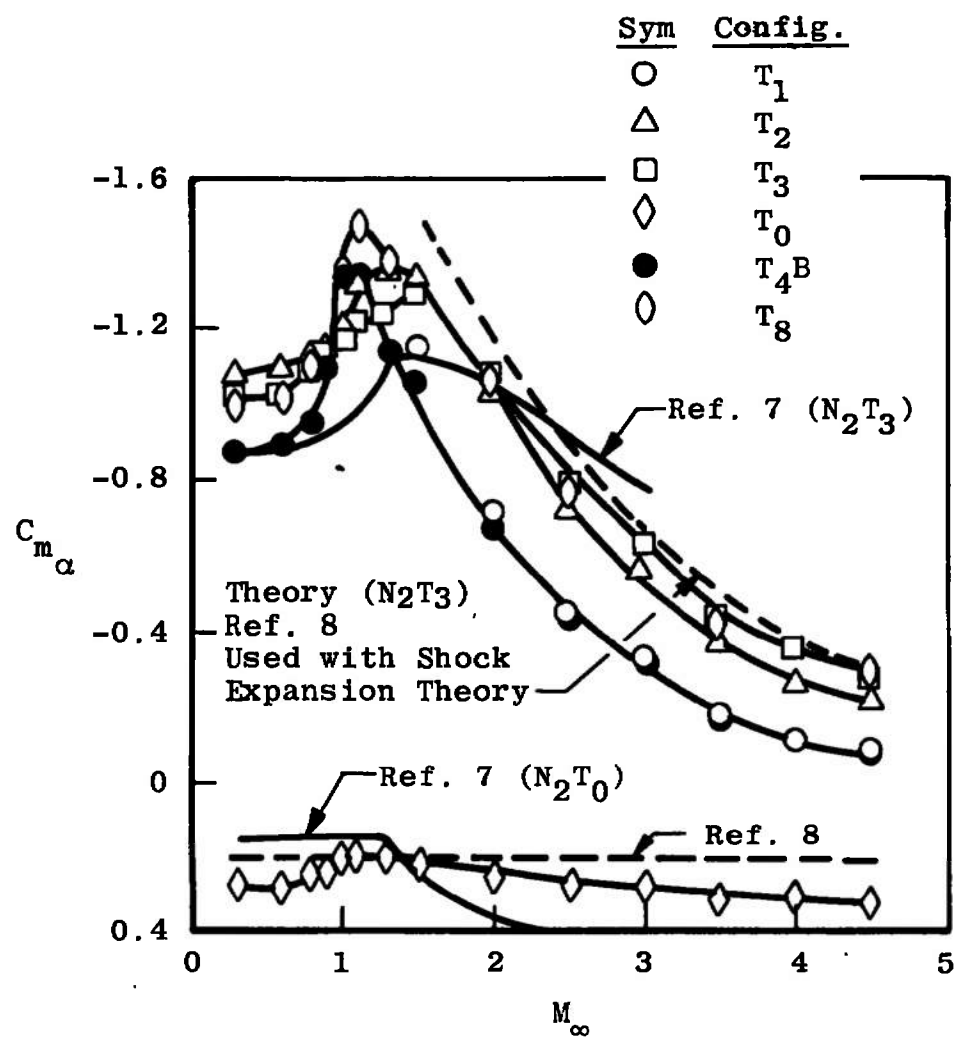


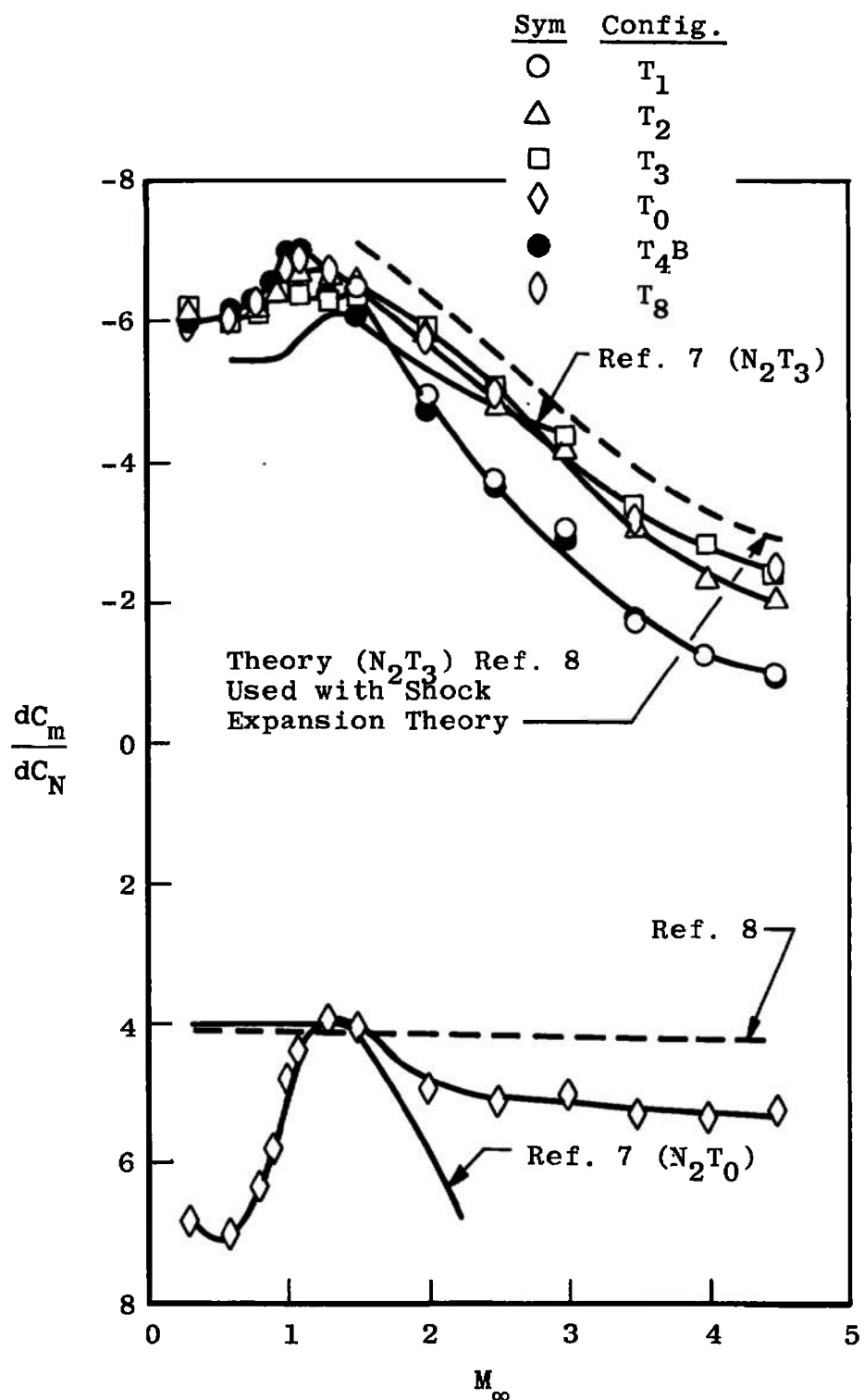
Fig. 4 Typical Variation of the Static Stability, Roll, and Axial-Force Coefficients with Angle of Attack, Configuration N₂ T₃



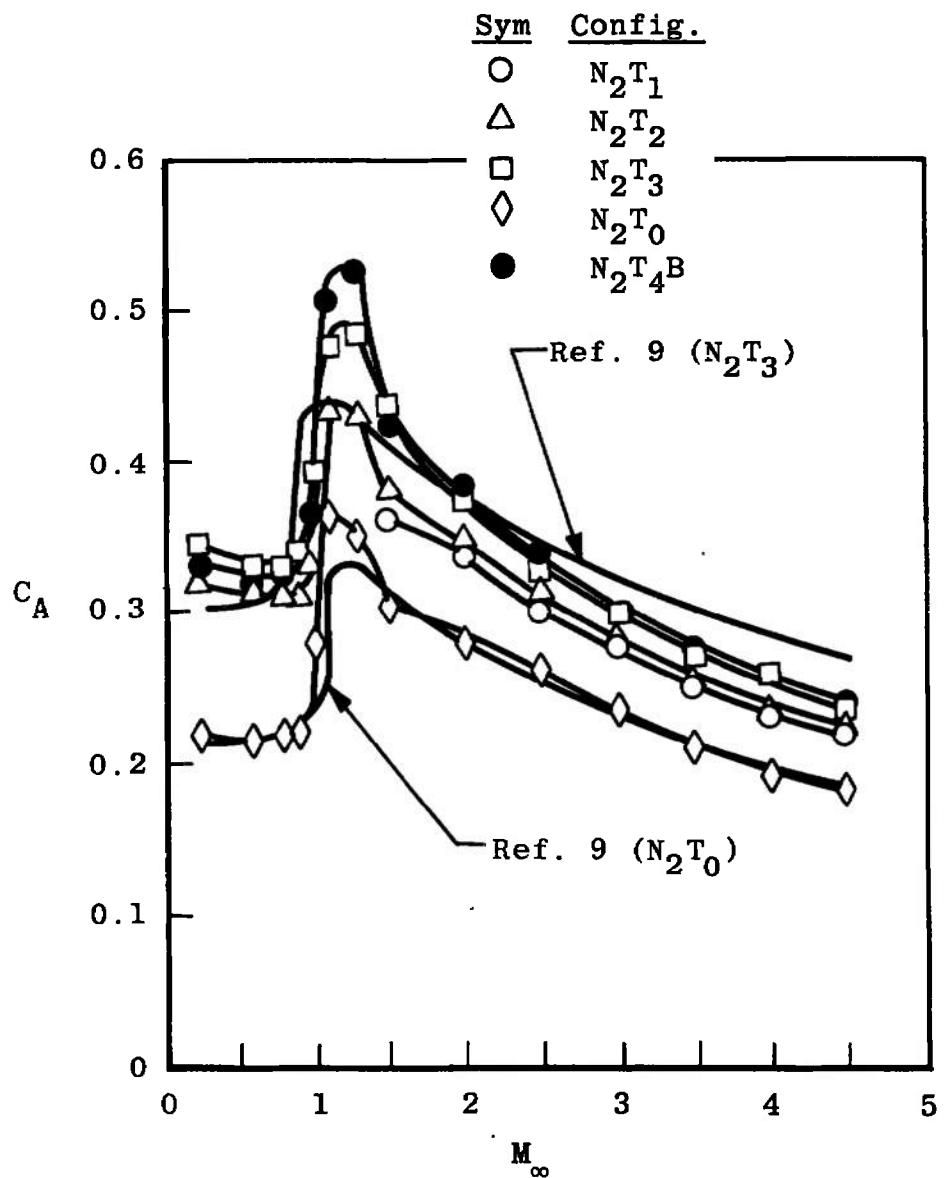
a. $C_{N\alpha}$ versus M_∞
**Fig. 5 Effect of Fin Configuration on the Stability Derivatives,
 Static Margin, and Axial Force at $\alpha = 0$**



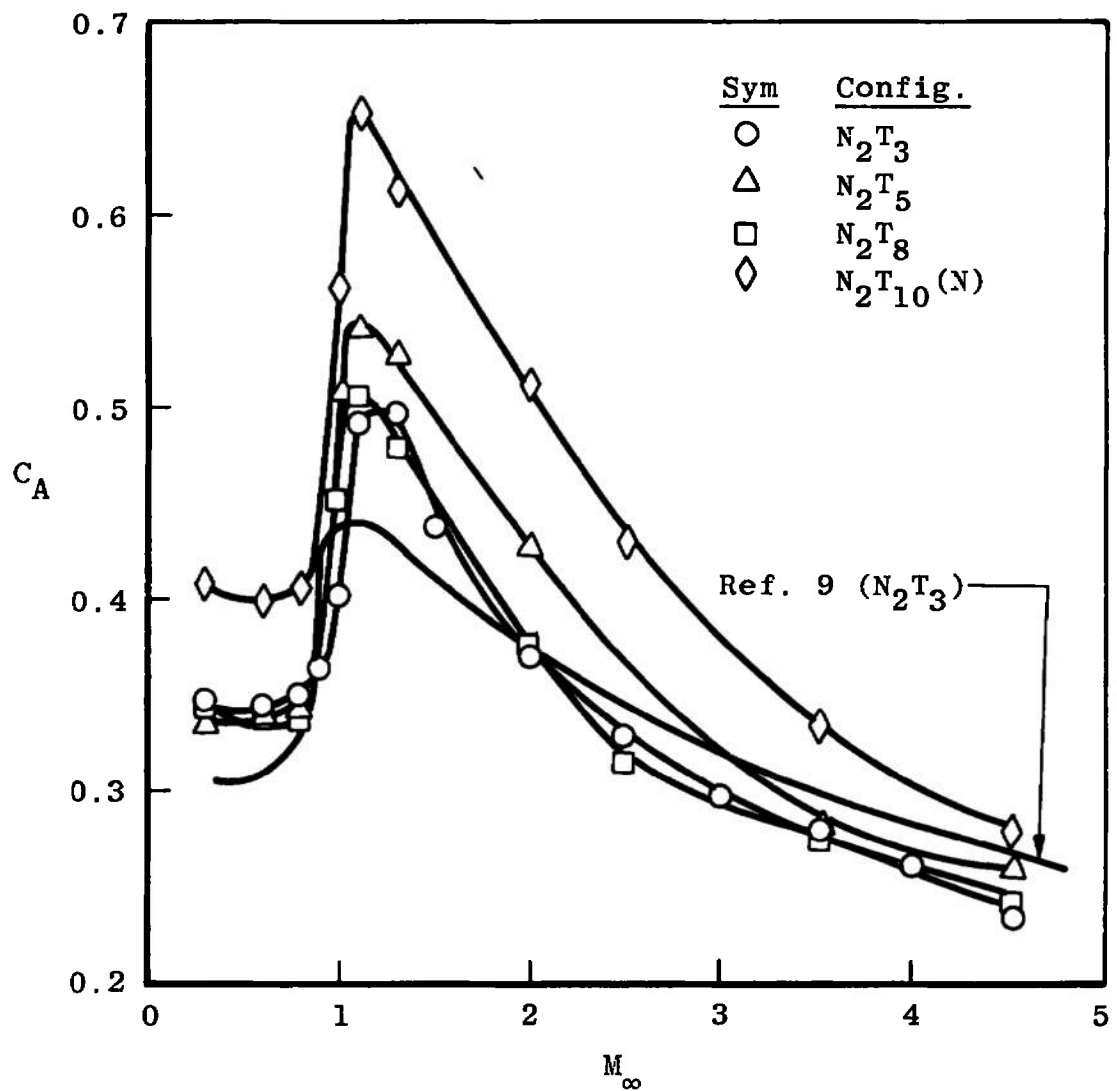
b. $C_{m\alpha}$ versus M_∞
 Fig. 5 Continued



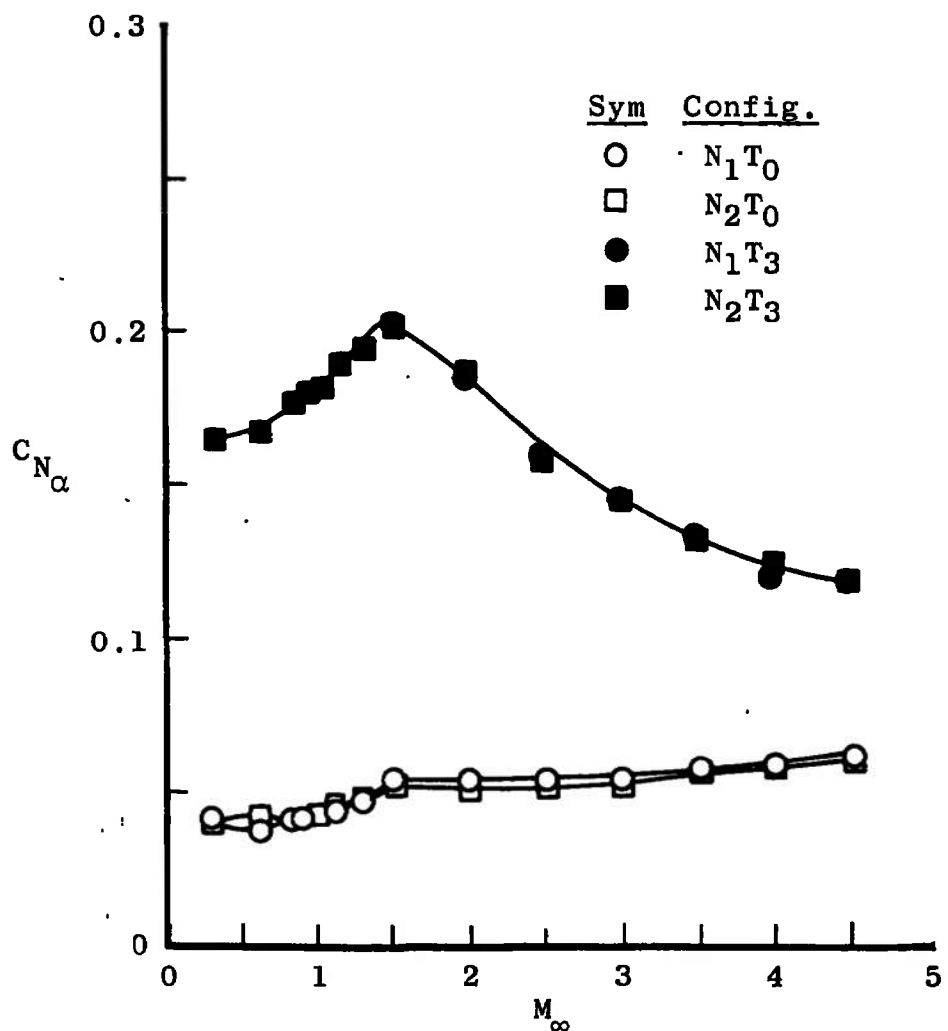
c. dC_m/dC_N versus M_∞
Fig. 5 Continued



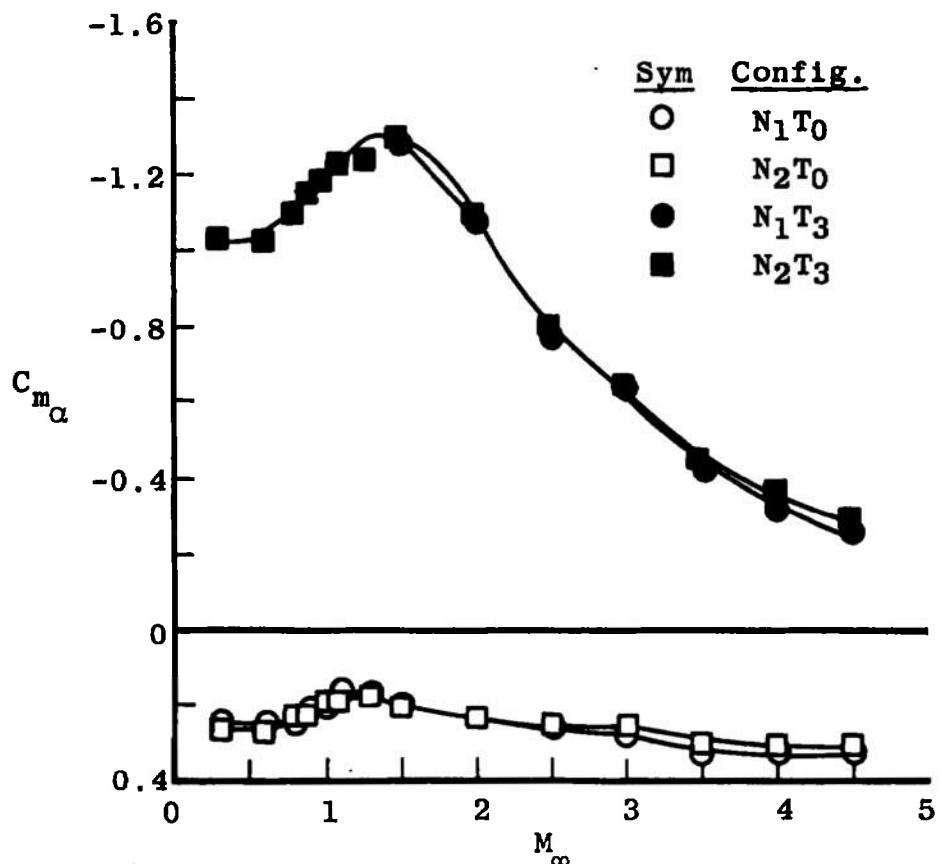
d. C_A versus M_∞ (Phase 1 Fins)
 Fig. 5 Continued



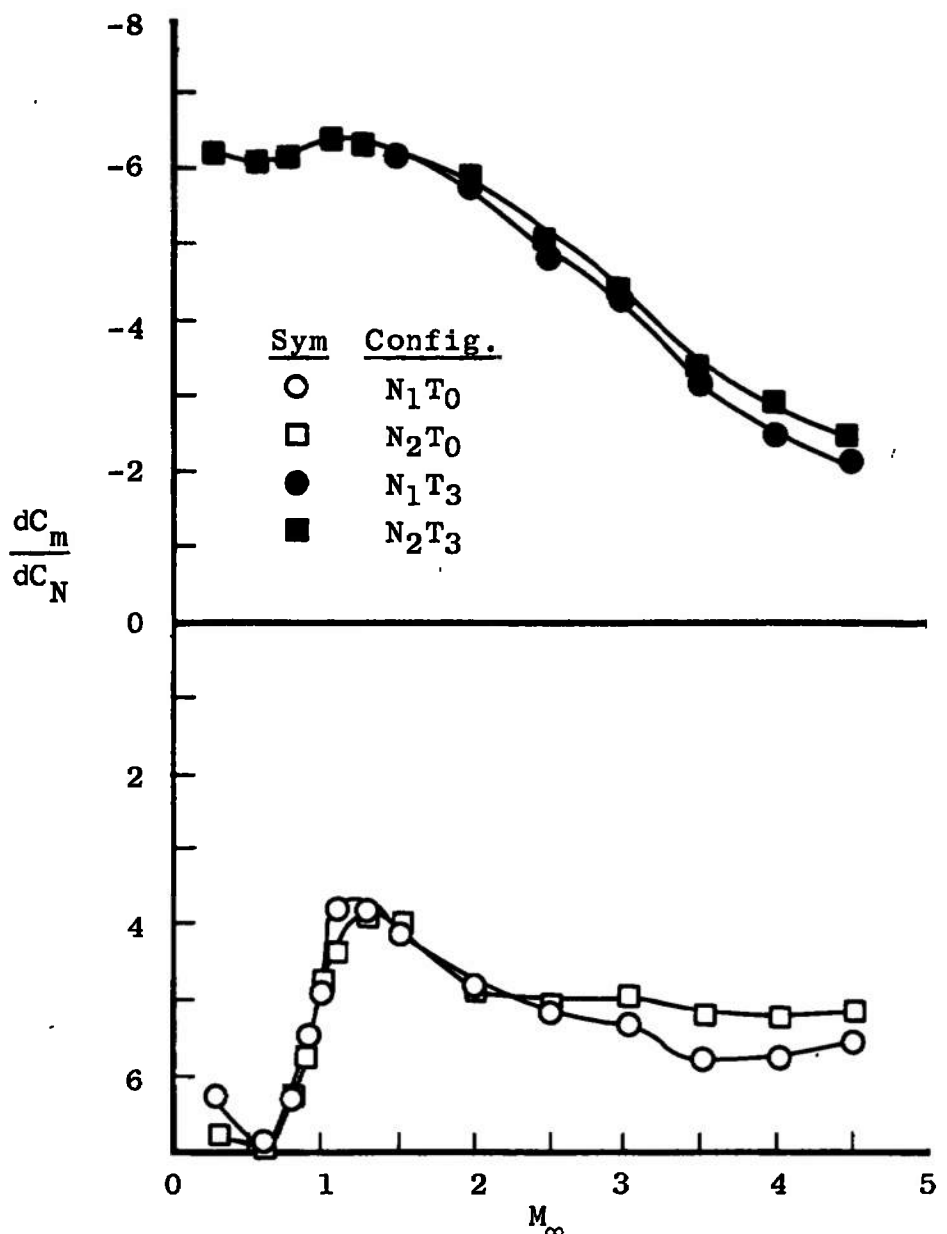
e. C_A versus M_∞ (T_3 and Phase 2 Fins)
 Fig. 5 Concluded



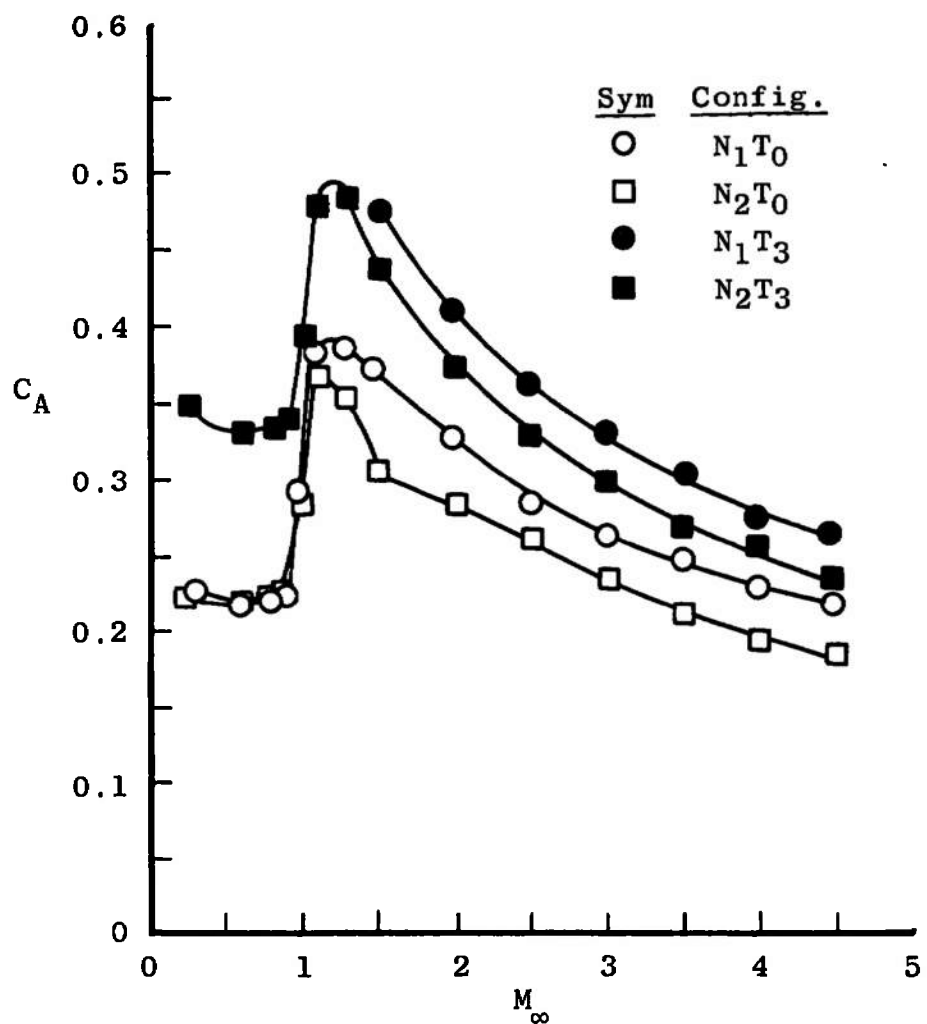
a. $C_{N\alpha}$ versus M_∞
Fig. 6 Effect of Nose Configuration on the Stability Derivatives, Static Margin, and Axial Force at $\alpha = 0$



b. C_{m_a} versus M_{∞}
Fig. 6 Continued



c. $\frac{dC_m}{dC_N}$ versus M_∞
Fig. 6 Continued



d. C_A versus M_∞
Fig. 6 Concluded

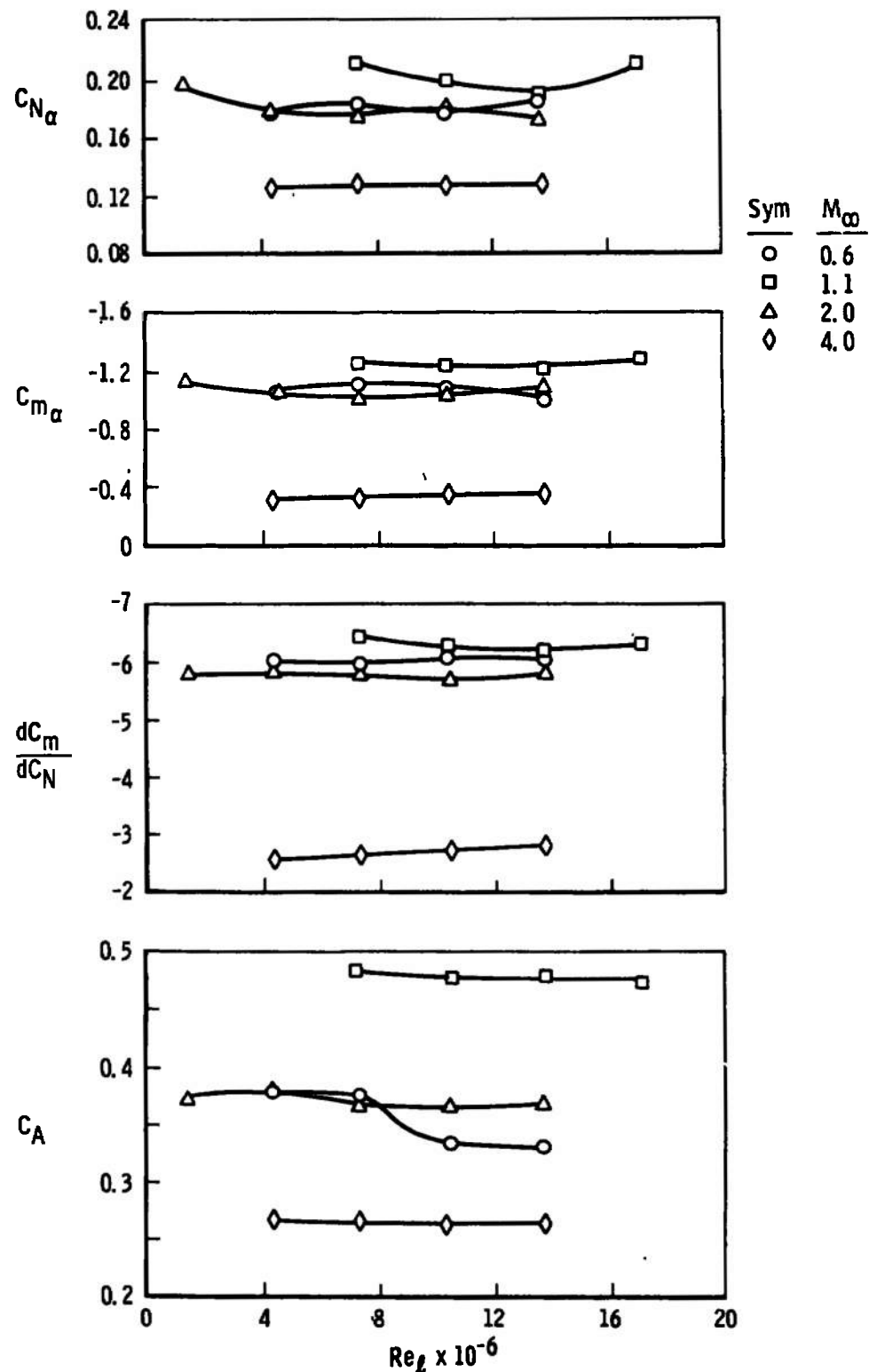


Fig. 7 Variation of the Stability Derivatives, Static Margin, and Axial Force with Reynolds Number at $\alpha = 0$, Configuration N₂T₃

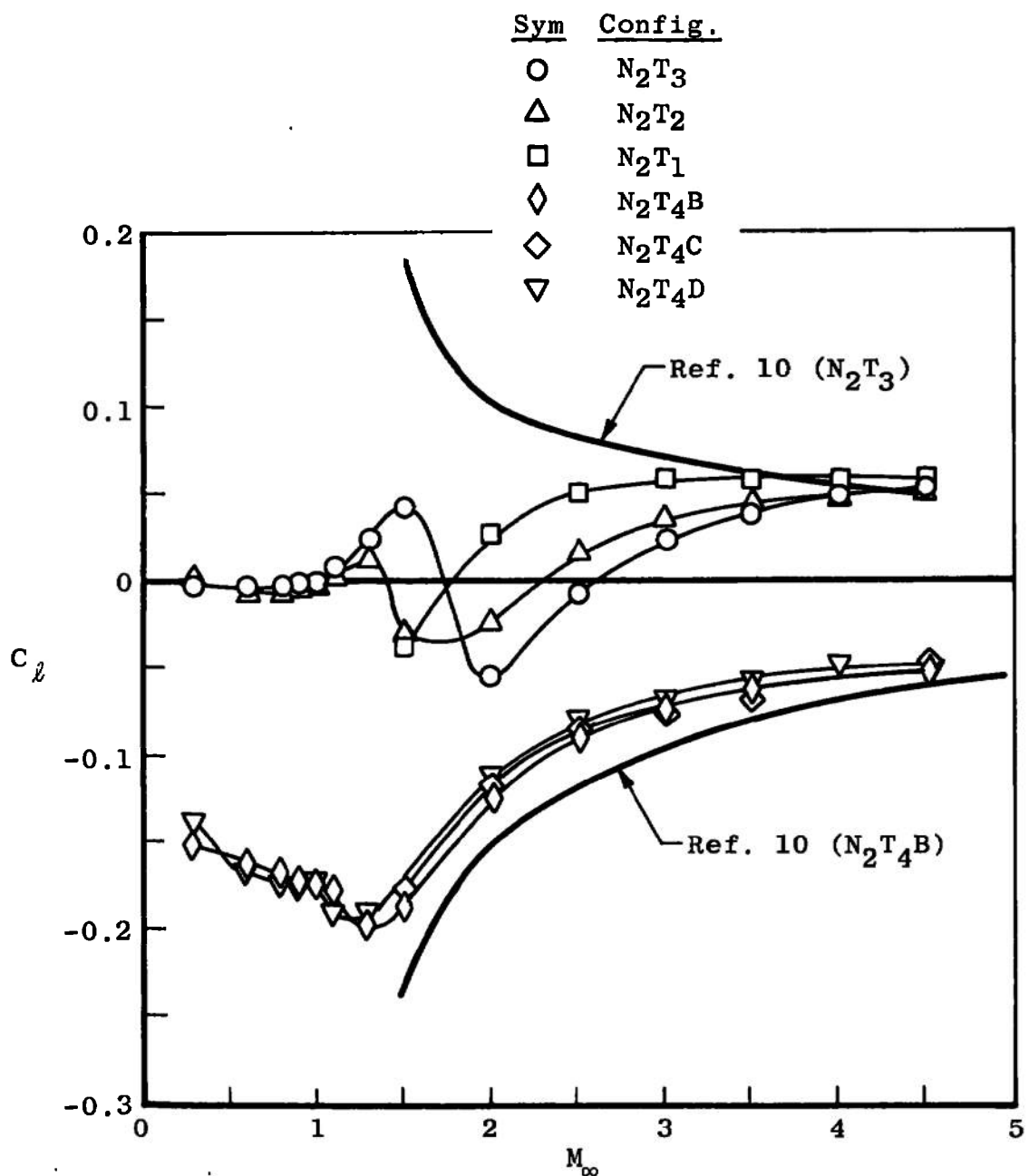


Fig. 8 Variation of the Roll-Moment Coefficient with Fin Configuration at $\alpha = 0$, Phase 1 Fins

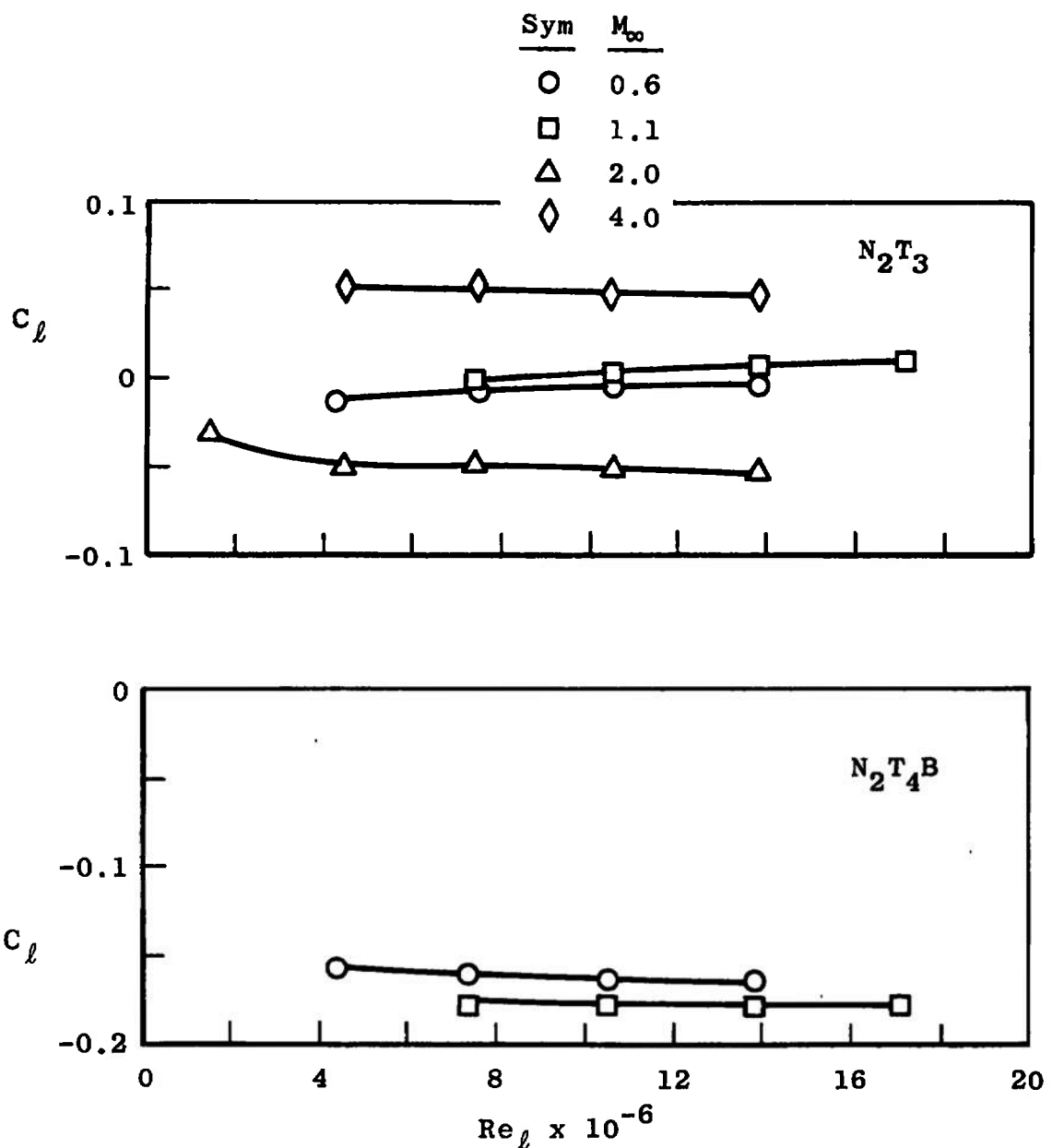


Fig. 9 Variation of the Roll-Moment Coefficient with Reynolds Number
at $\alpha = 0$

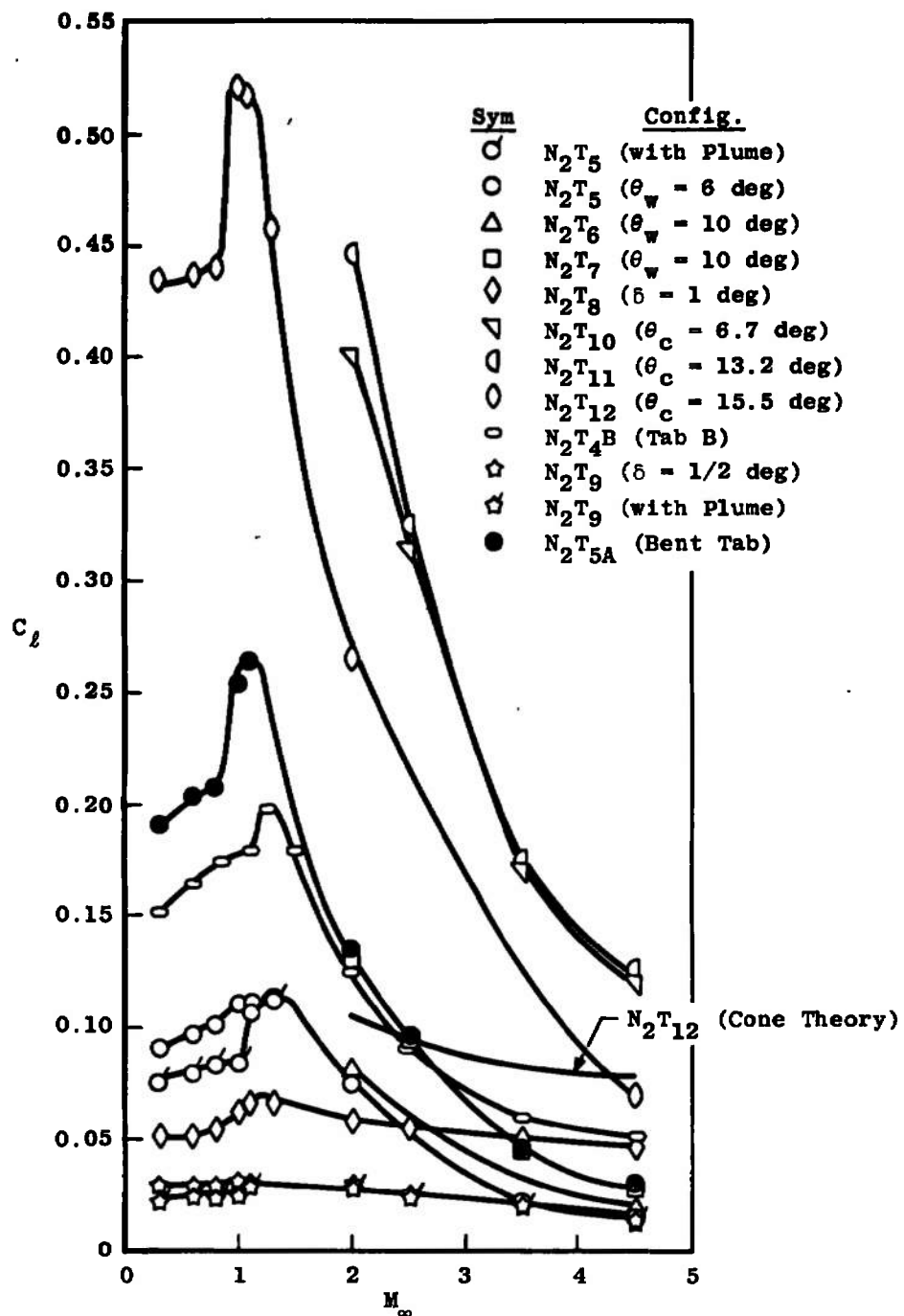
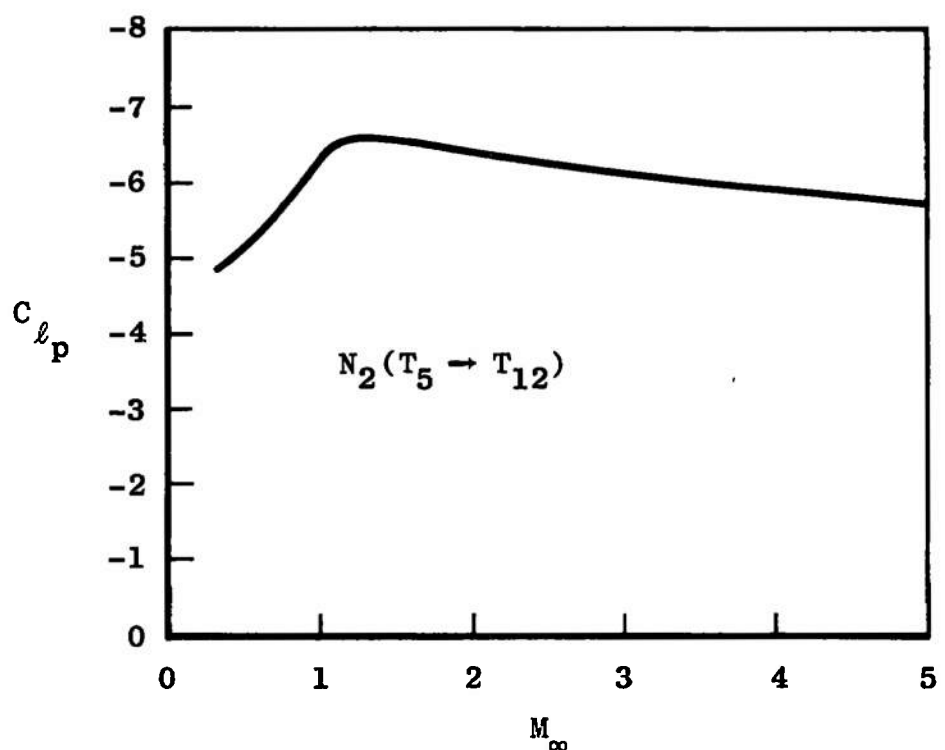
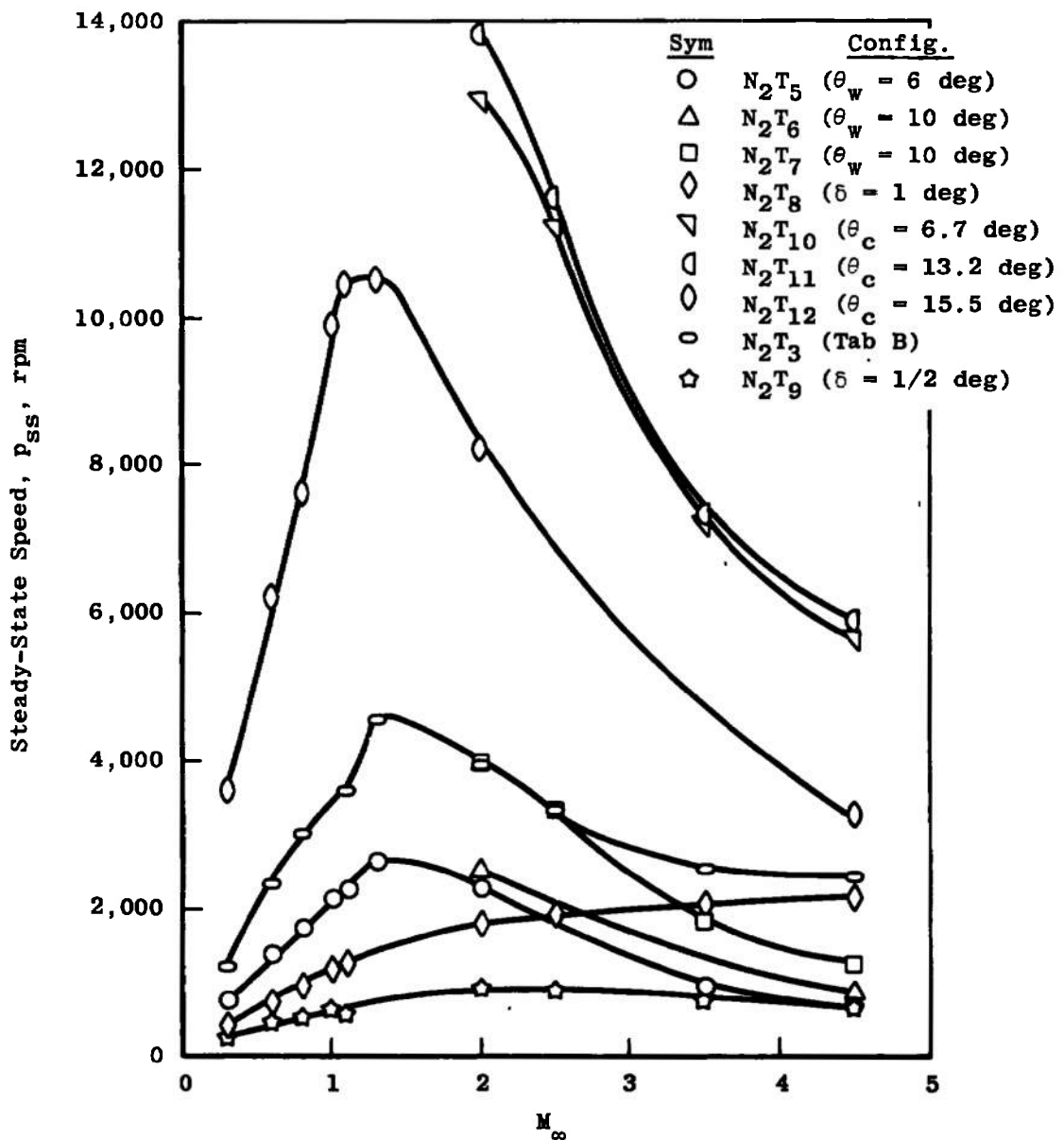
a. C_l versus M_∞

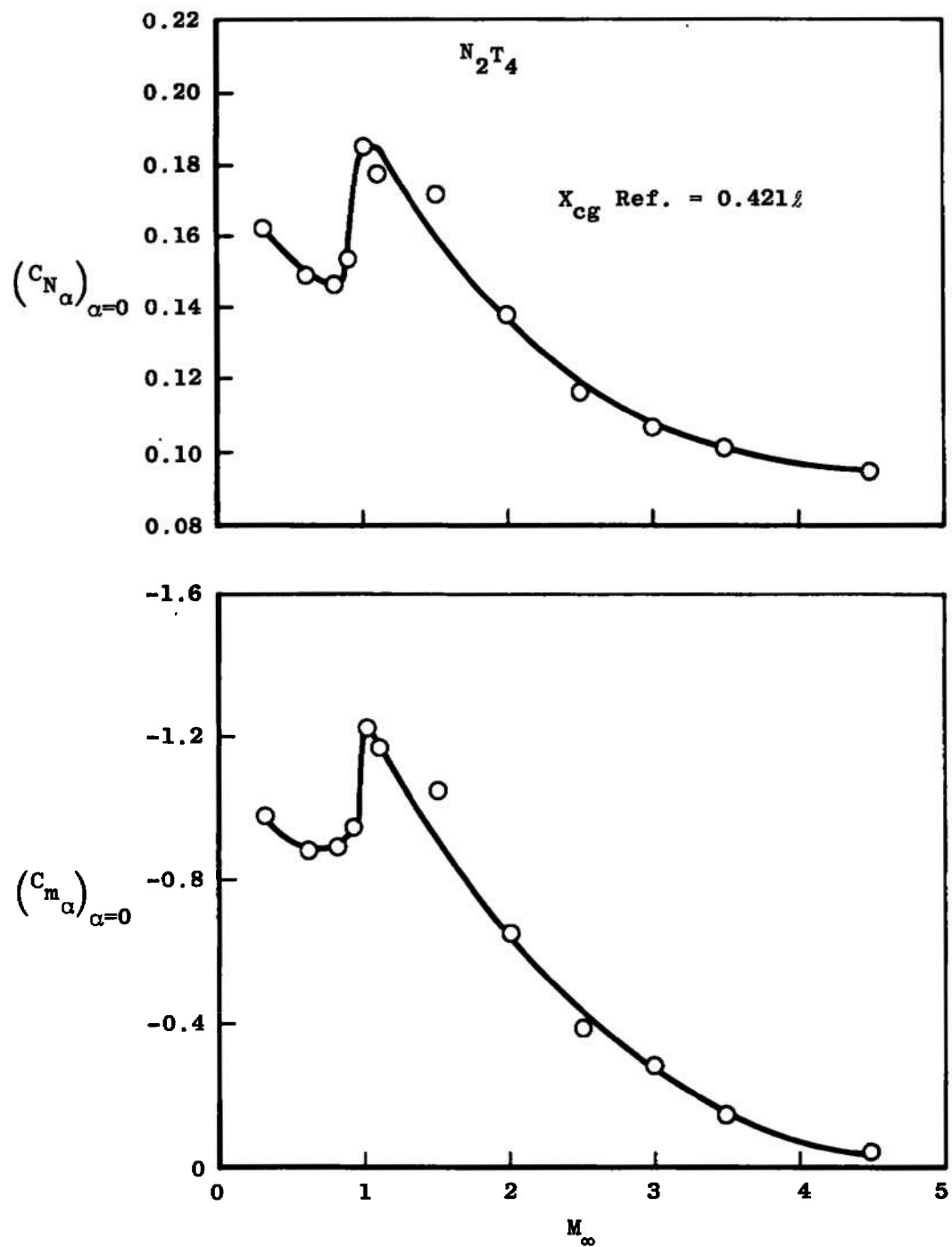
Fig. 10 Variation of the Roll-Moment Coefficient at $\alpha = 0$ with Fin Configuration



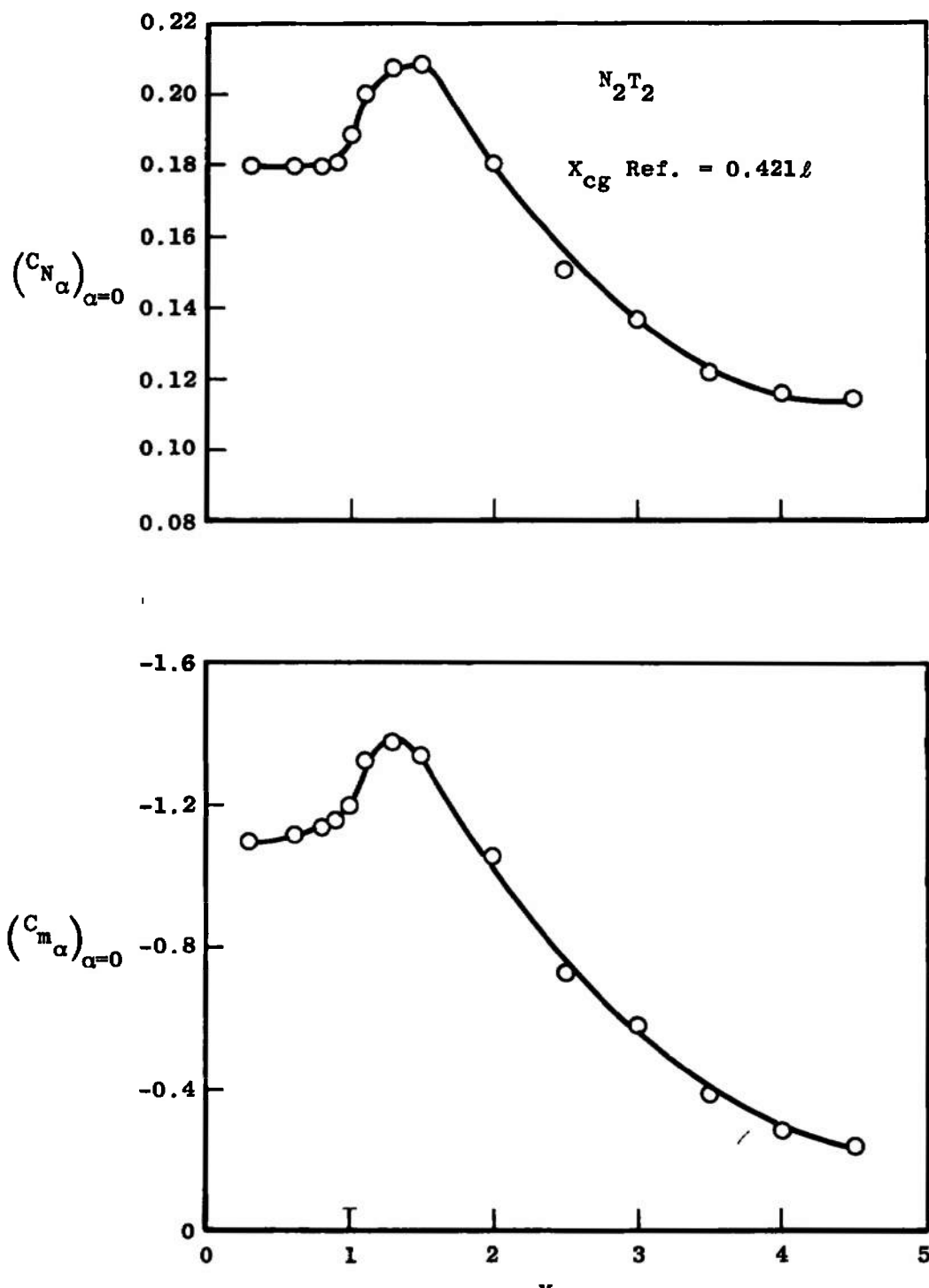
a. C_{l_p} versus M_∞
Fig. 10 Continued



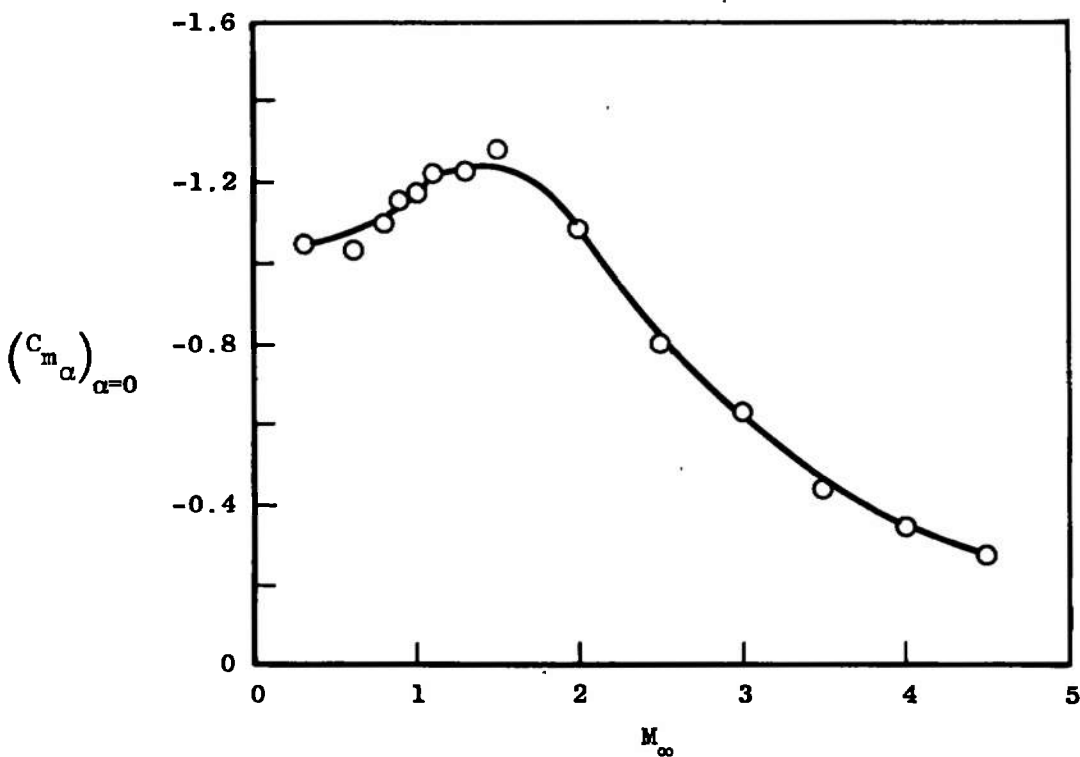
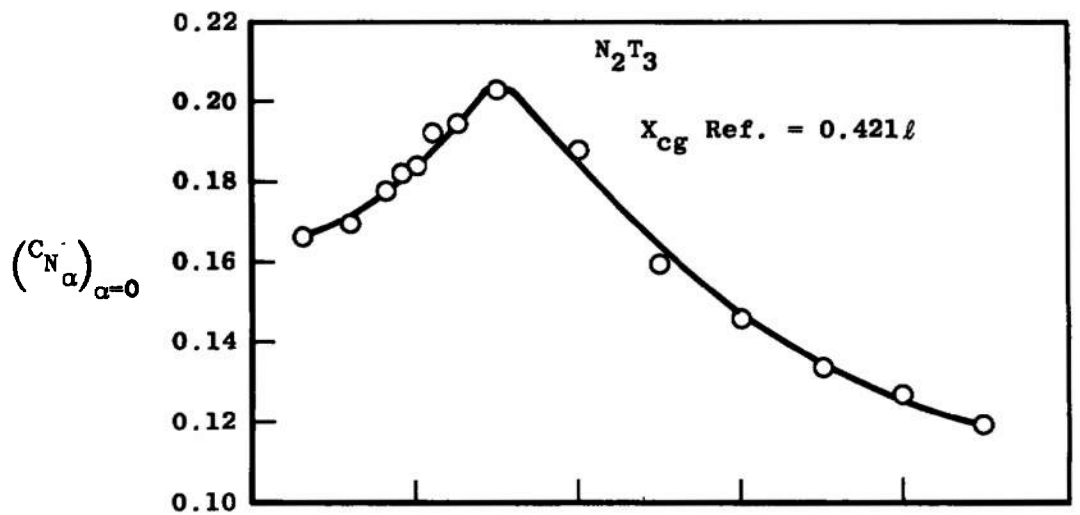
c. p_{ss} versus M_∞
Fig. 10 Concluded



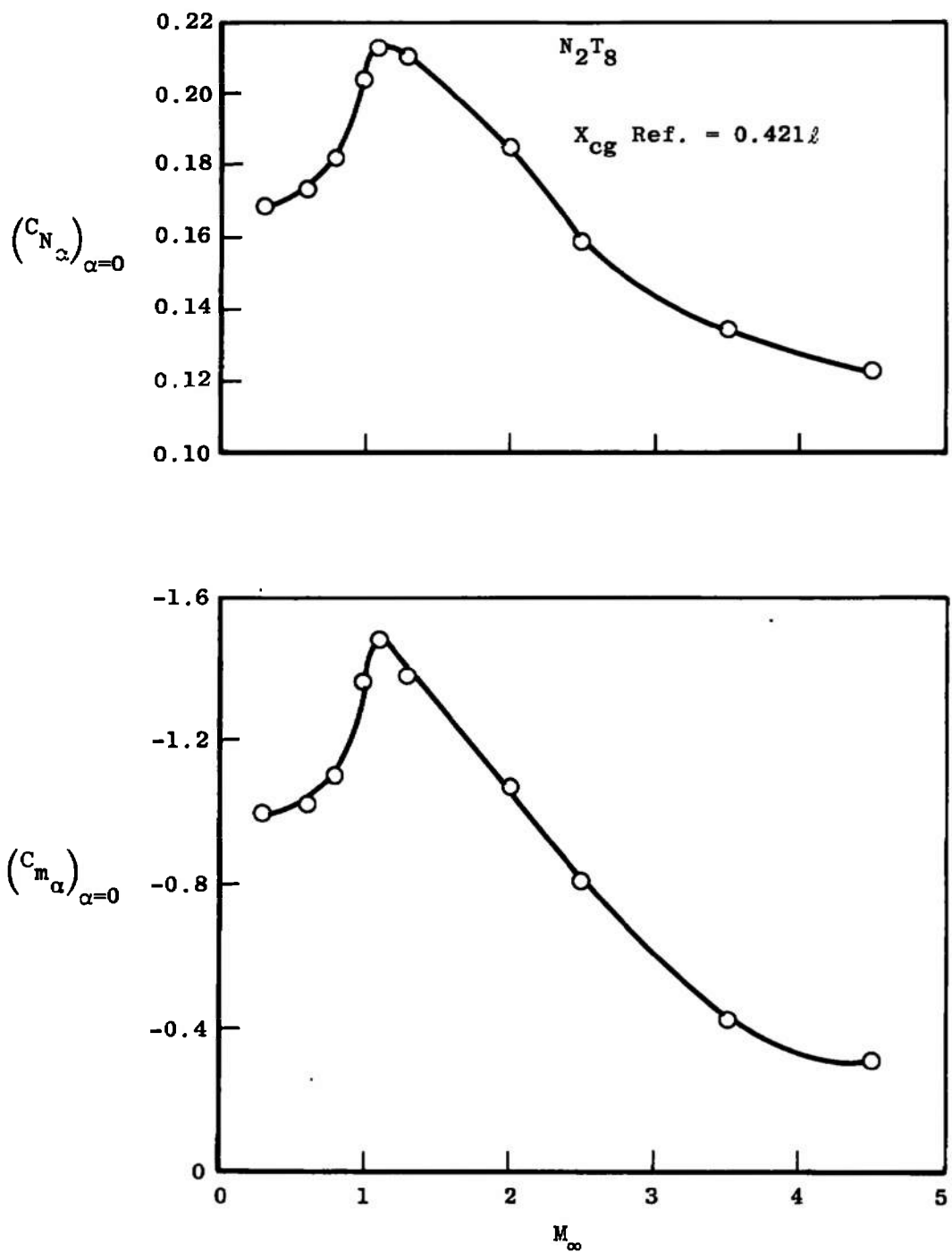
a. $N_2 T_4$
Fig. 11 $C_{N_{\alpha}}$ and $C_{m_{\alpha}}$ versus M_{∞}



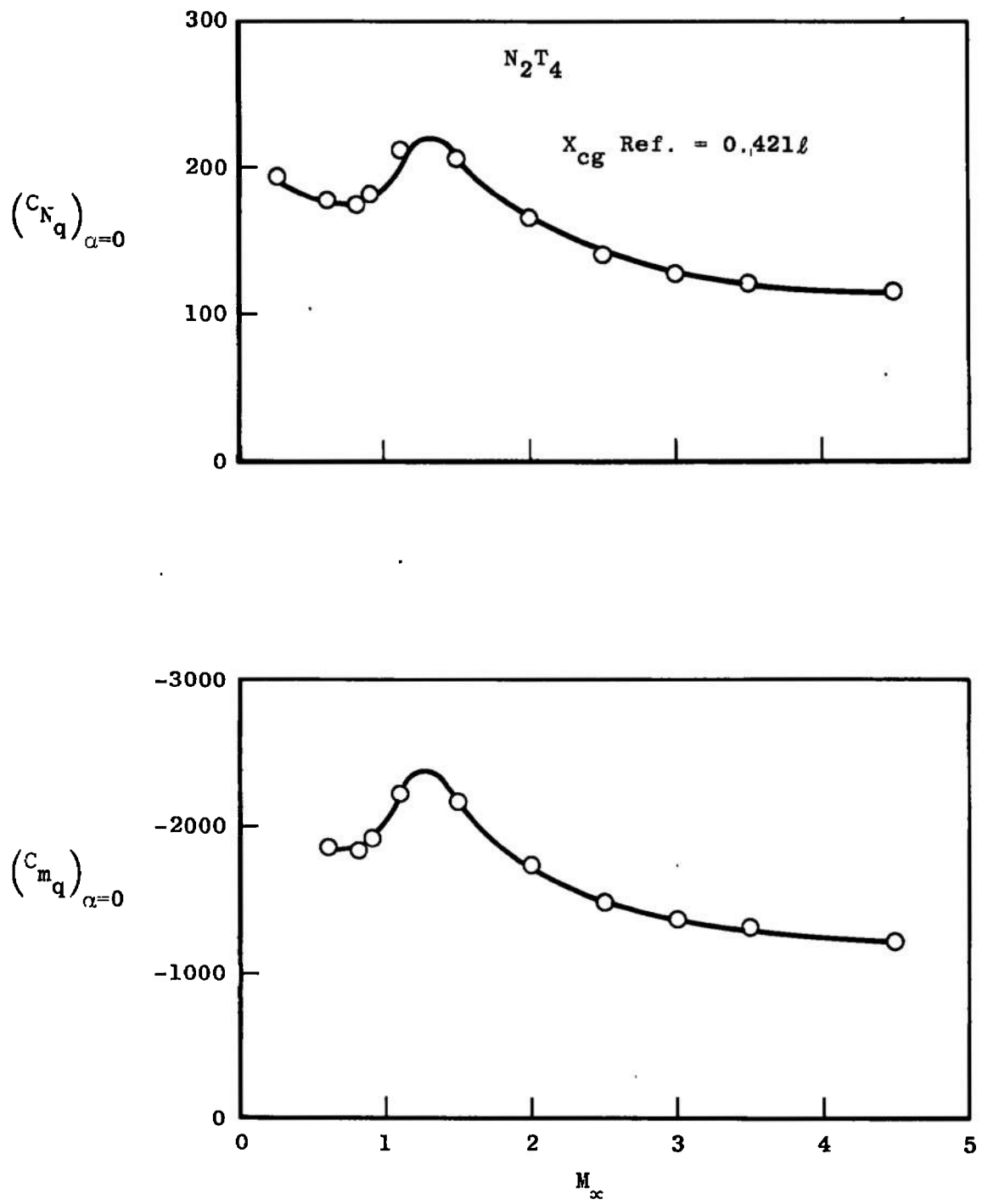
b. $N_2 T_2$
Fig. 11 Continued



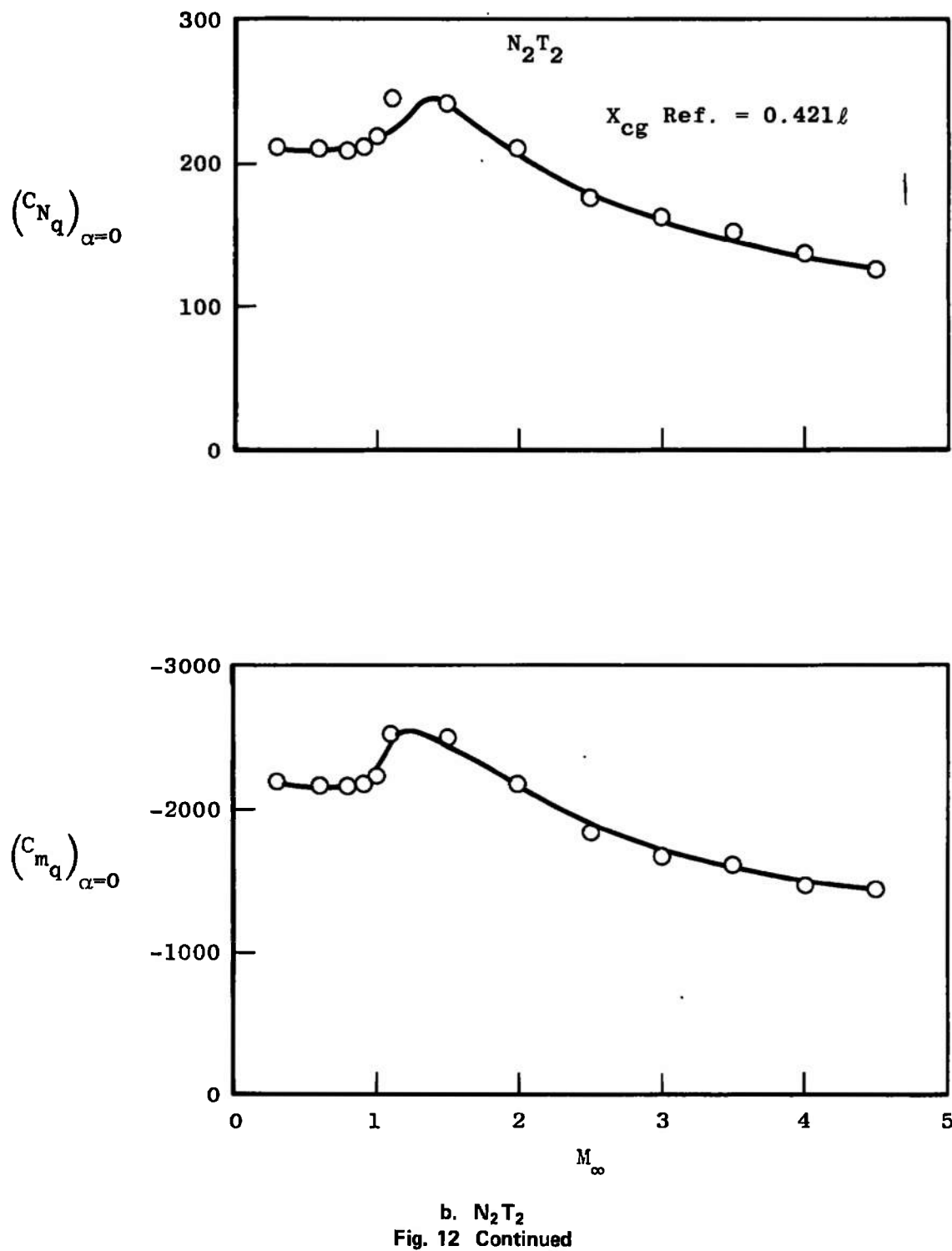
c. N_2T_3
Fig. 11 Continued

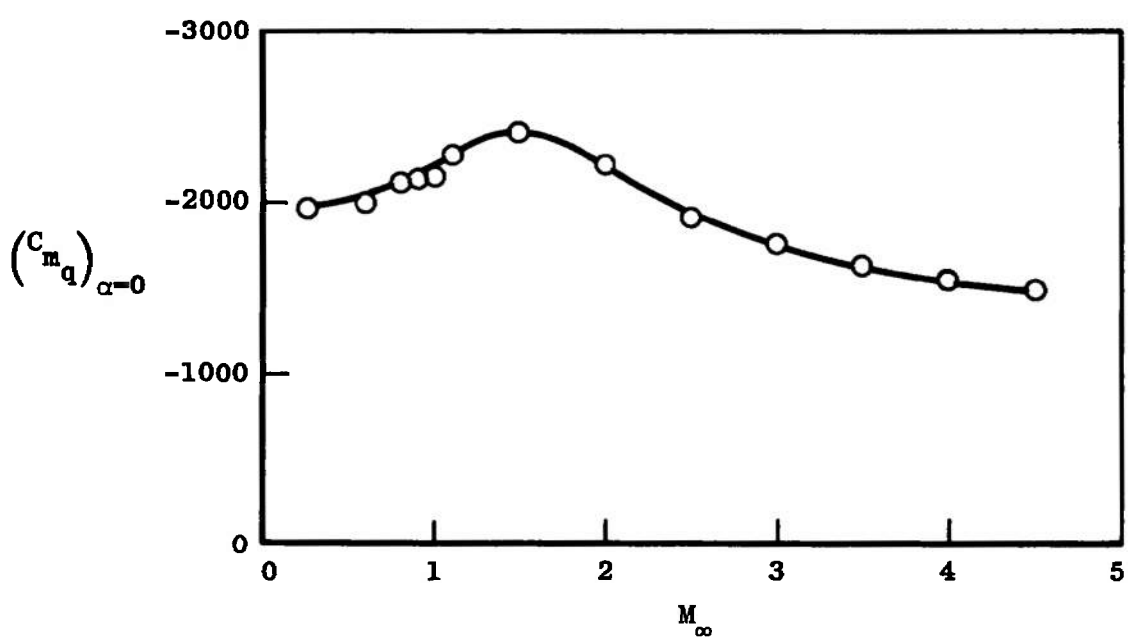
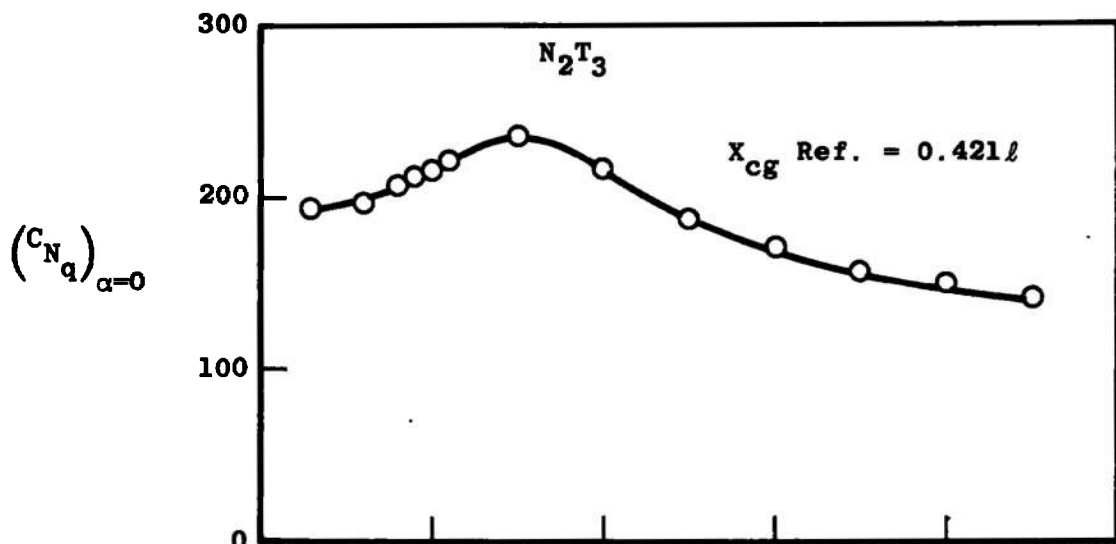


d. $N_2 T_8$
Fig. 11 Concluded

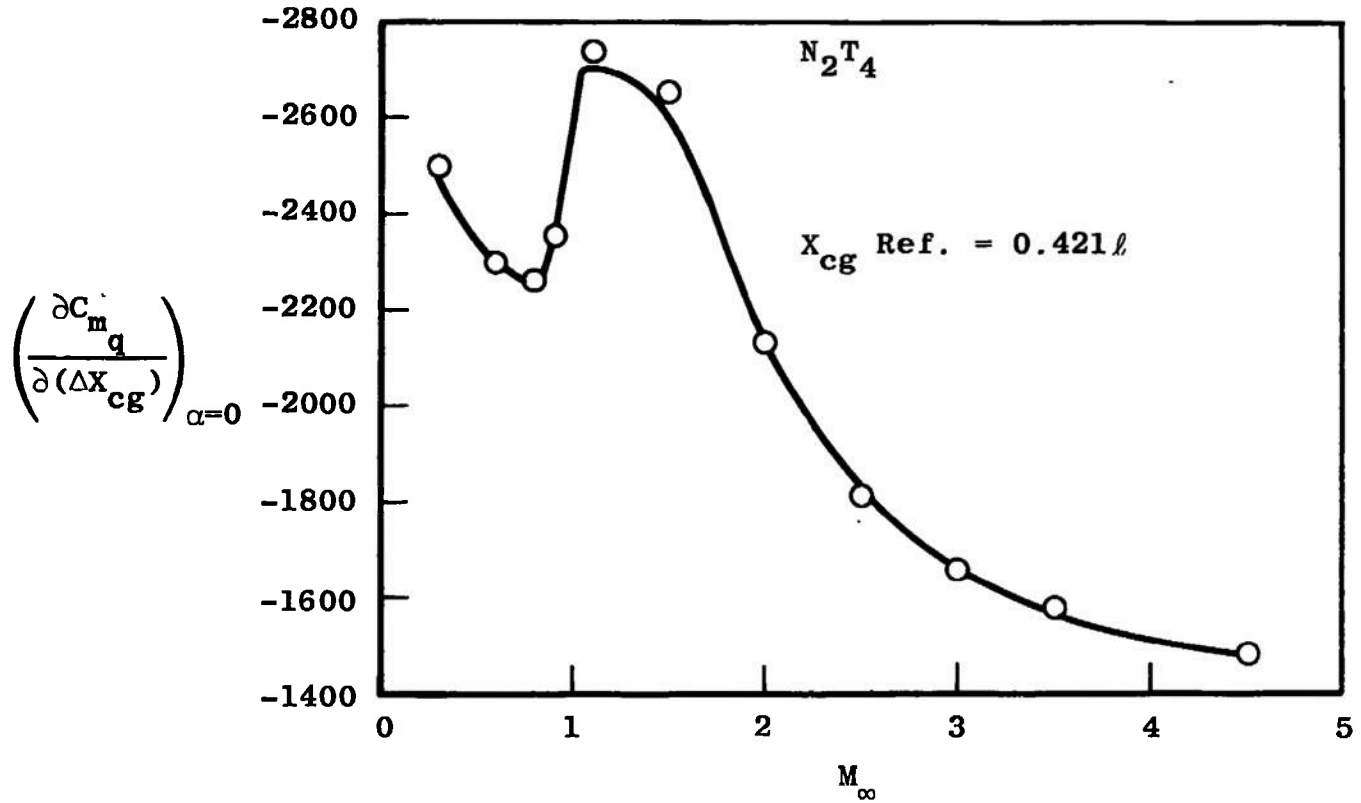


a. $N_2 T_4$
Fig. 12 C_{Nq} and C_{mq} versus M_{∞}

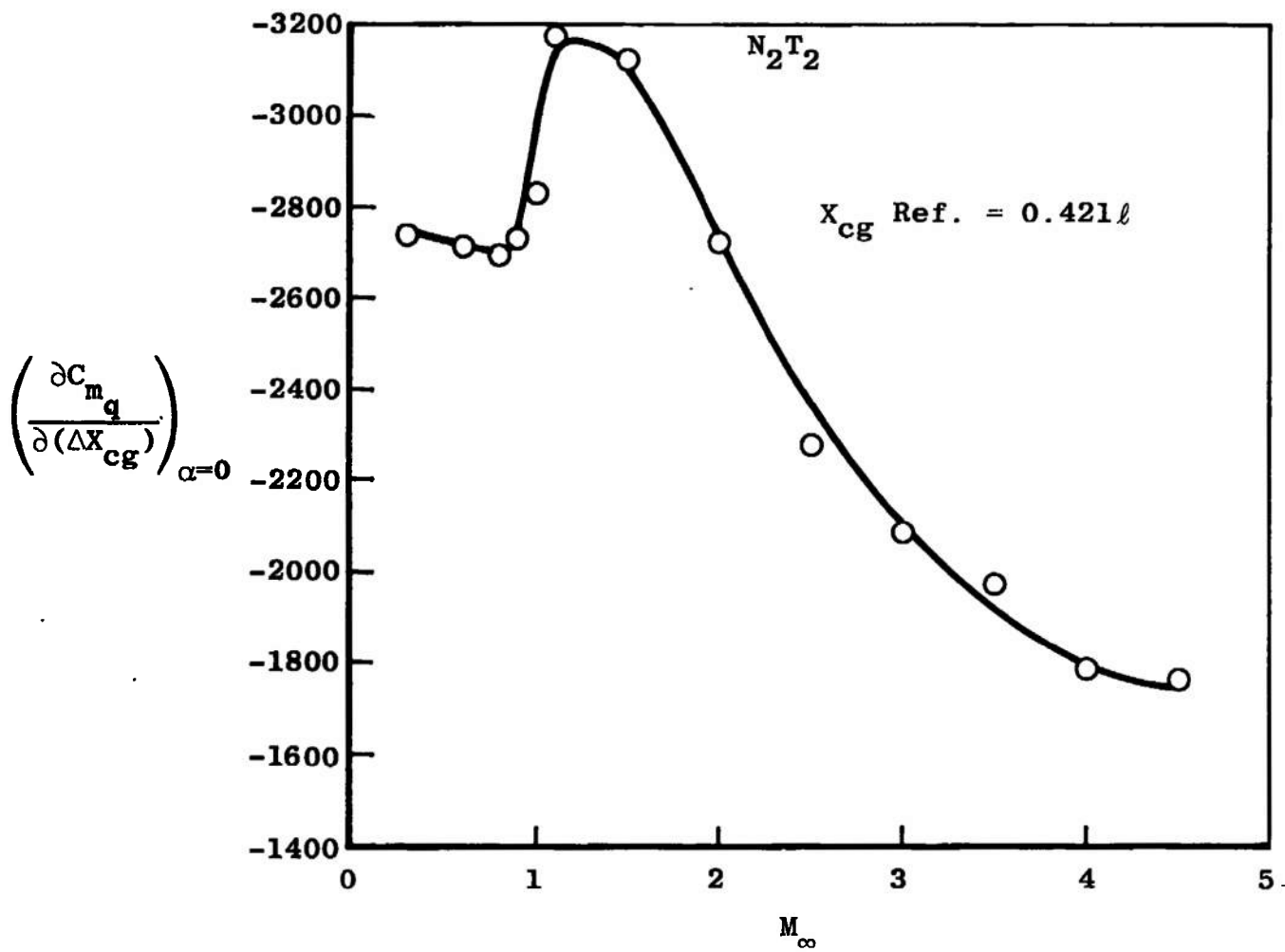




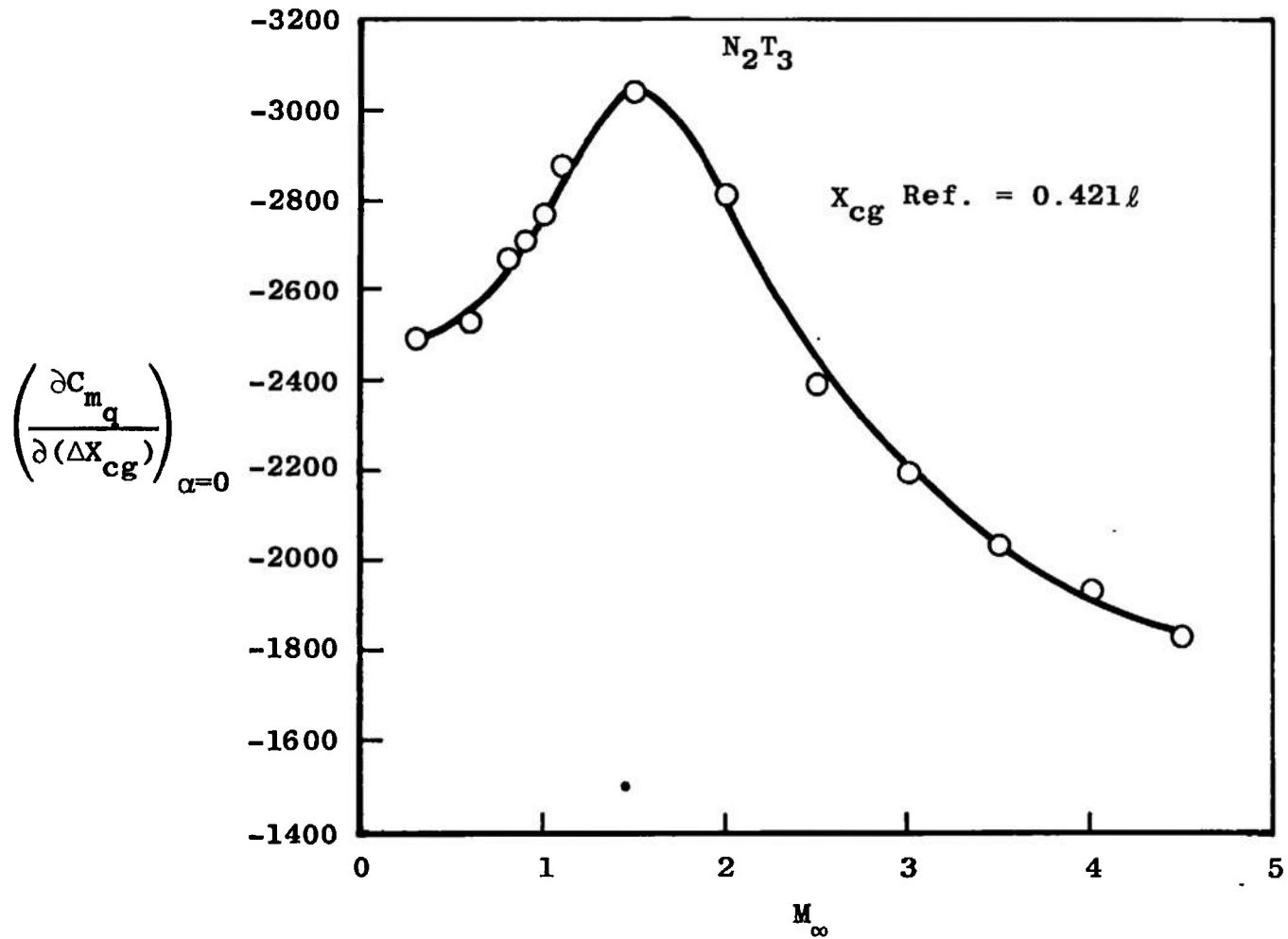
c. N_2T_3 and N_2T_8
Fig. 12 Concluded



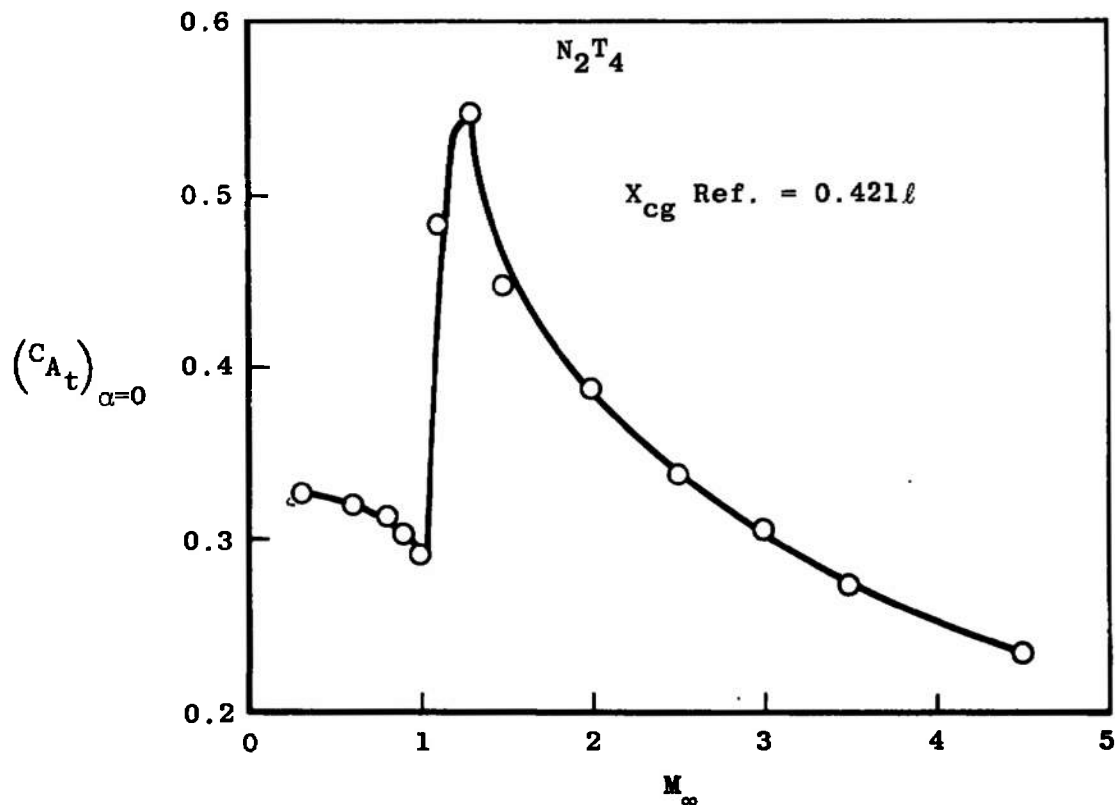
a. $N_2 T_4$
Fig. 13 $\partial C_{m_q} / \partial (\Delta X_{cg})$ versus M_∞



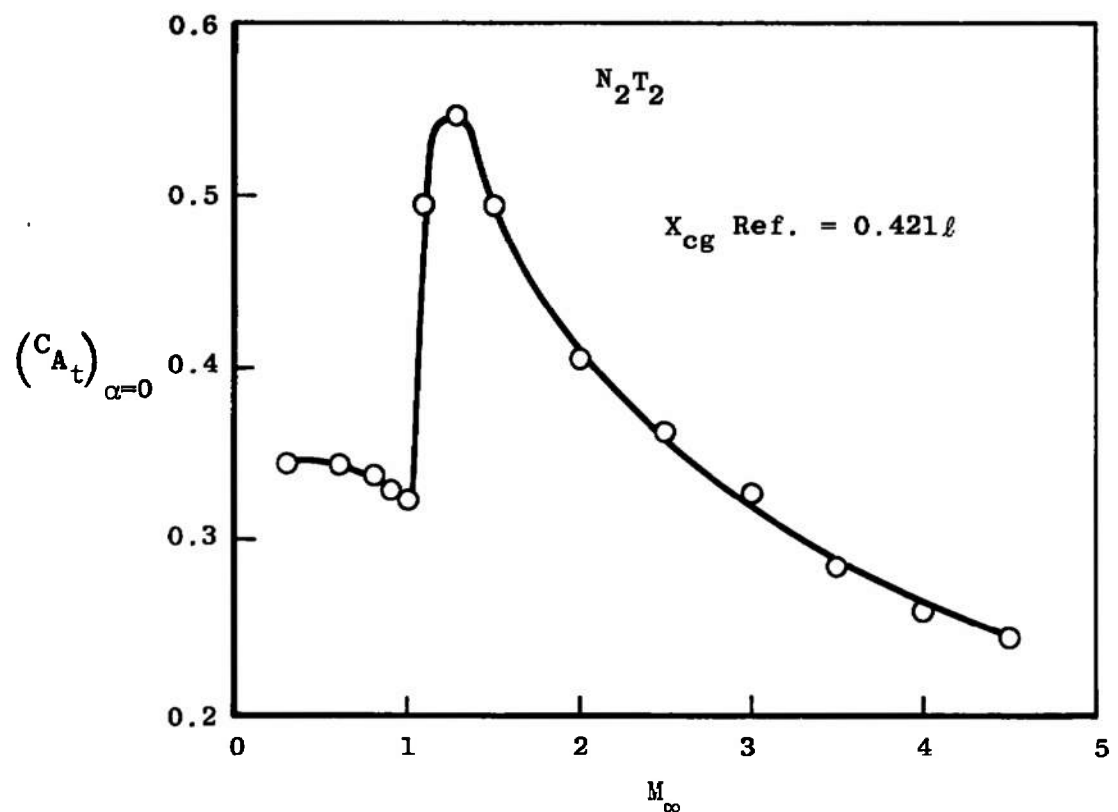
b. $N_2 T_2$
Fig. 13 Continued



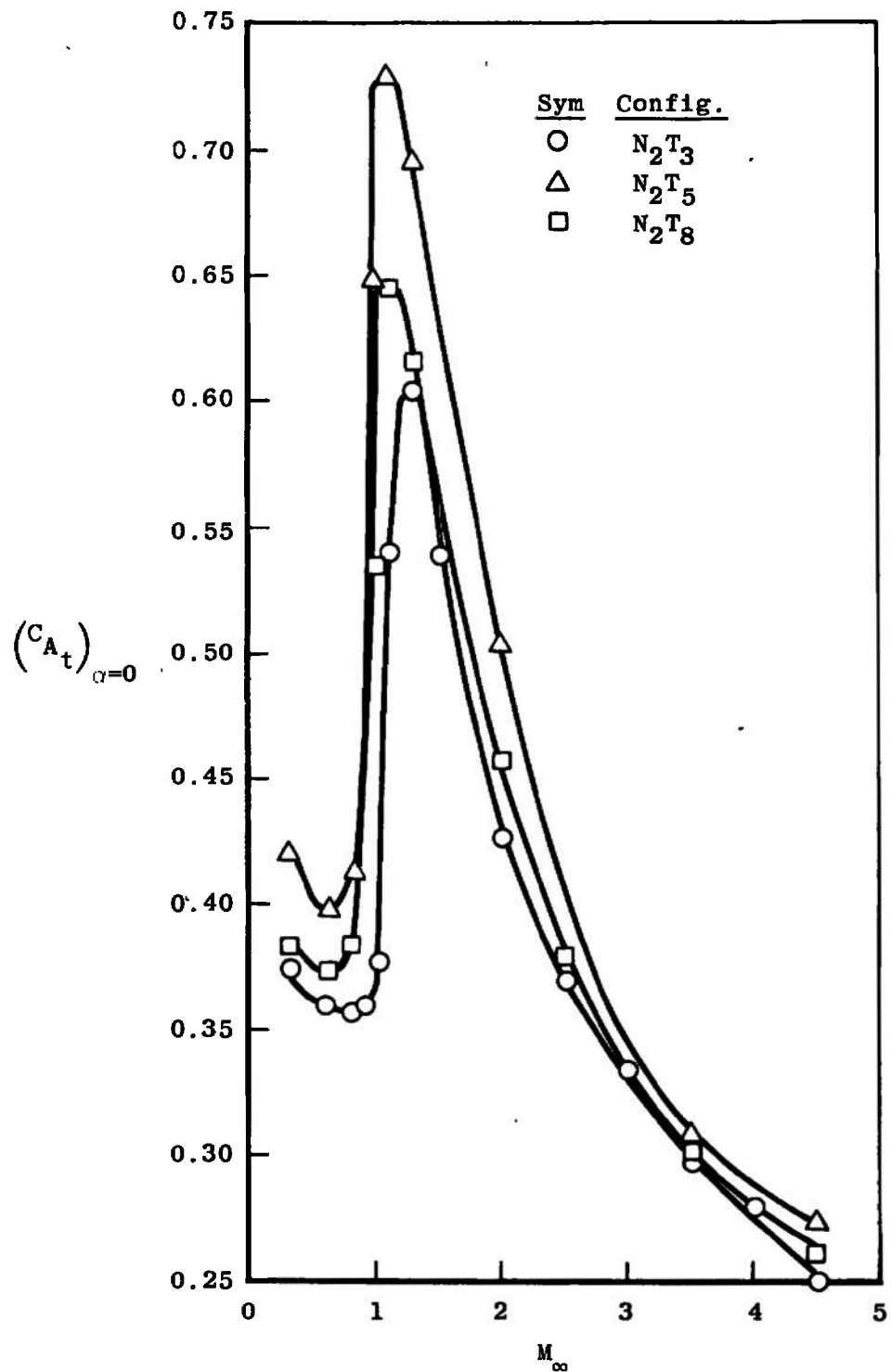
c. $N_2 T_3$
Fig. 13 Concluded



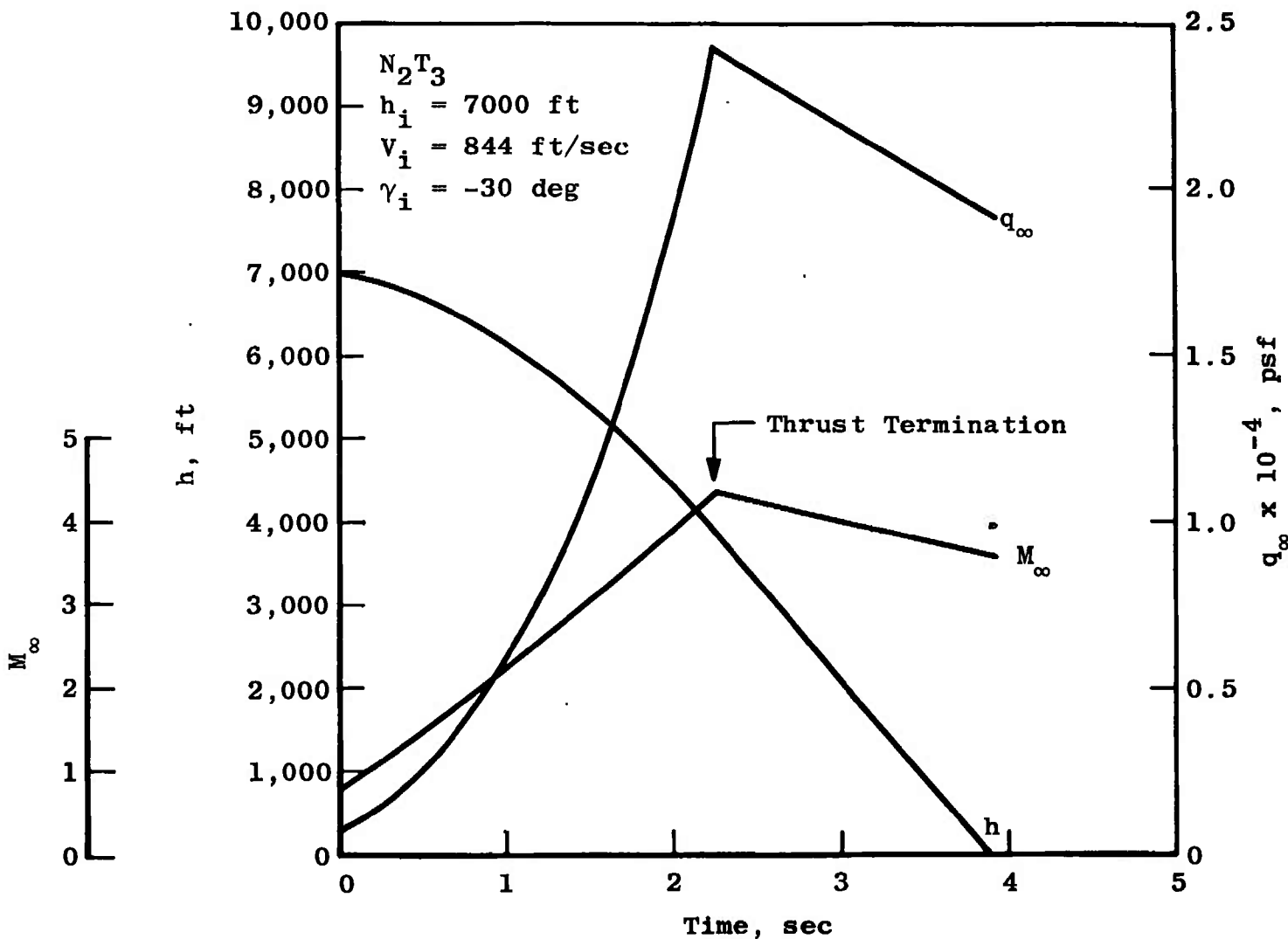
a. $N_2 T_4$
Fig. 14 $(C_{A_t})_{\alpha=0}$ versus M_∞



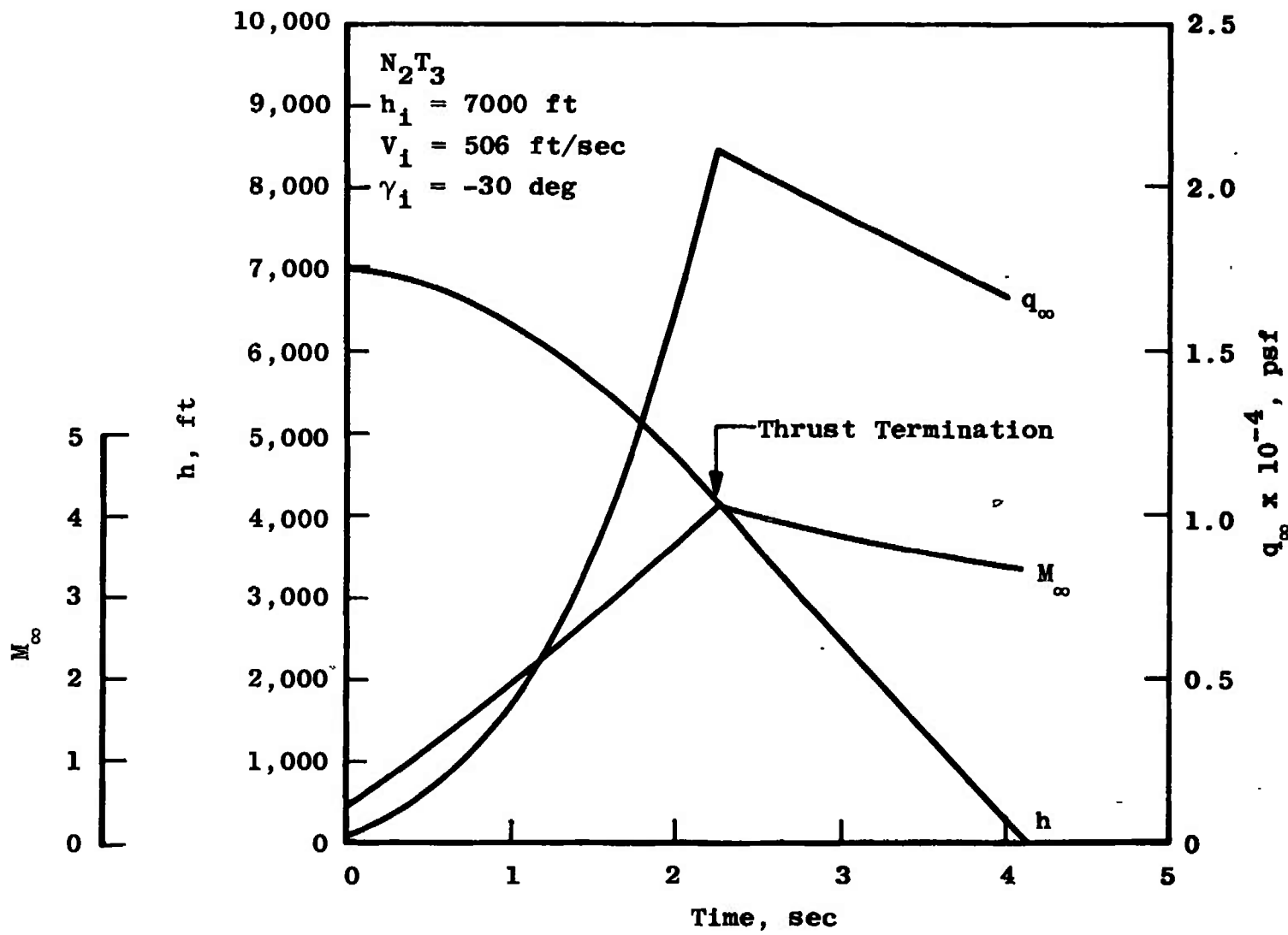
b. $N_2 T_2$
Fig. 14 Continued



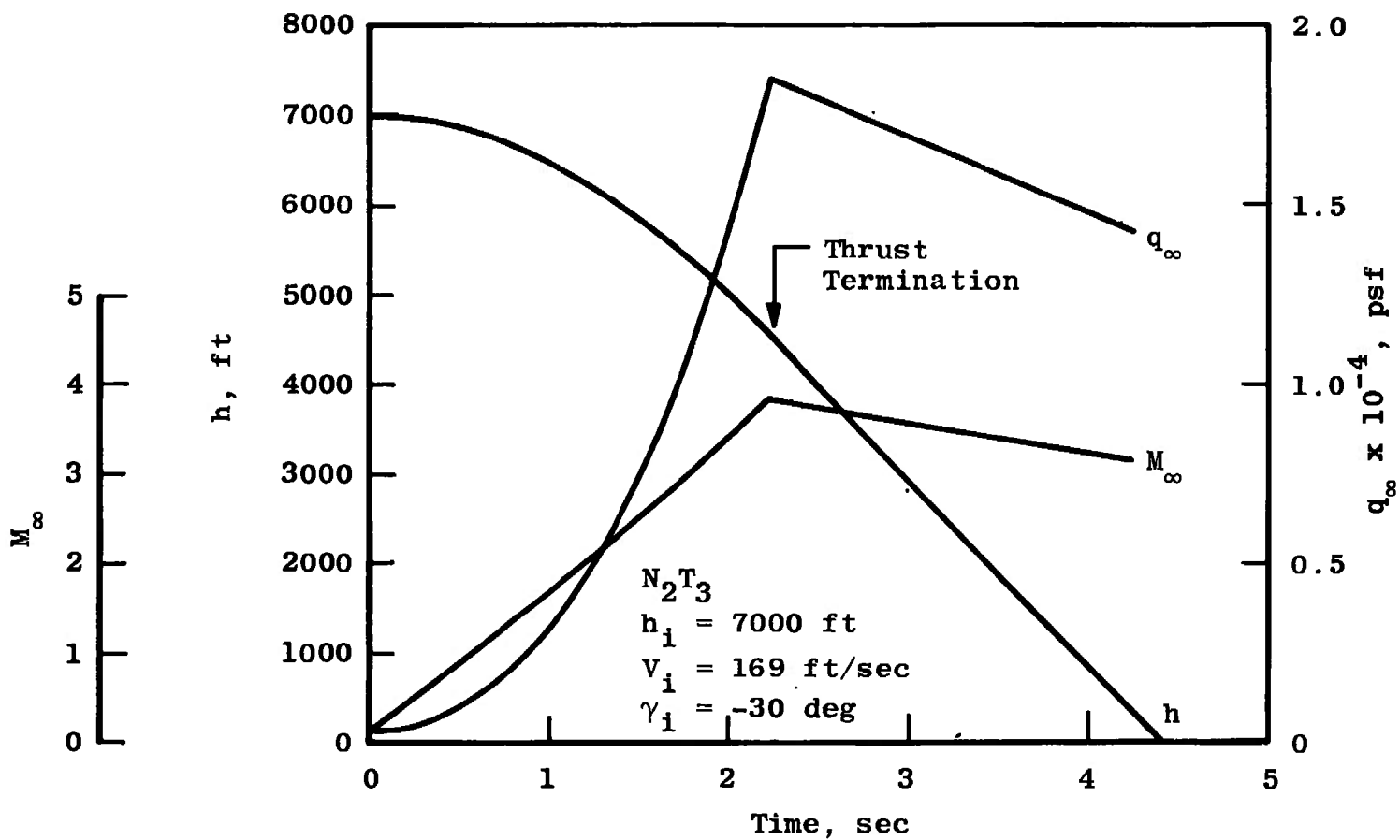
c. $N_2 T_3$, $N_2 T_5$, and $N_2 T_8$
Fig. 14 Concluded



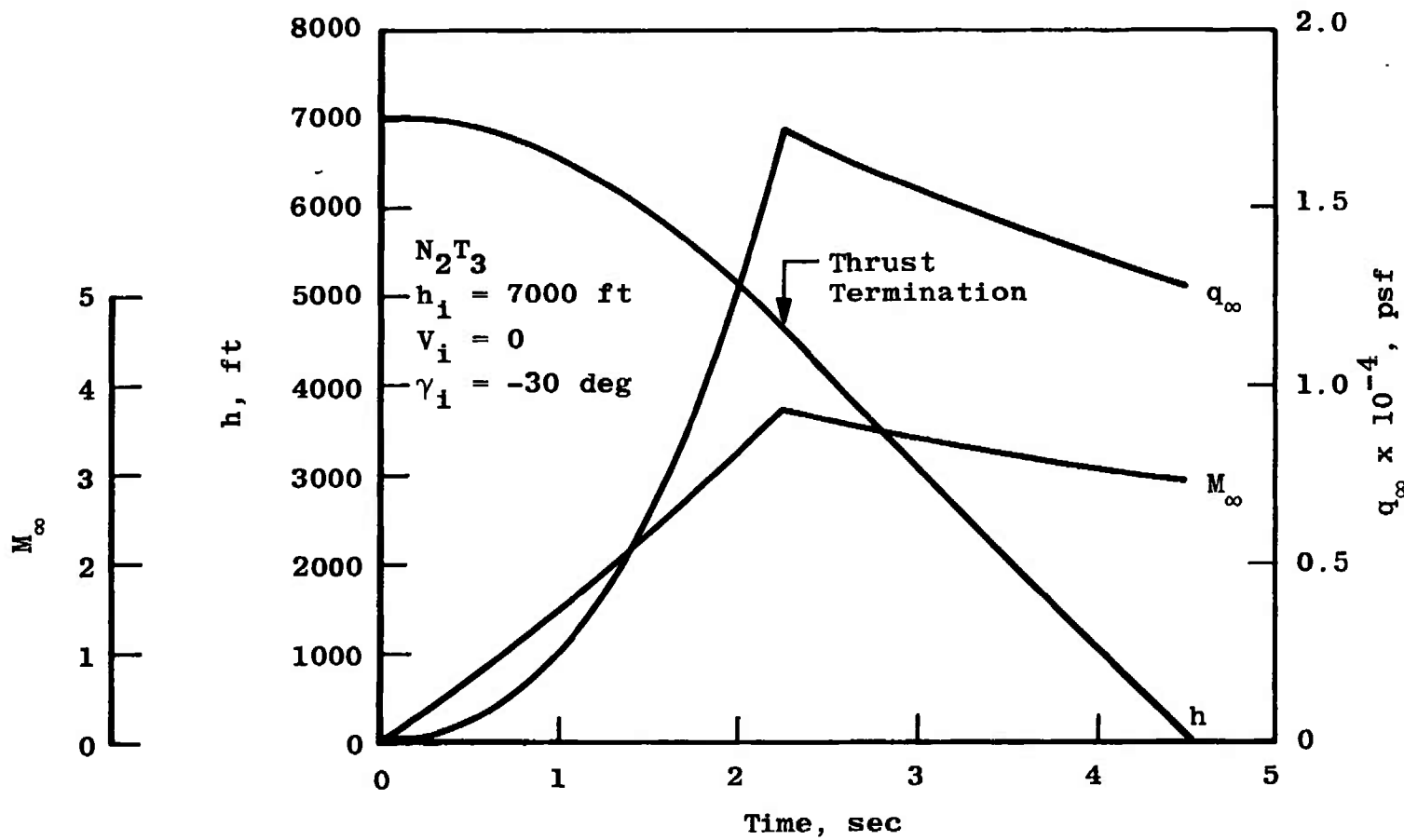
a. $h_i = 7000$ ft, $V_i = 844$ ft/sec
Fig. 15 Variation of h , q_∞ , and M_∞ with Time for the ATR Configuration $N_2 T_3$ Trajectory



b. $h_i = 7000 \text{ ft}$, $V_i = 506 \text{ ft/sec}$
Fig. 15 Continued

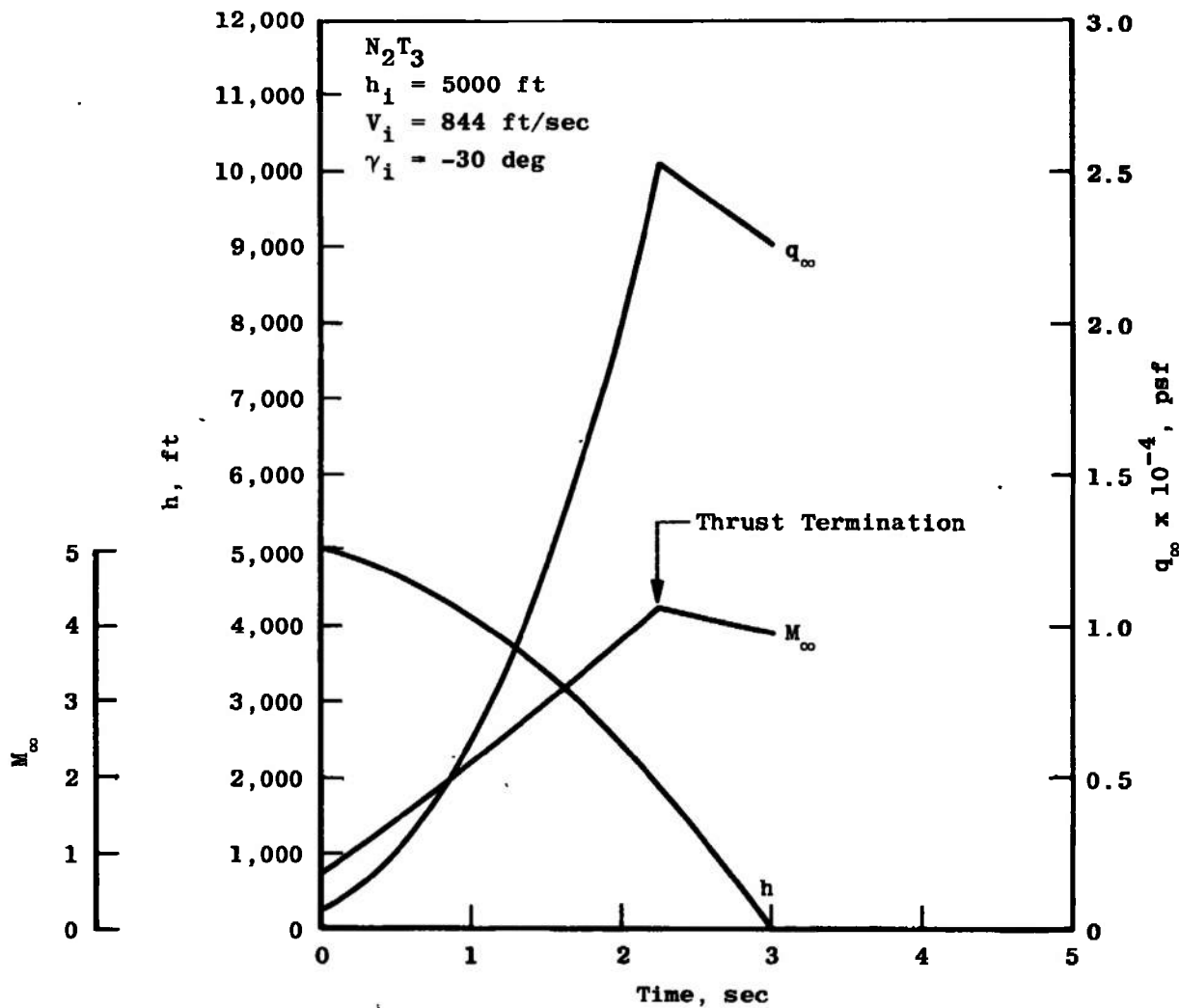


c. $h_i = 7000$ ft, $V_i = 169$ ft/sec
Fig. 15 Continued



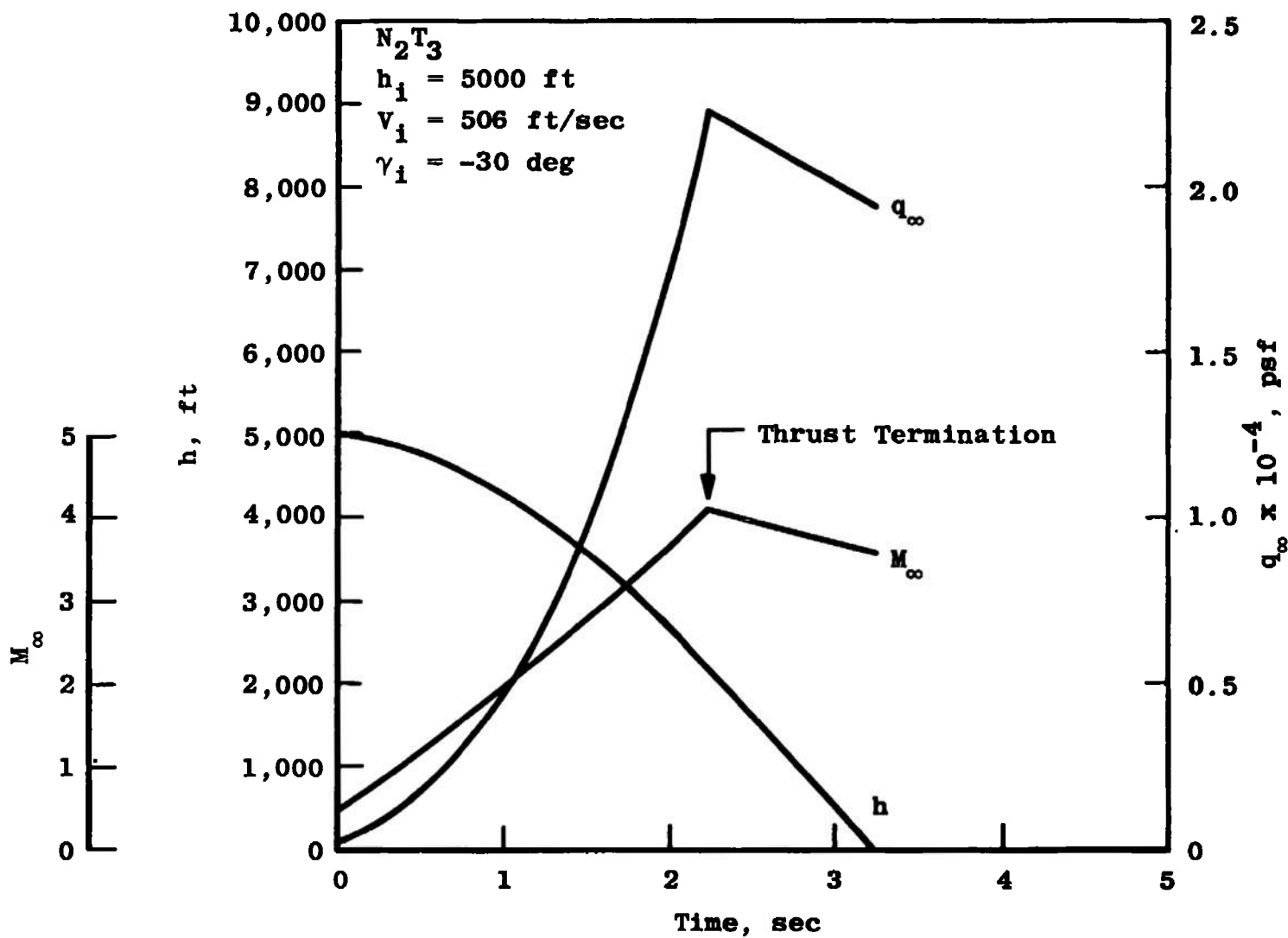
d. $h_i = 7000$ ft, $V_i = 0$

Fig. 15 Continued

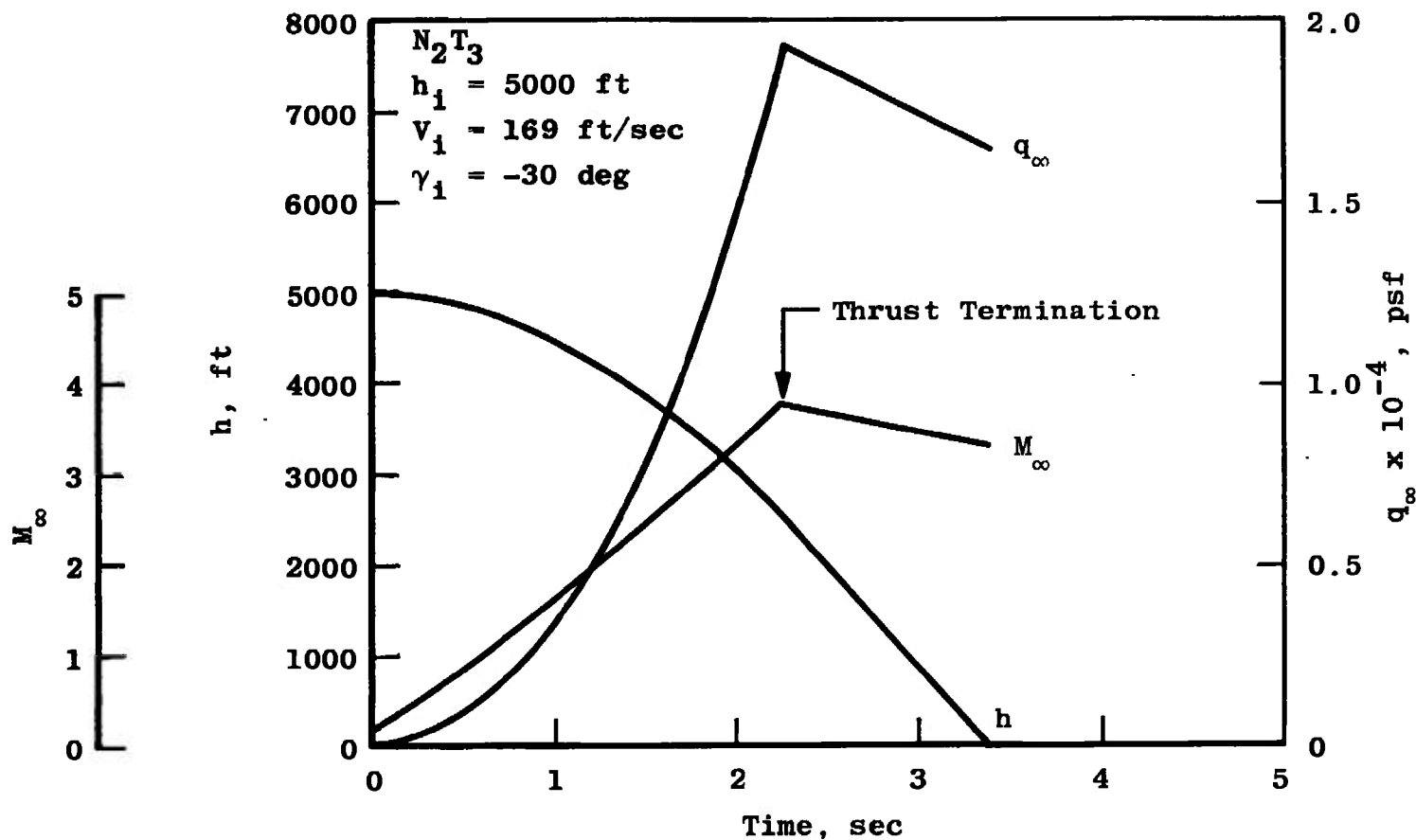


e. $h_i = 5000$ ft, $V_i = 844$ ft/sec

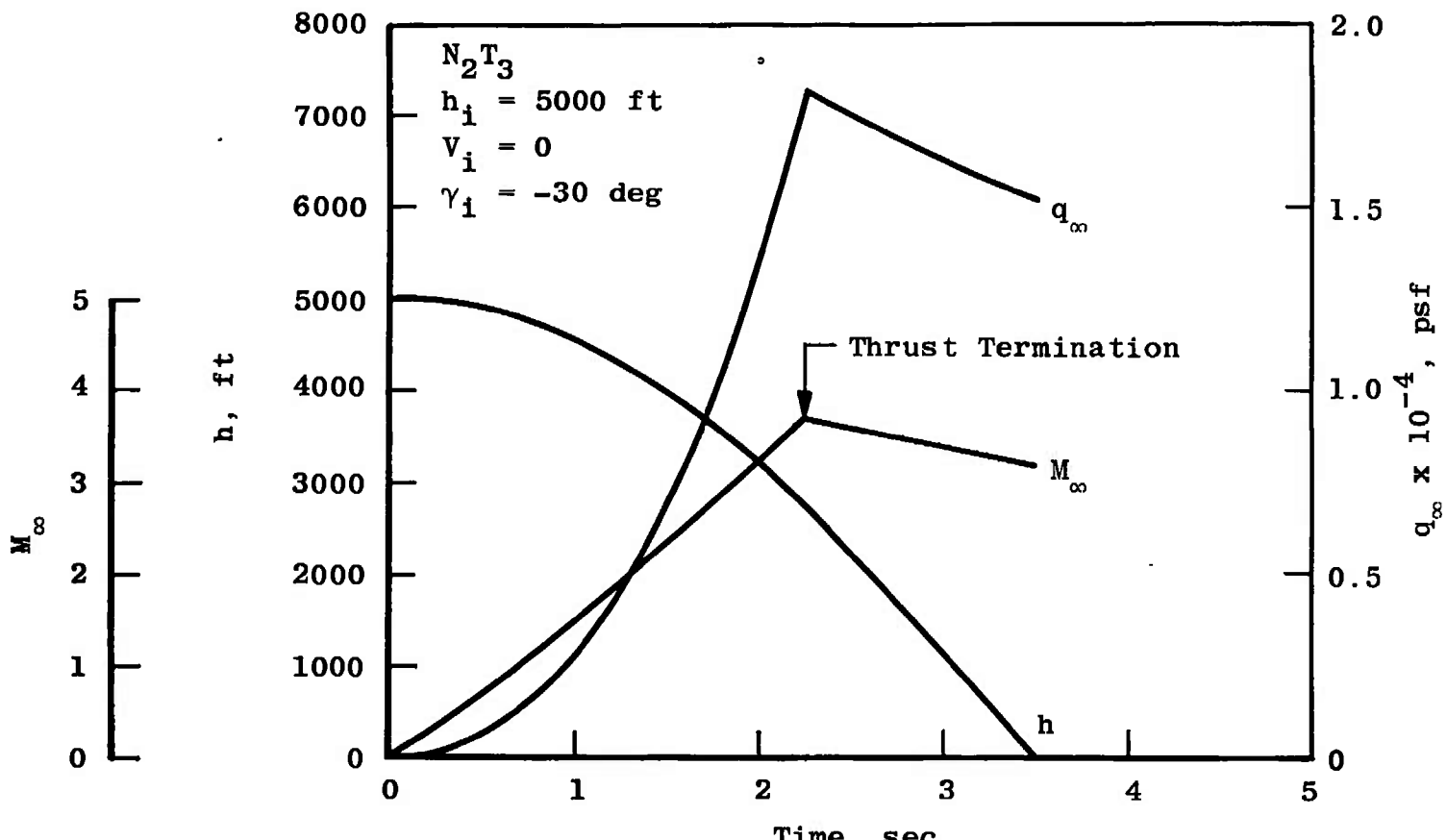
Fig. 15 Continued



f. $h_i = 5000 \text{ ft}$, $V_i = 506 \text{ ft/sec}$
Fig. 15 Continued

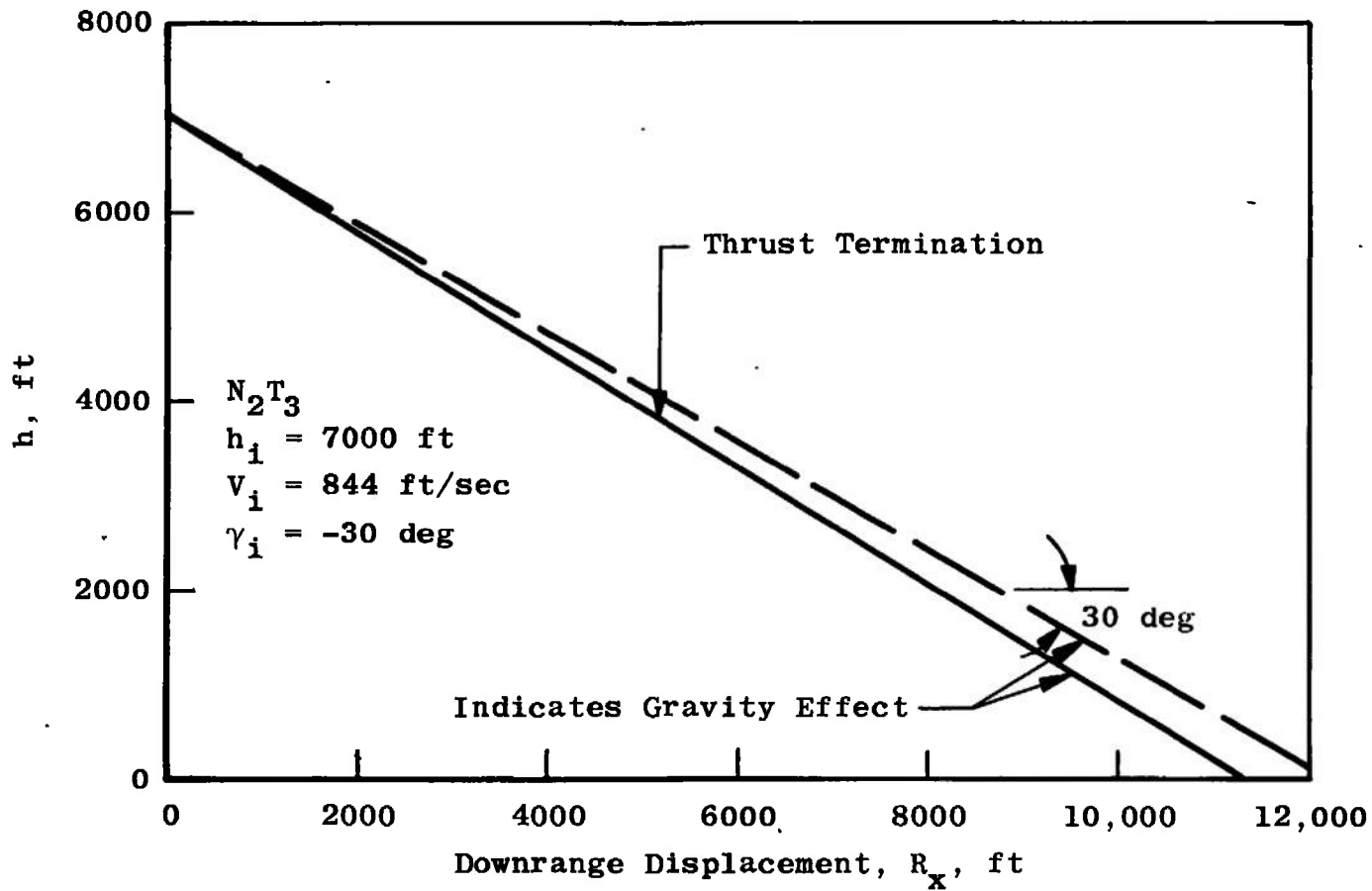


g. $h_i = 5000 \text{ ft}$, $V_i = 169 \text{ ft/sec}$
 Fig. 15 Continued



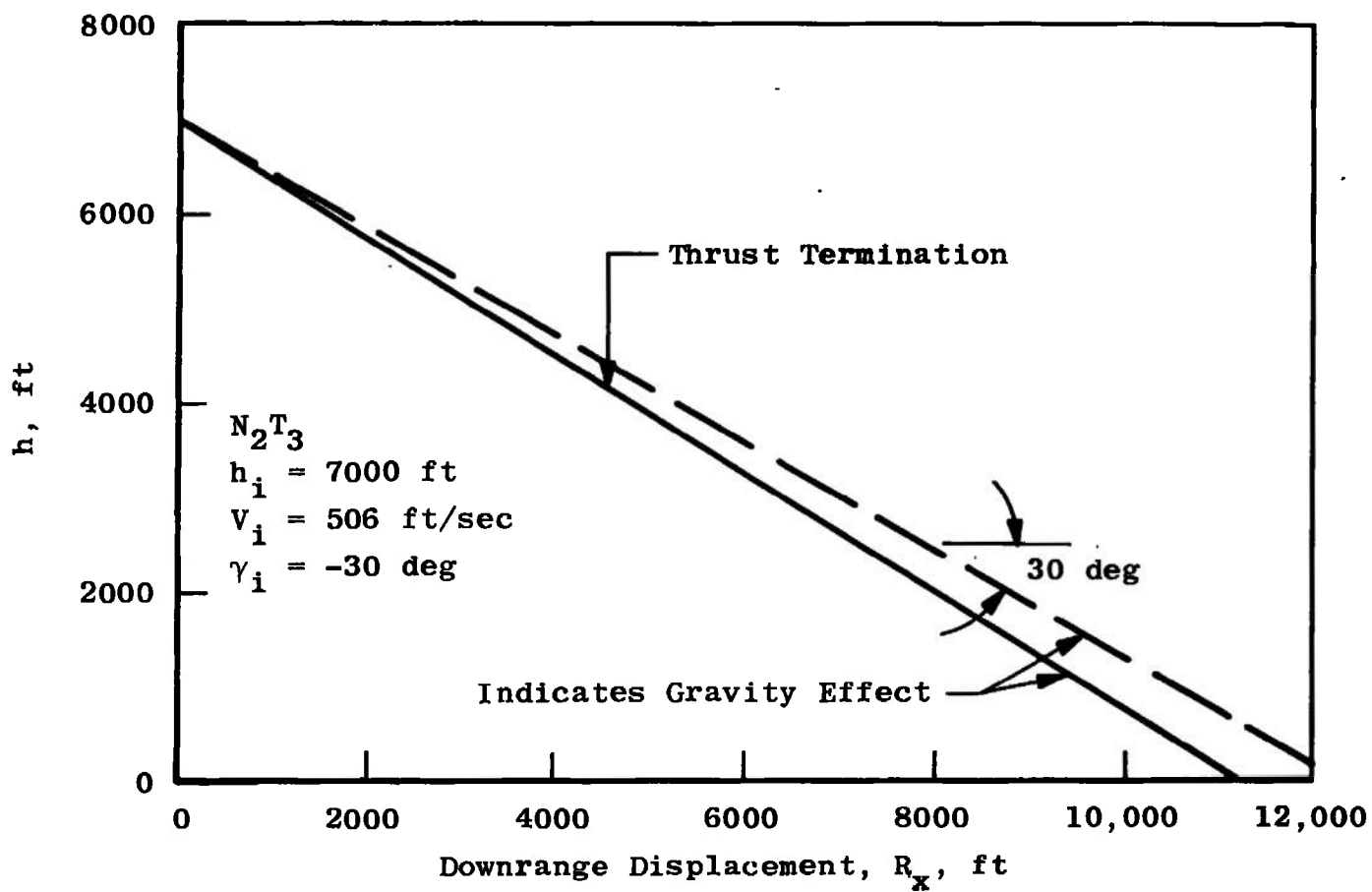
h. $h_i = 5000$ ft, $V_i = 0$

Fig. 15 Concluded



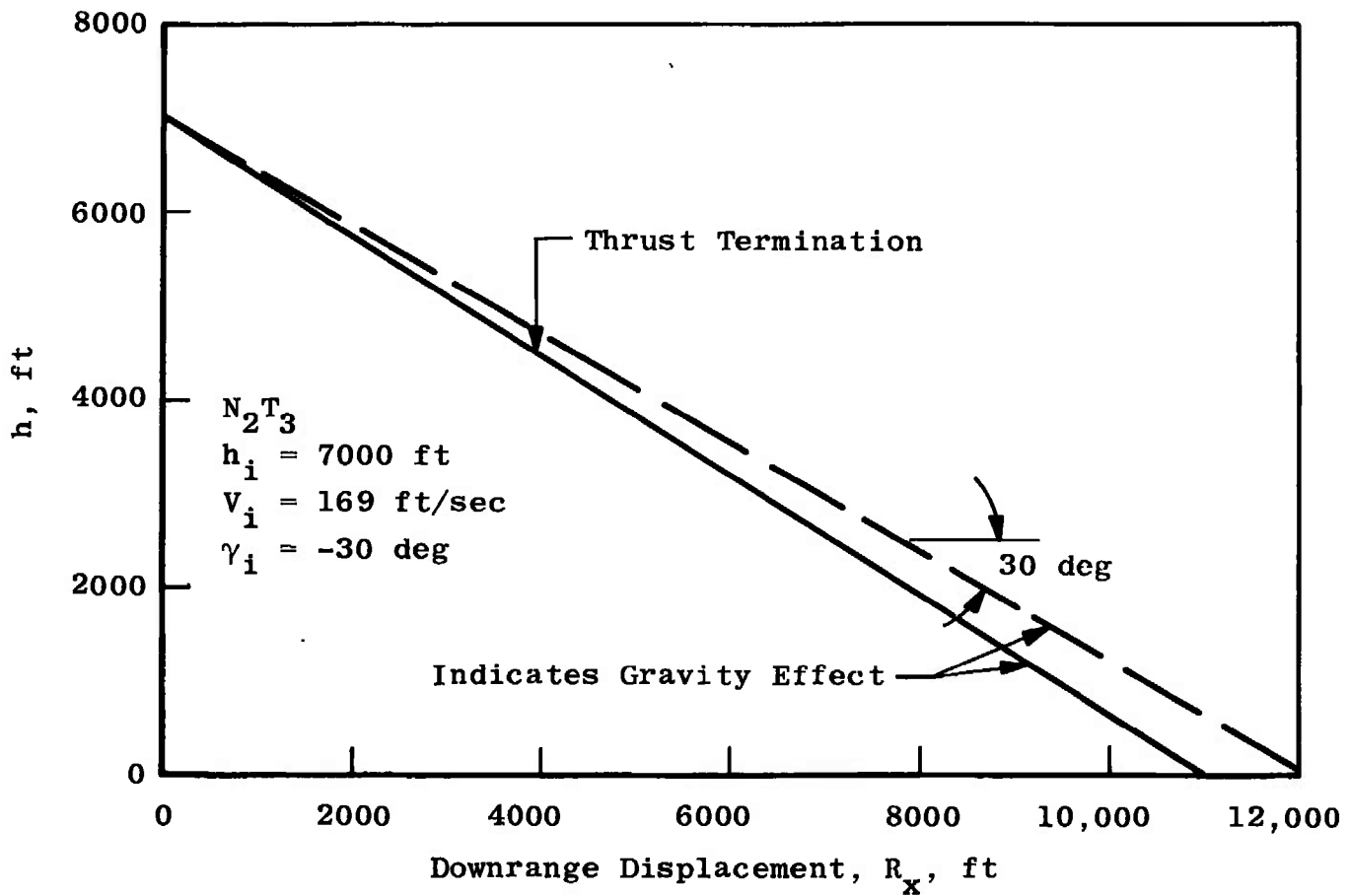
a. $h_i = 7000 \text{ ft}$, $V_i = 844 \text{ ft/sec}$

Fig. 16 Altitude versus Downrange Distance for the ATR Configuration $N_2 T_3$ Trajectory



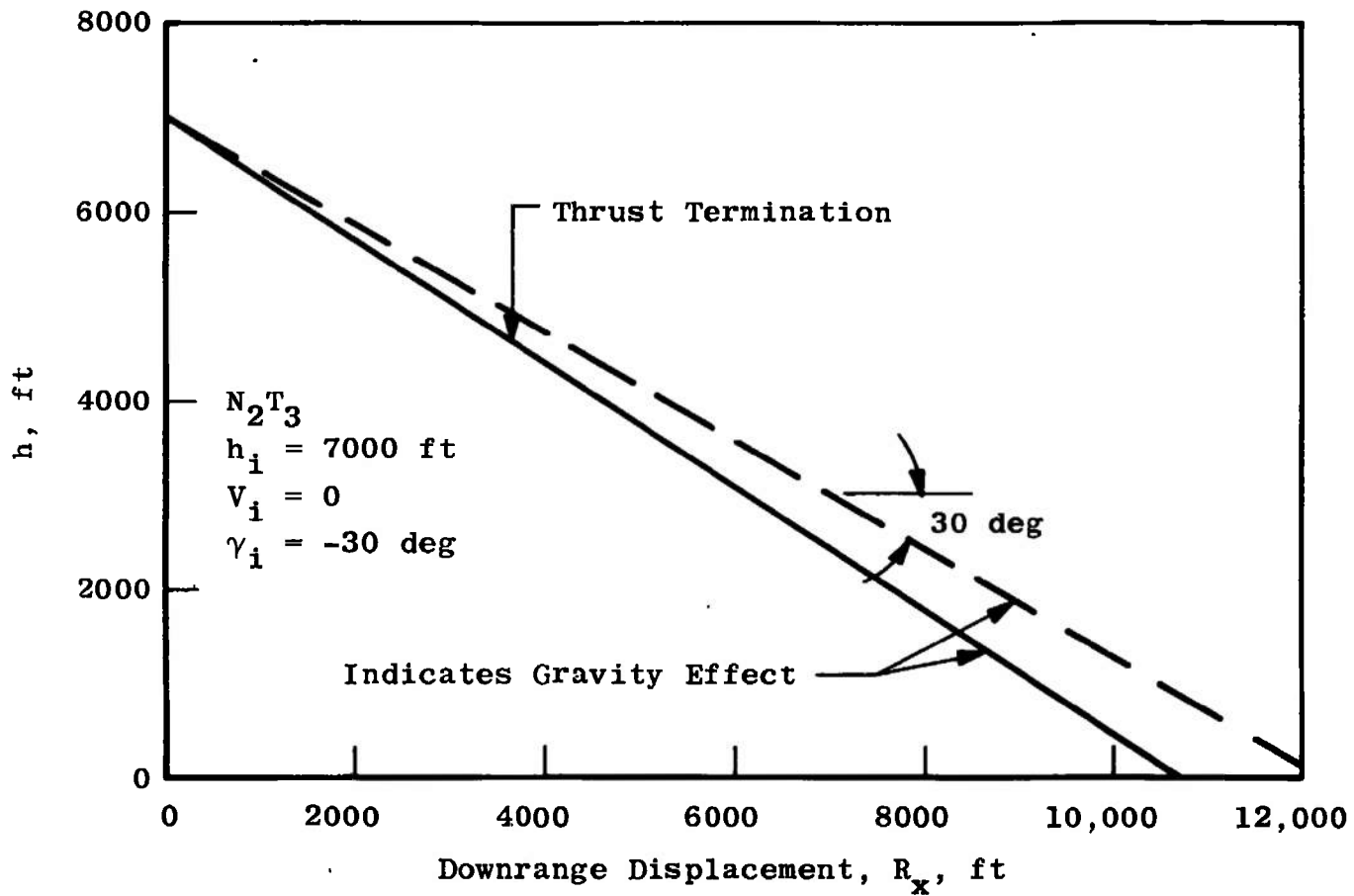
b. $h_i = 7000$ ft, $v_i = 506$ ft/sec

Fig. 16 Continued



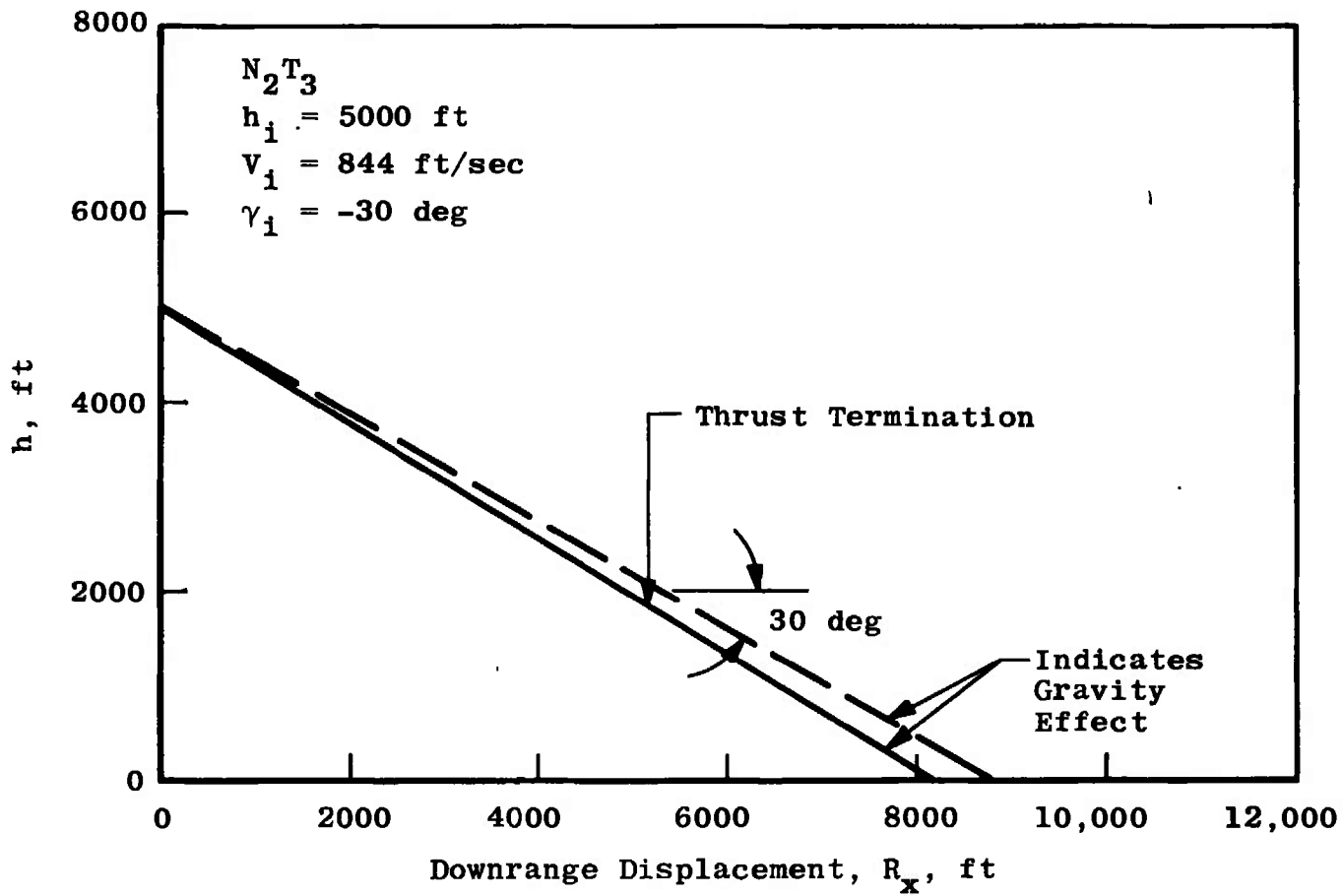
c. $h_i = 7000$ ft, $V_i = 169$ ft/sec

Fig. 16 Continued



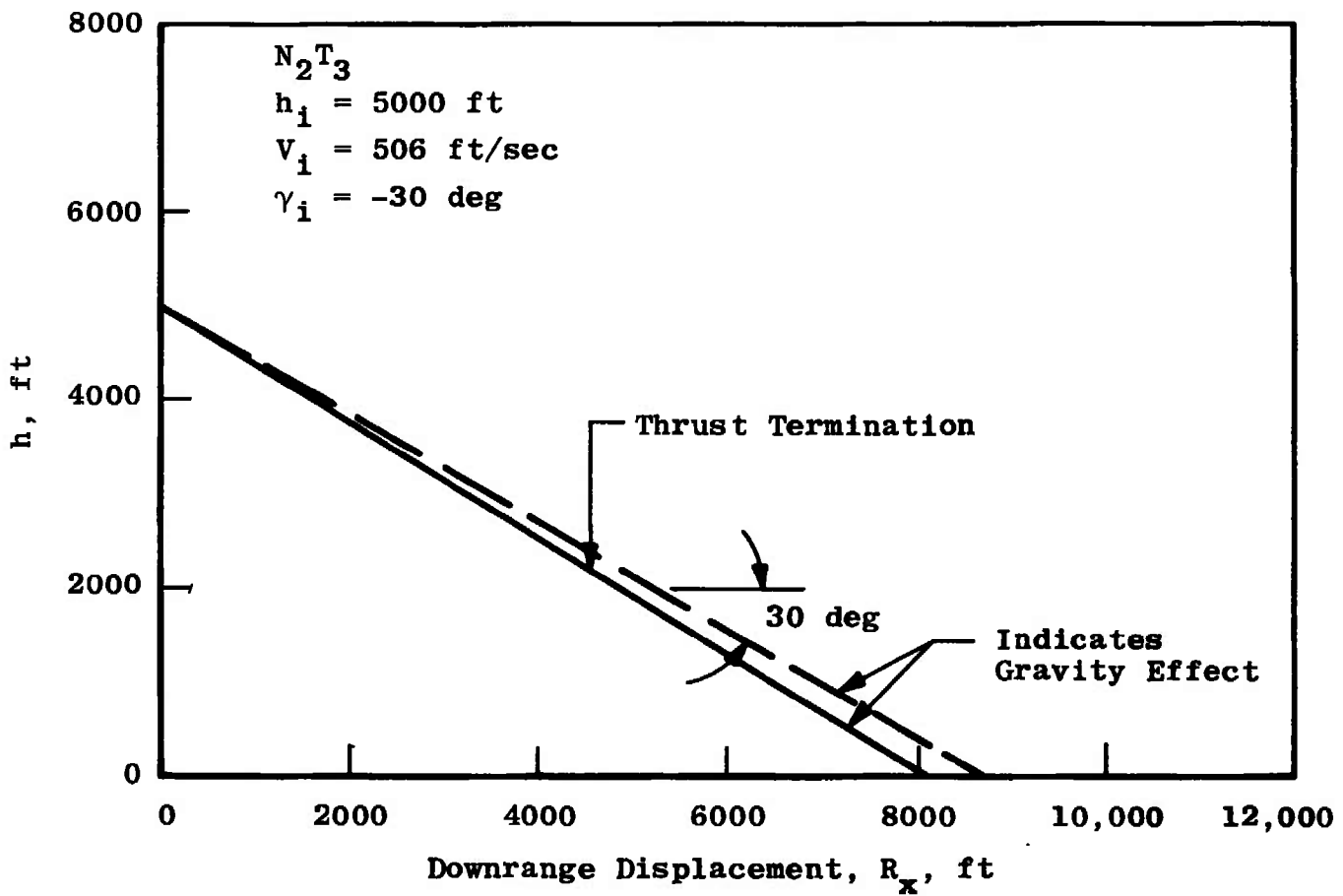
d. $h_i = 7000 \text{ ft}$, $V_i = 0$

Fig. 16 Continued



e. $h_i = 5000 \text{ ft}$, $V_i = 844 \text{ ft/sec}$

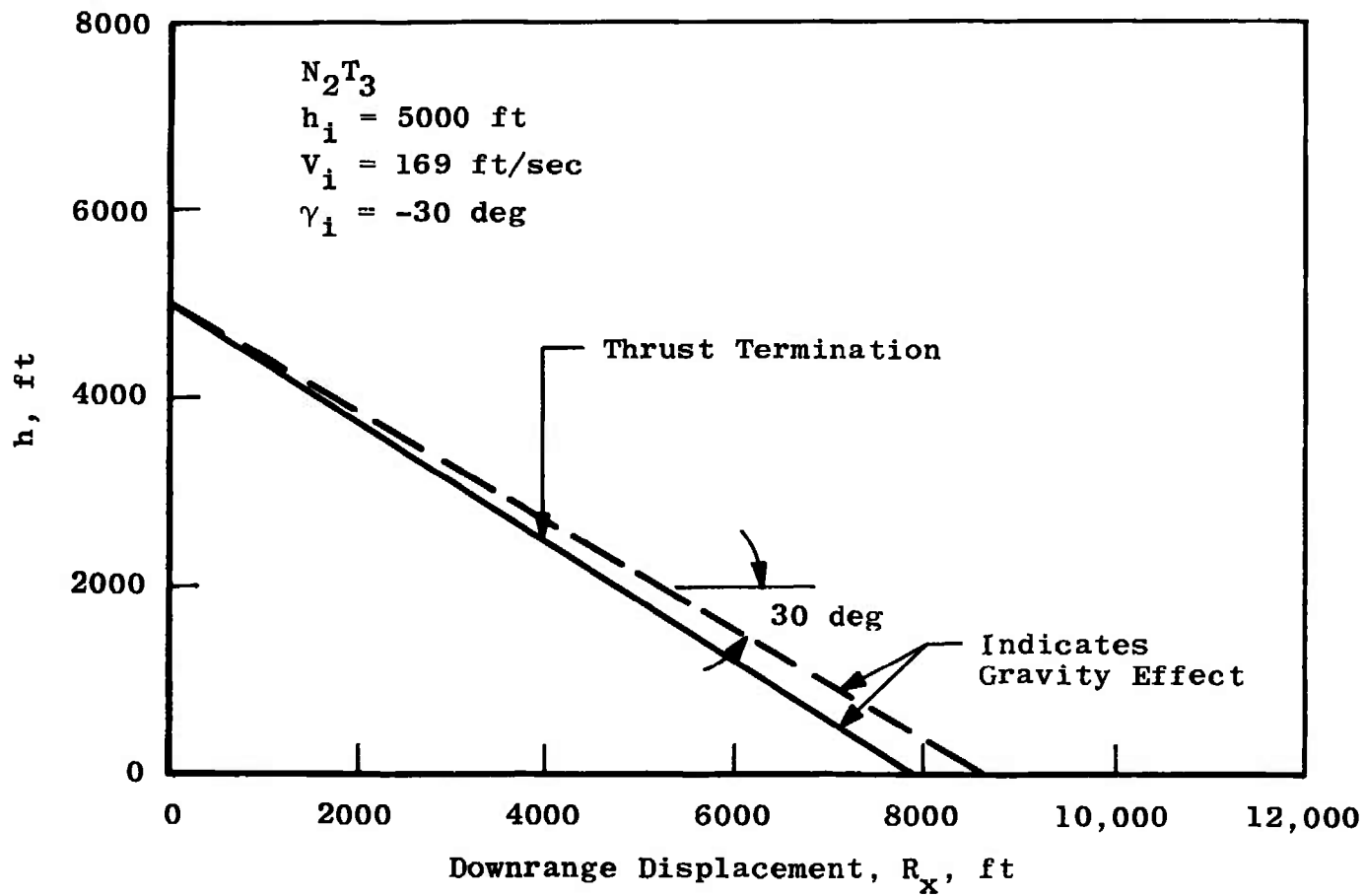
Fig. 16 Continued



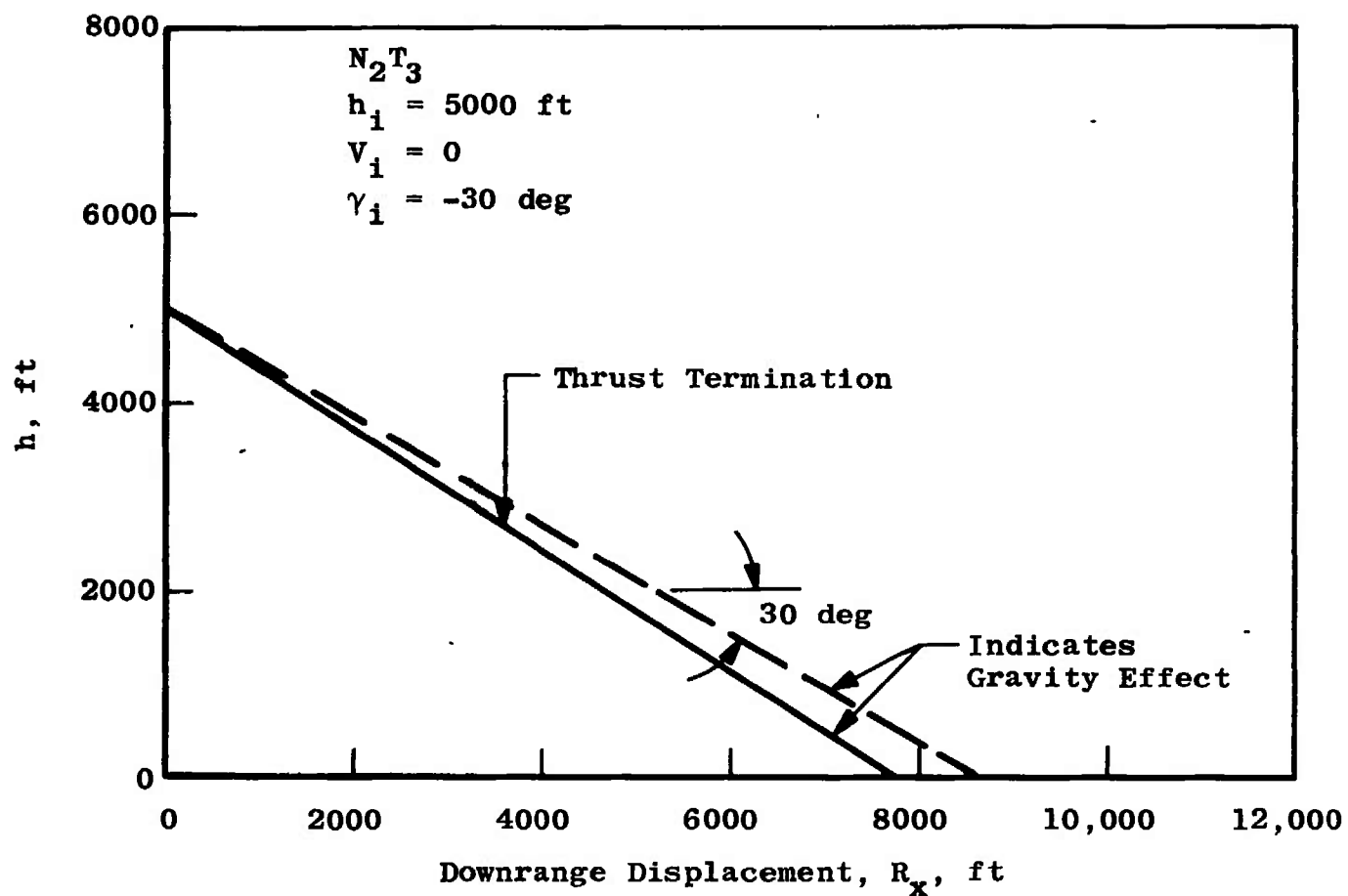
f. $h_i = 5000 \text{ ft}$, $V_i = 506 \text{ ft/sec}$

Fig. 16 Continued

5L



g. h_i = 5000 ft, V_i = 169 ft/sec
Fig. 16 Continued



h. $h_i = 5000$ ft, $V_i = 0$
Fig. 16 Concluded

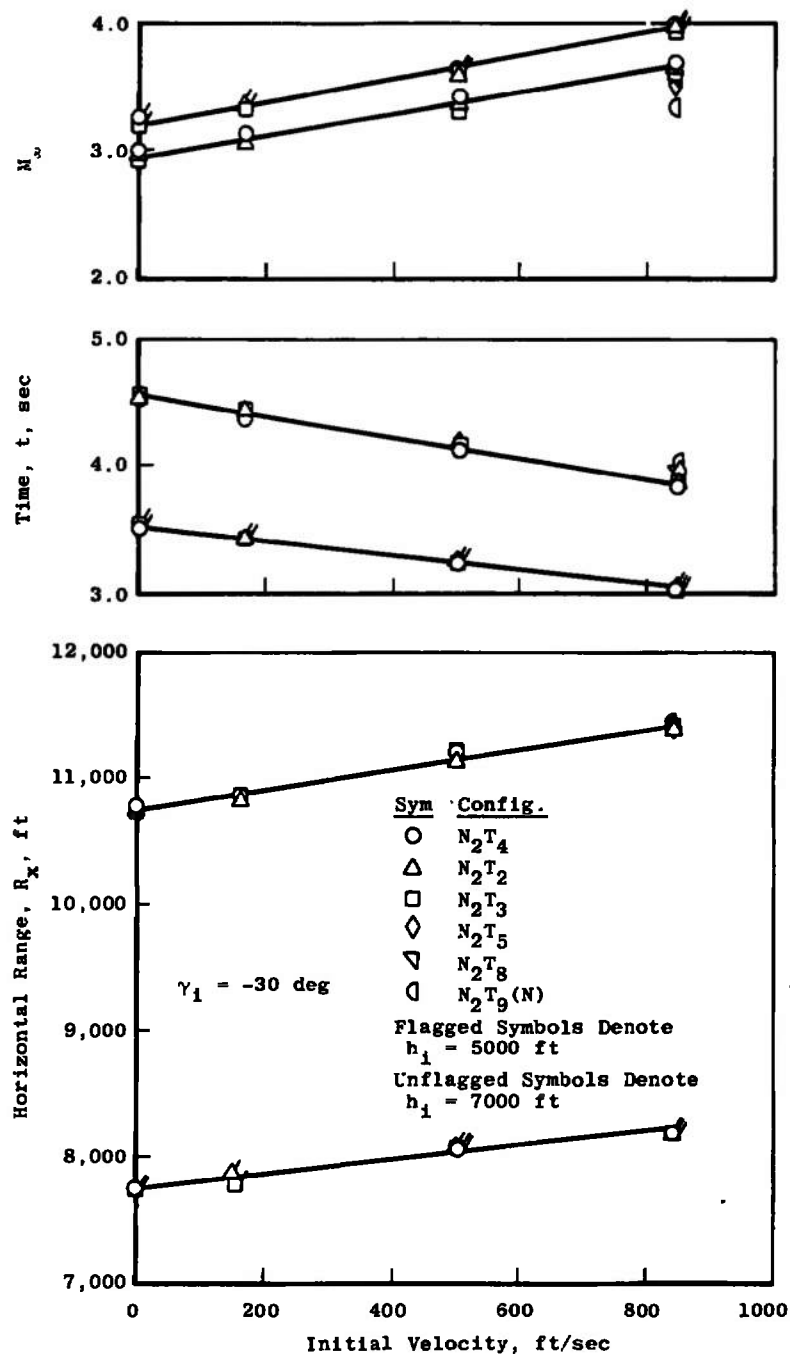


Fig. 17 Variation of Impact M_{∞} , Time, and Horizontal Range with Initial Velocity

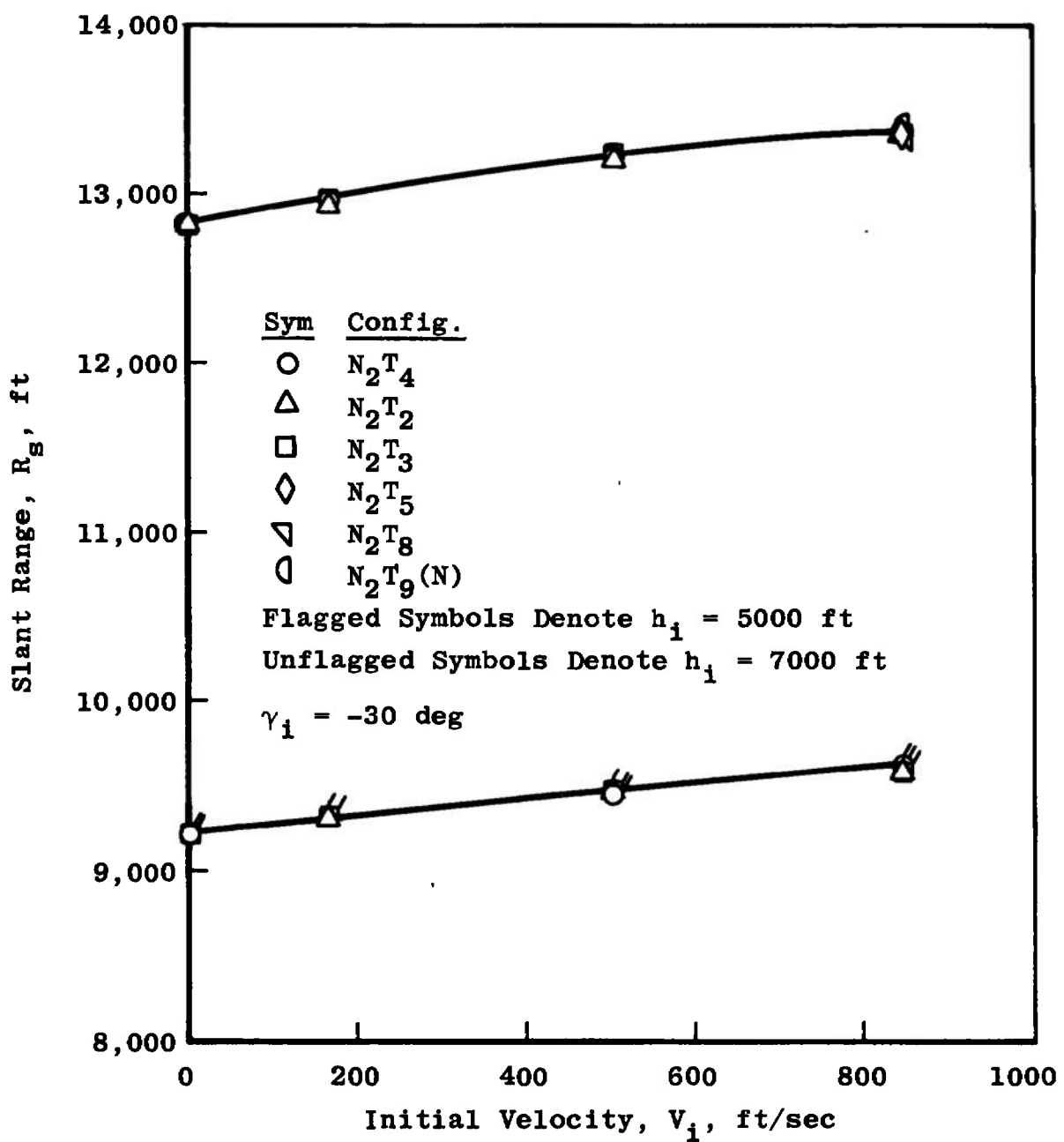


Fig. 18 Variation of Slant Range with Initial Velocity

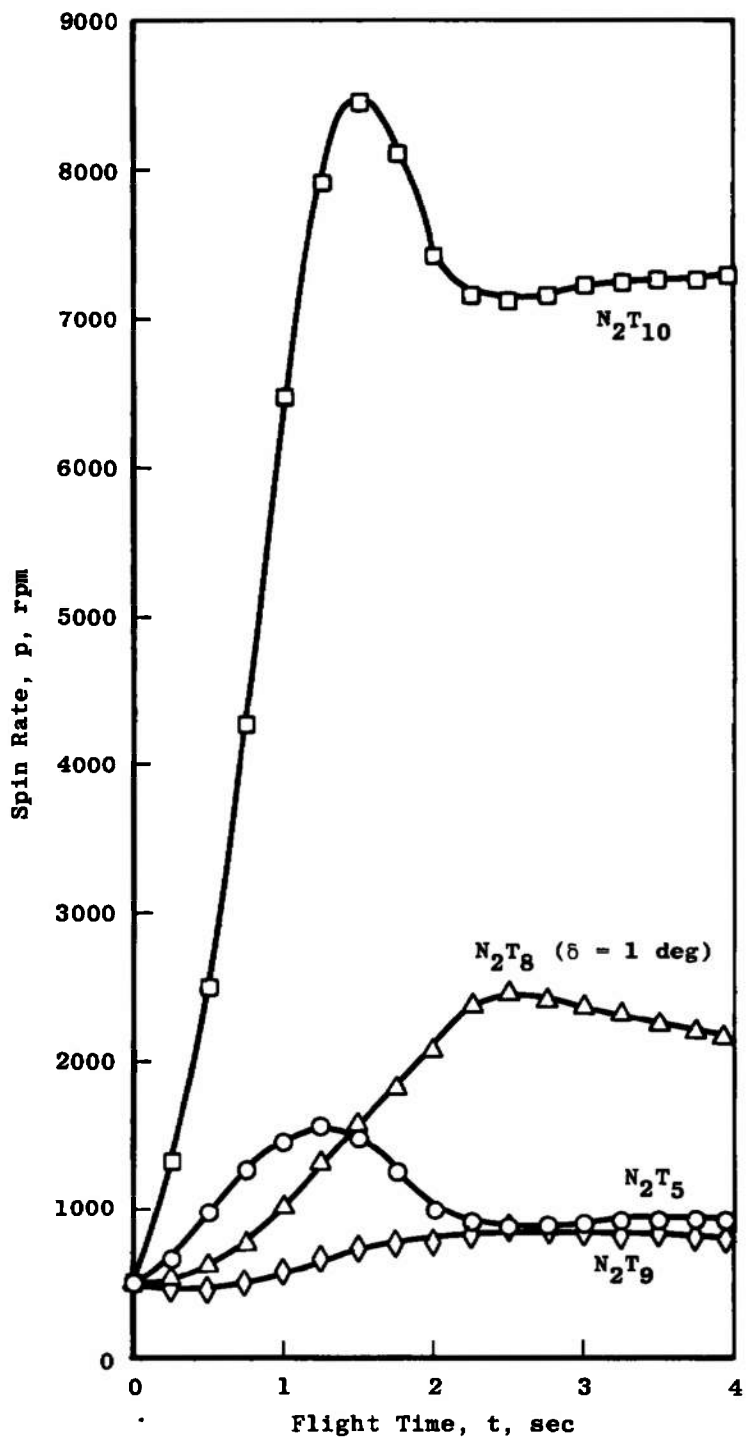


Fig. 19 Variation of Spin Rate with Flight Time for N_2T_5 , N_2T_8 , N_2T_9 and N_2T_{10} with $h_i = 7000$ ft and $V_i = 844$ ft/sec

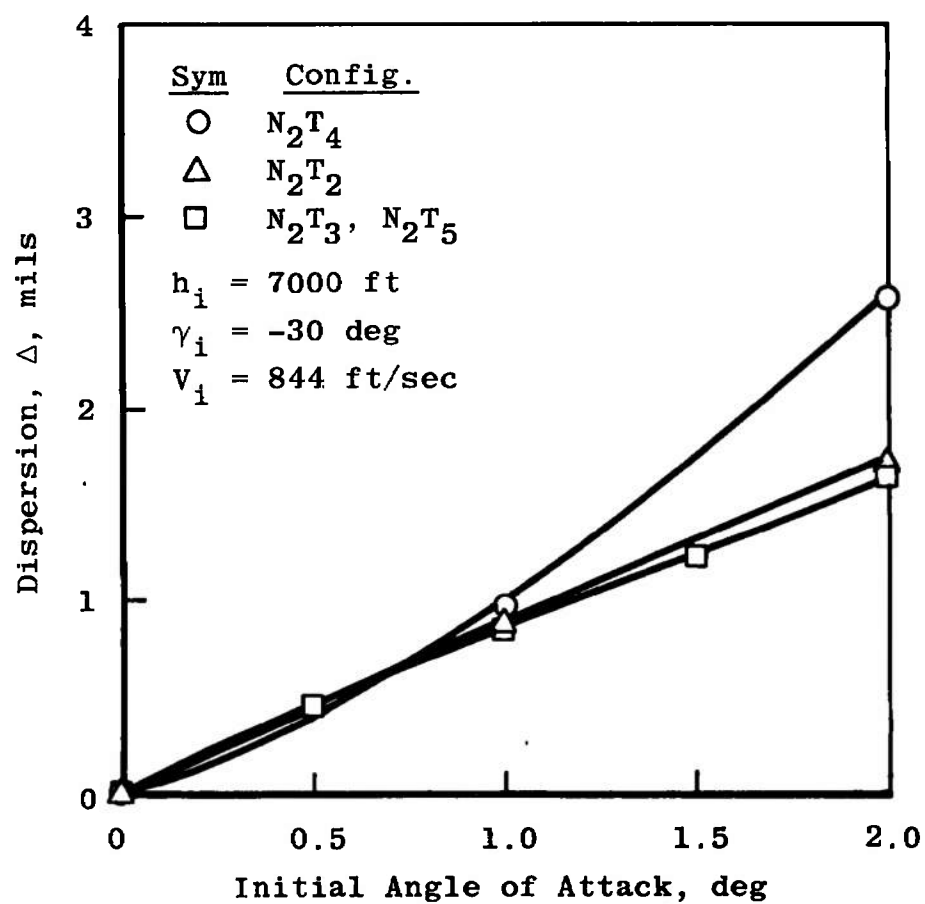


Fig. 20 Effects of Initial Angle of Attack on Missile Dispersion

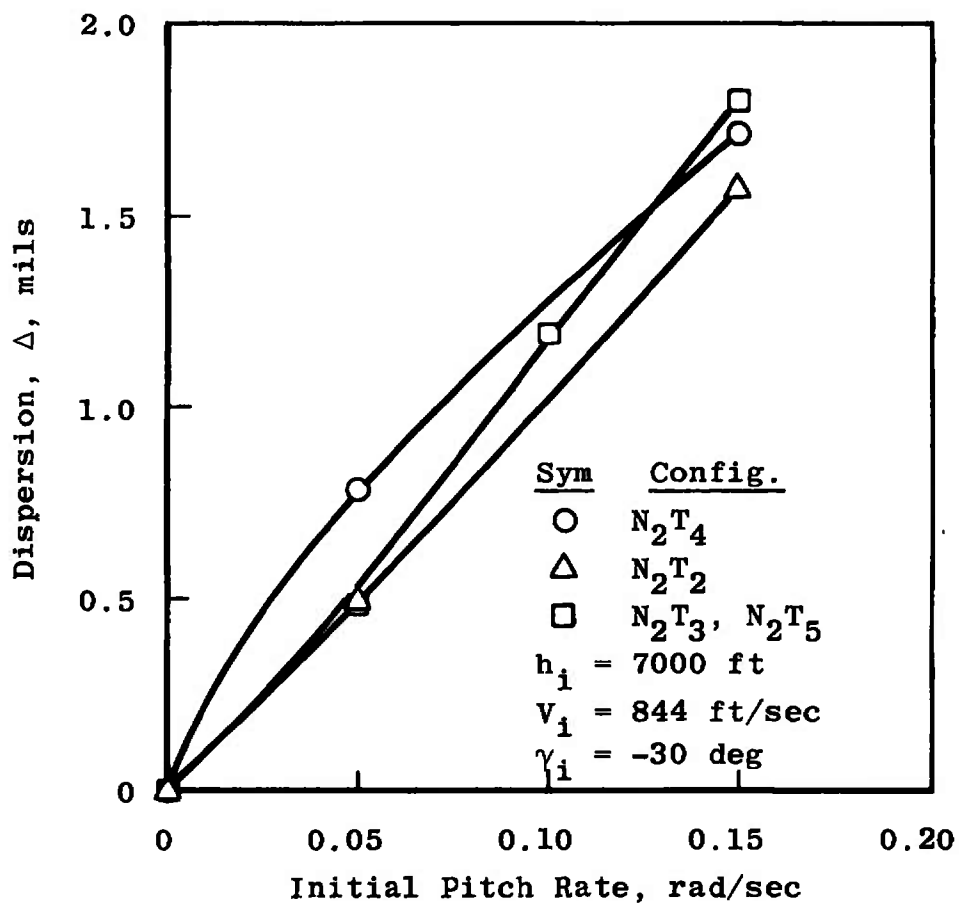
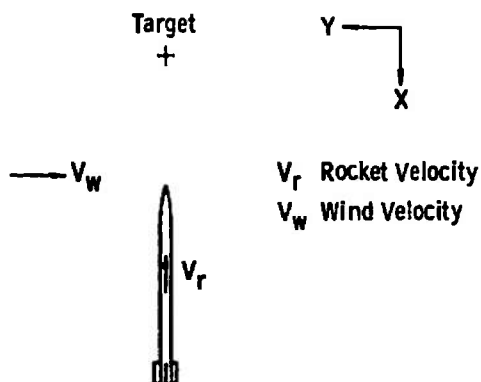
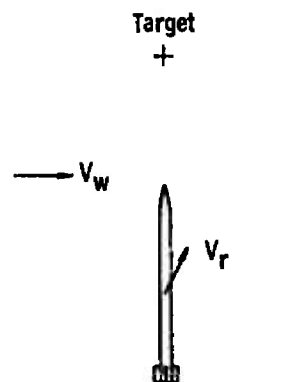


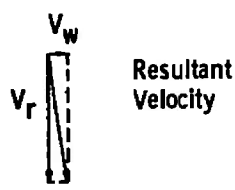
Fig. 21 Effects of Initial Pitch Rate on Missile Dispersion



a. Initial Velocity Diagram
Relative to Ground



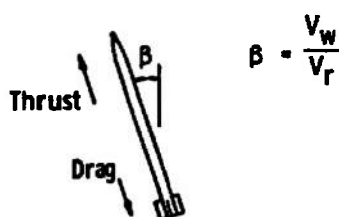
a. Initial Velocity Diagram
Relative to Ground



b. Initial Velocity Diagram
Relative to Rocket



b. Initial Velocity Diagram
Relative to Rocket



A statically stable rocket will weathercock into the wind. The thrust force will then be directed at an angle β to the target and the rocket will be forced away from the target.

c. Force Diagram

Rocket Launched at Target from Plane with Velocity Directly at the Target



$v_w = v_{r_y}$; therefore, the rocket will not turn.

The thrust vector will be parallel to the line between the target and the initial release point. The rocket will only drift off target.

c. Force Diagram

Rocket Launched at Target from Plane with Cross Velocity Equal to the Crosswind Velocity

Fig. 22 Illustration of Wind Effects

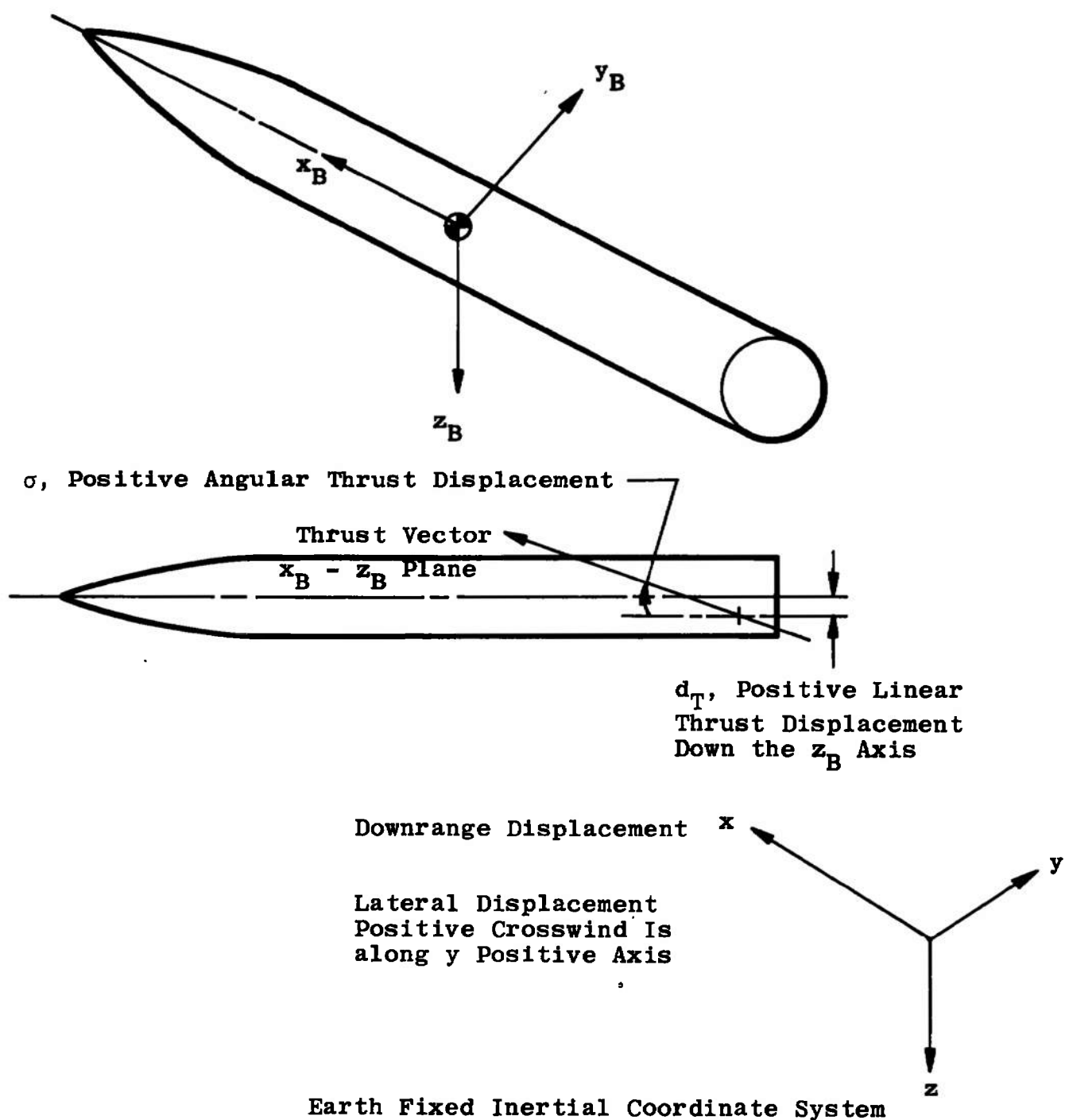


Fig. 23 Illustration of the Thrust and Body Coordinate Nomenclature

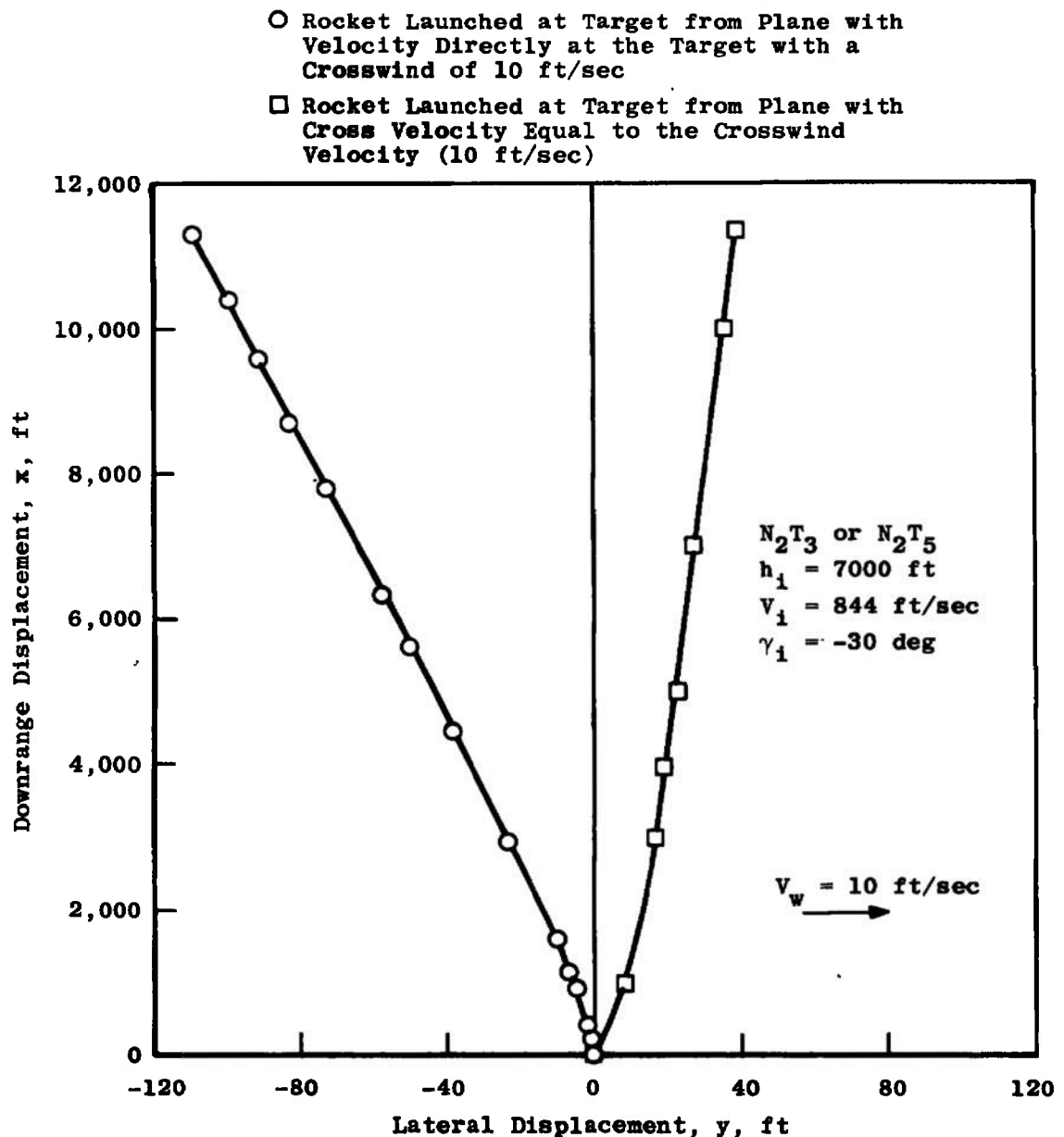


Fig. 24 Variation of the Vehicle Lateral Displacement with Downrange Distance for a 10-ft/sec Crosswind

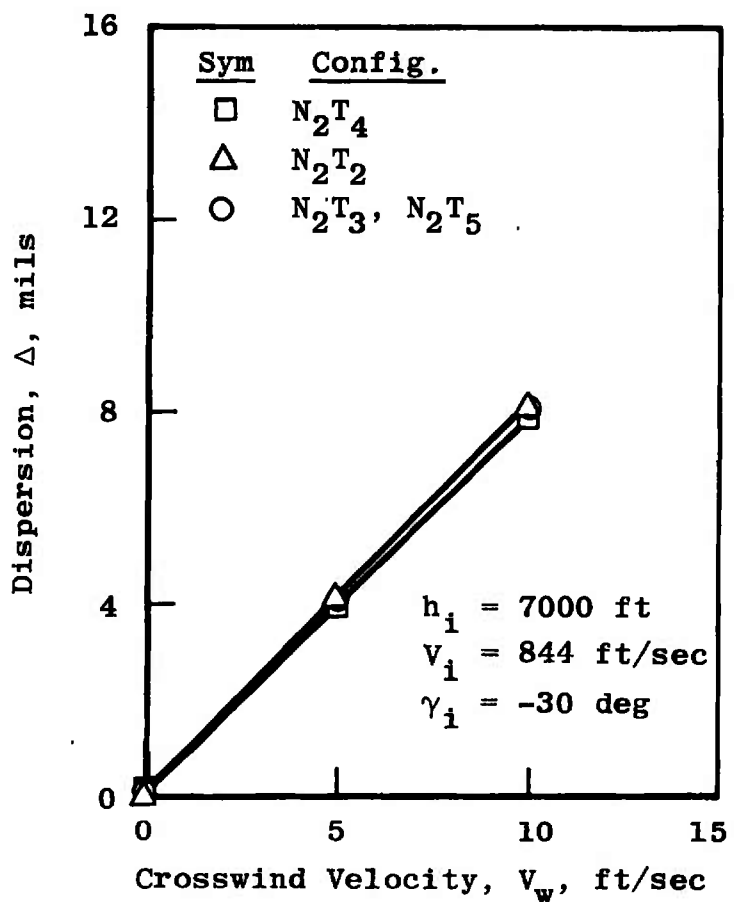


Fig. 25 Variation of Dispersion with Crosswind Velocity

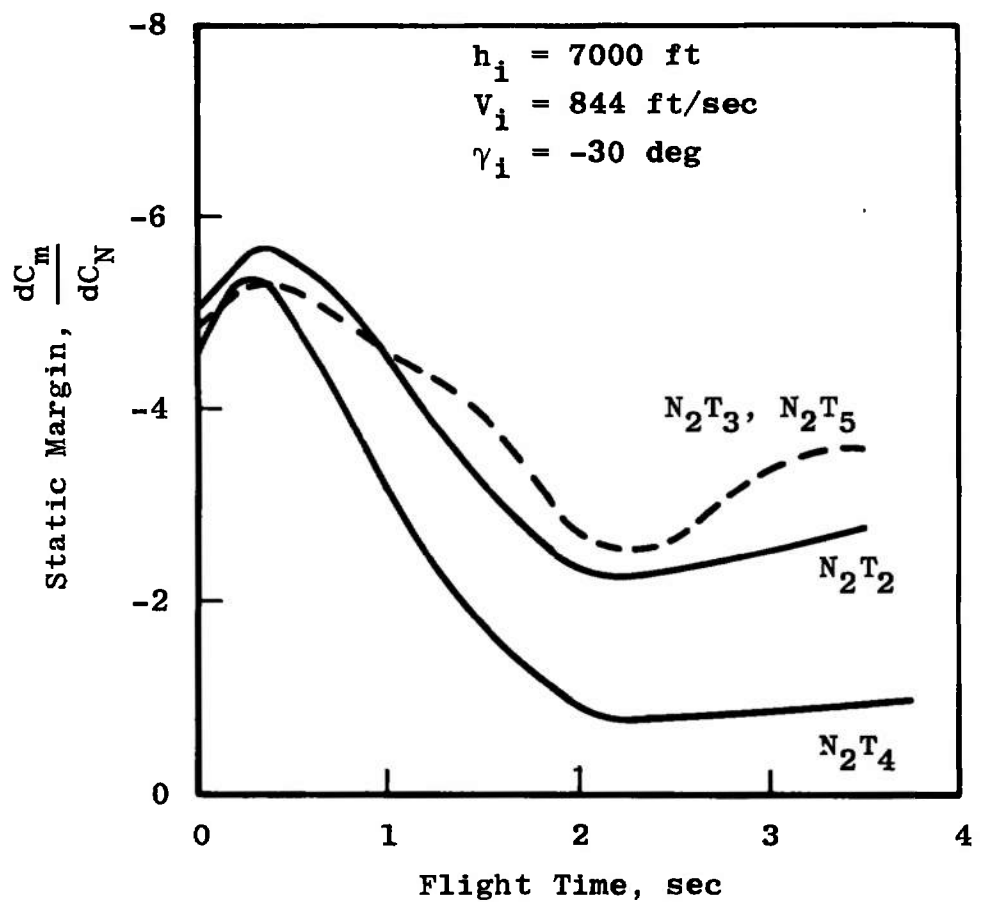


Fig. 26 Variation of Vehicle Static Margin with Flight Time

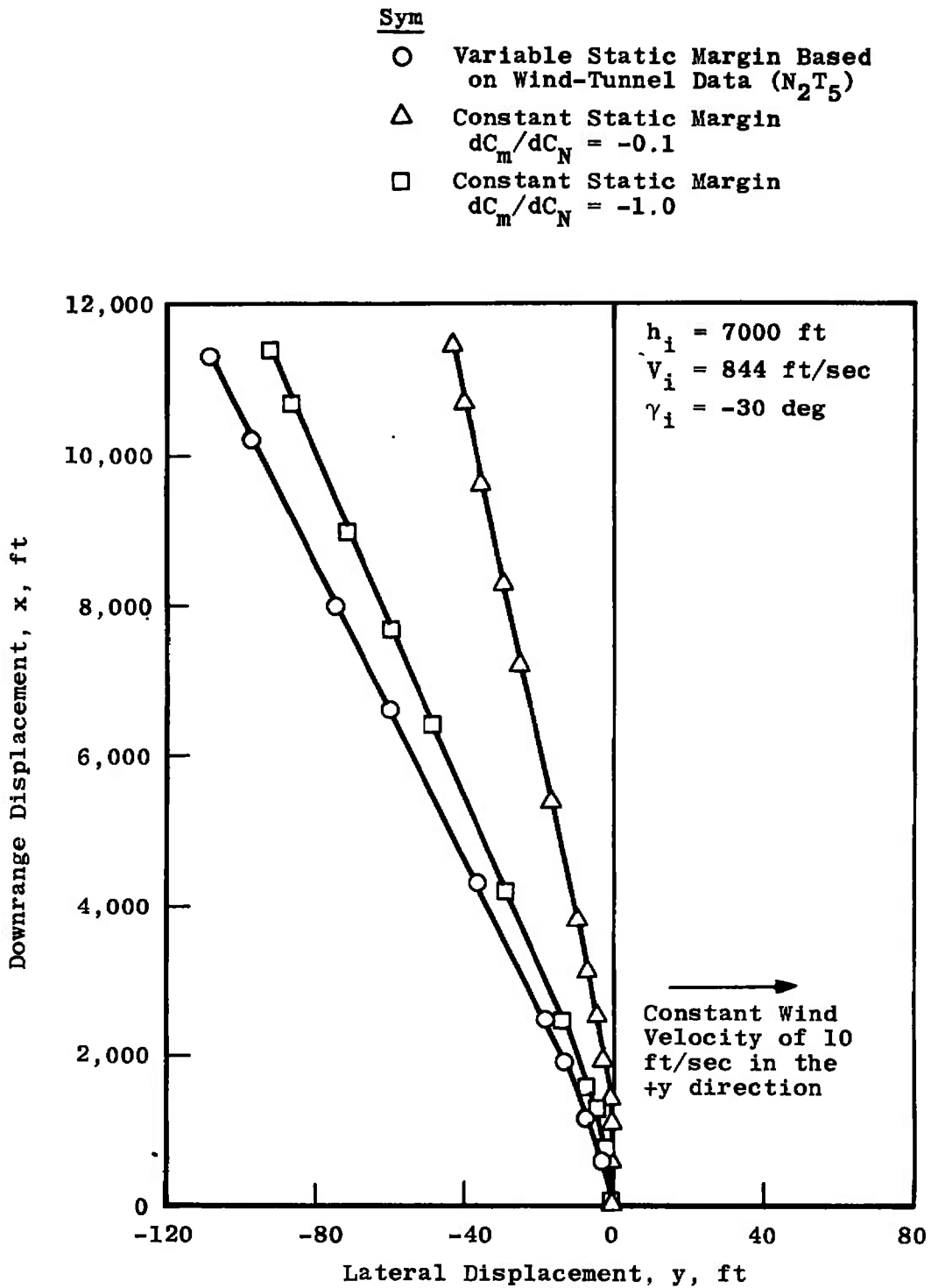


Fig. 27 Effect of Static Margin on the Vehicle Lateral Displacement Caused by Crosswinds

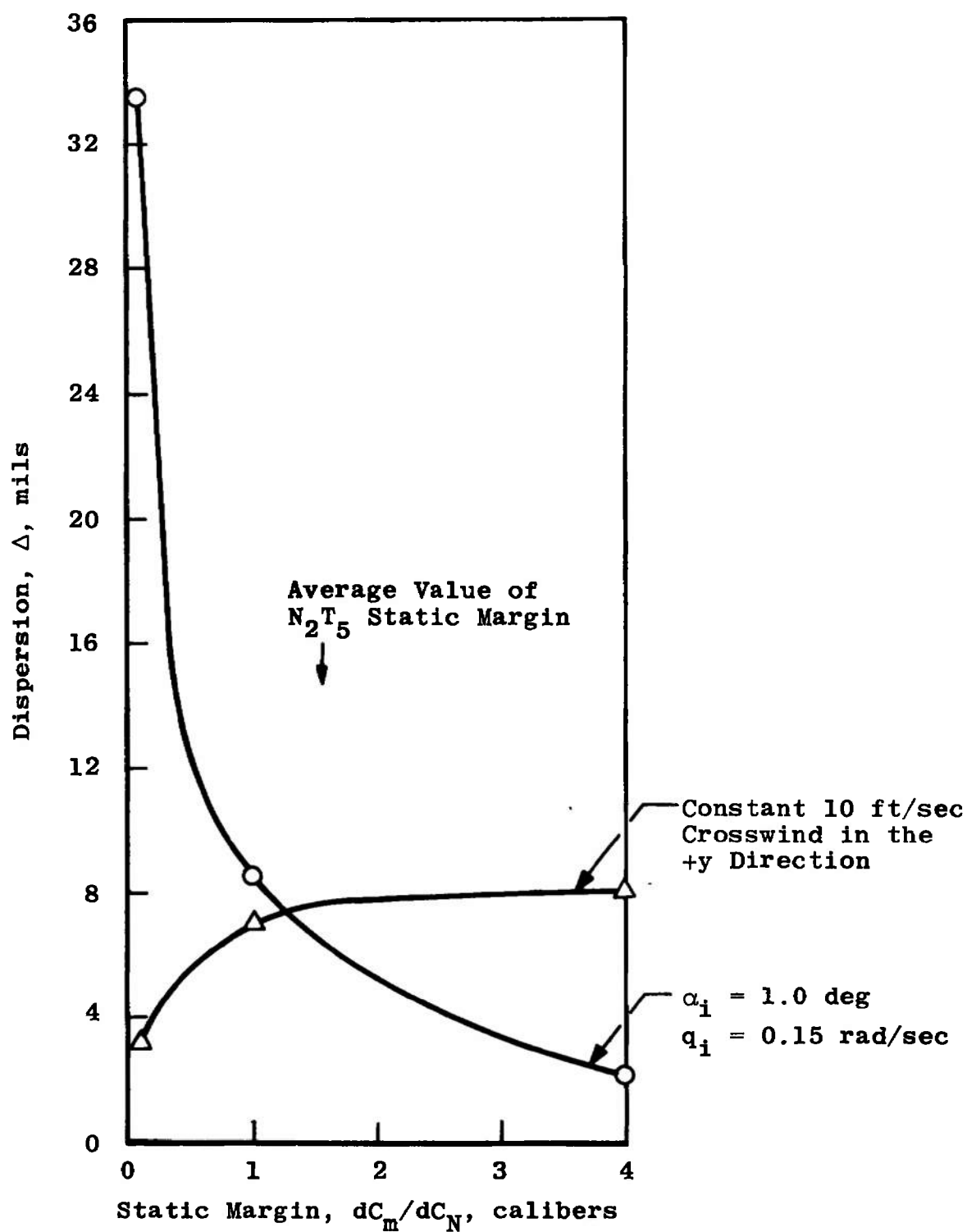


Fig. 28 Comparison of the Effects of Wind and Launch Error on Dispersion when Reducing the Static Margin of the Vehicle

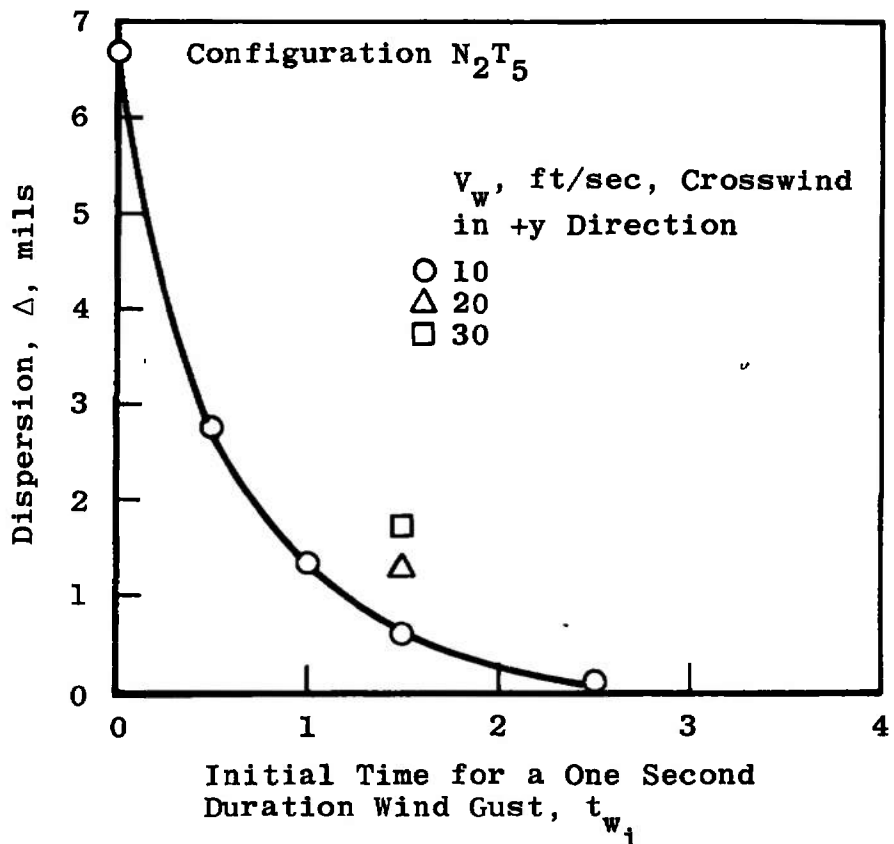


Fig. 29 Variation of Dispersion with Starting Time for a Wind Gust Lasting for One Second

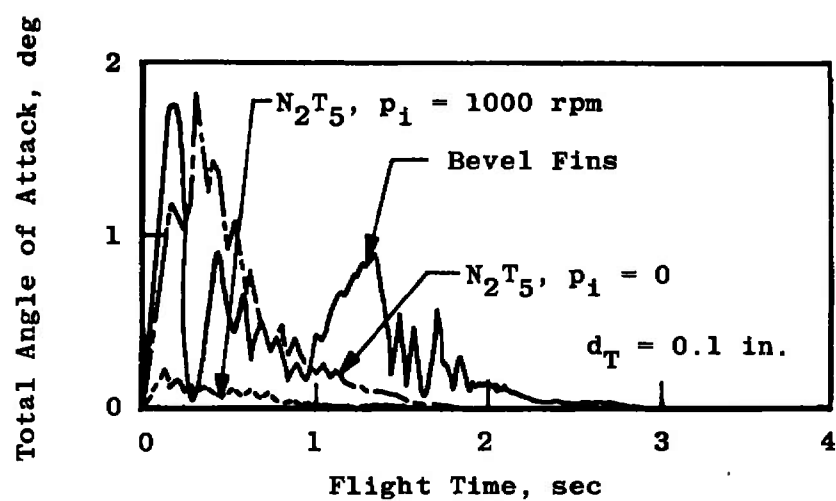
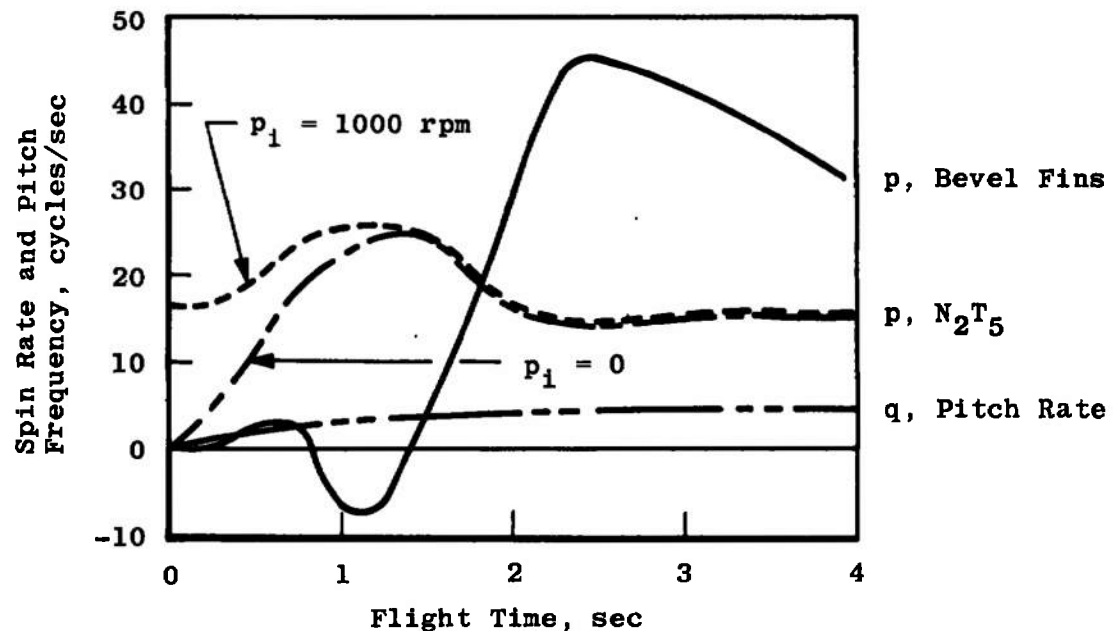


Fig. 30 Variation of the Vehicle Roll Rate and Total Angle of Attack with Flight Time

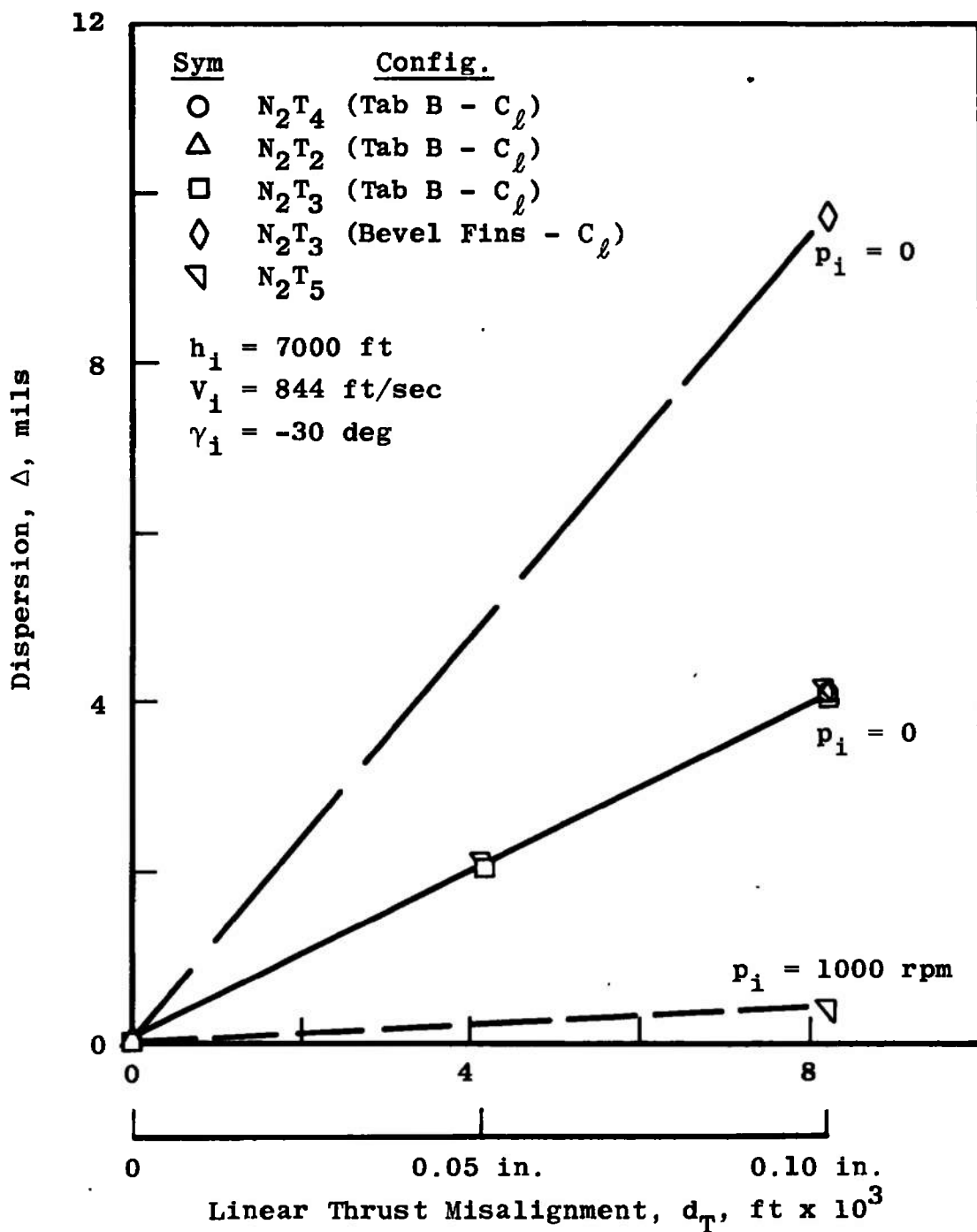


Fig. 31 Effect of Linear Thrust Misalignment on Missile Dispersion

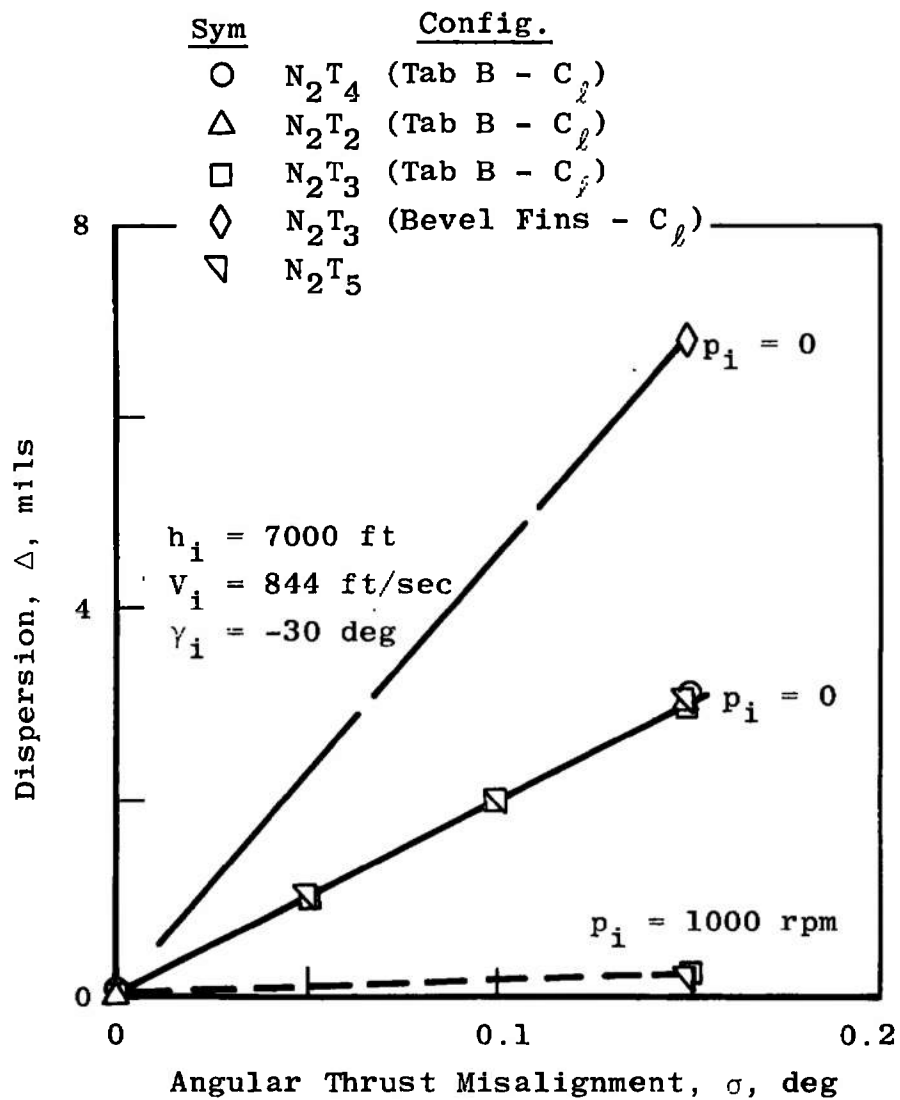


Fig. 32 Effect of Angular Thrust Misalignment on Missile Dispersion

Note: Two fins 180 deg apart were assumed to be misaligned by the angle, λ , and the force and moment produced by this misalignment were obtained from the static data and used in the 6-DOF trajectory.

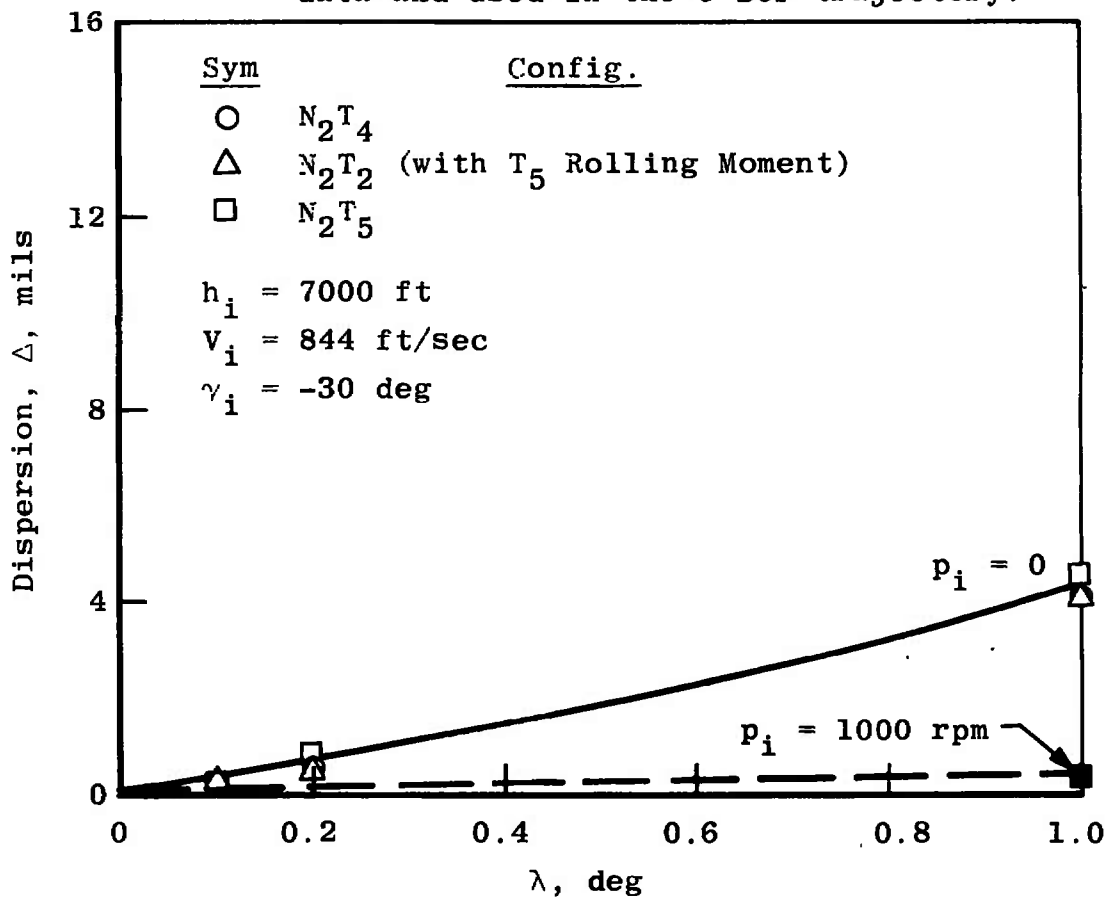


Fig. 33 Effects of Fin Misalignment on Missile Dispersion

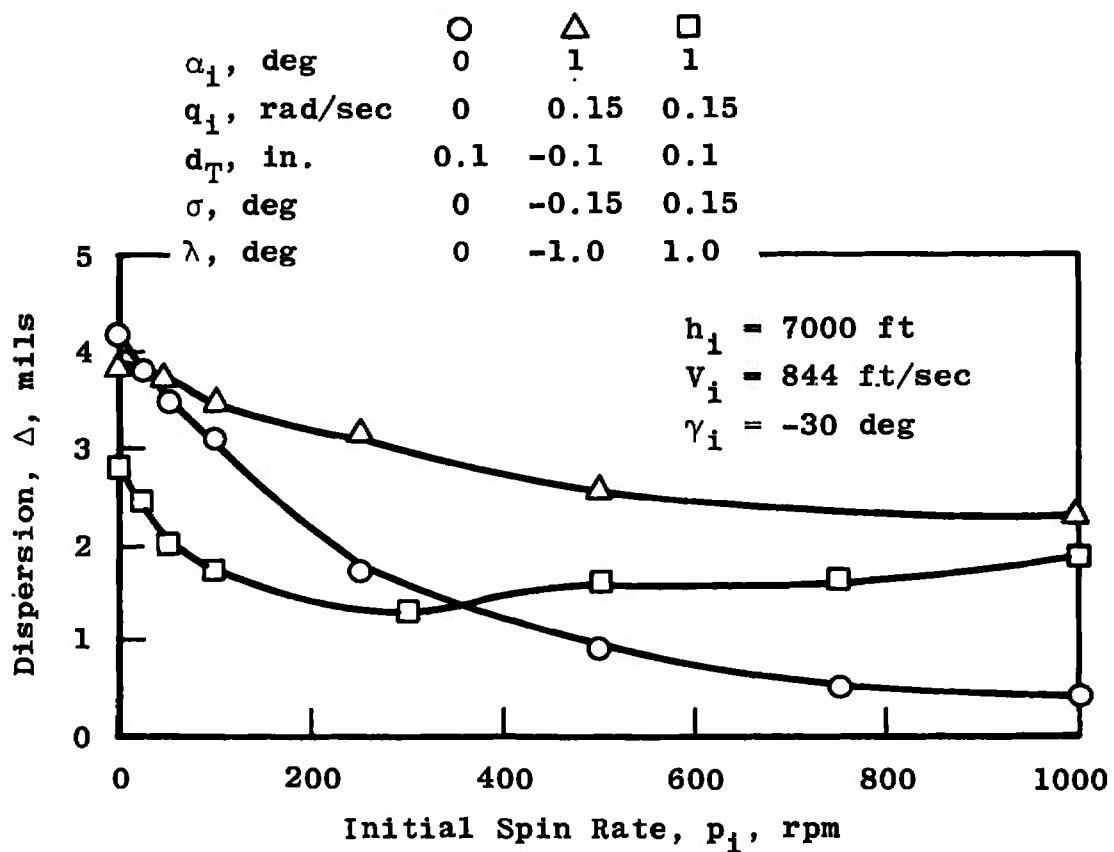


Fig. 34 Variation of Dispersion with Initial Spin Rate

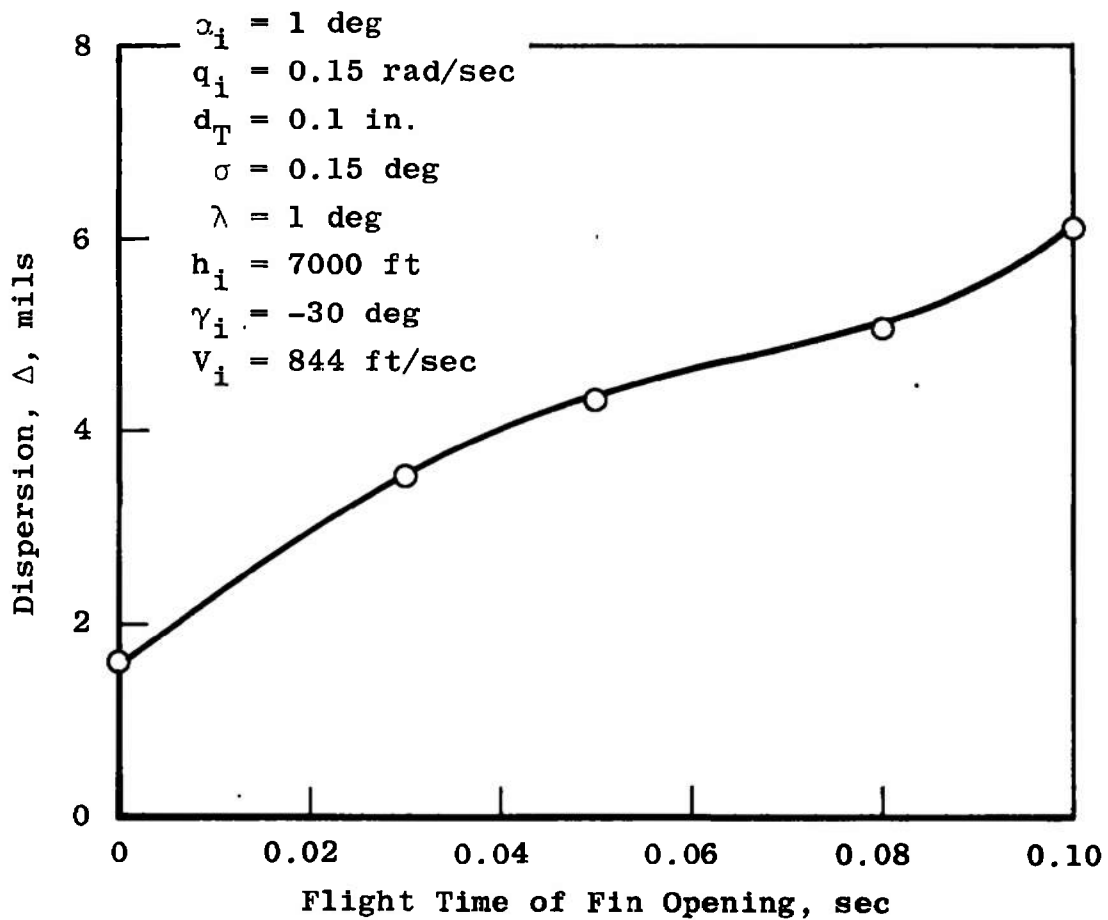


Fig. 35 Effects of Fin Opening Time on Dispersion

TABLE I
TEST SUMMARY
a. Phase 1

M_∞	$Re_\delta \times 10^{-6}$	Configuration											
		N ₁ T ₀	N ₁ T ₁	N ₁ T ₂	N ₁ T ₃	N ₂ T ₀	N ₂ T ₁	N ₂ T ₄	N ₂ T _{4B}	N ₂ T _{4C}	N ₂ T _{4D}	N ₂ T ₂	N ₂ T ₃
0.3	8.3	x		x		x		x	x		x	x	x
0.6	13.8	x		x		x		x	x		x	x	x
	10.5			x		x		x	x				x
	7.4			x		x		x	x				x
	4.4			x		x		x	x				x
0.8	13.8	x		x		x		x	x		x	x	x
0.9	13.8	x		x		x		x	x		x	x	x
1.0	13.8	x		x		x		x	x		x	x	x
1.1	17.1	x		x		x		x	x		x	x	x
	13.8			x		x		x	x		x	x	x
	10.5			x		x		x	x		x	x	x
	7.4			x		x		x	x		x	x	x
1.3	13.8	x		x		x		x	x		x	x	x
1.5	13.8	x	x	x	x	x	x	x	x	x	x	x	x
2.0	13.8	x		x		x		x	x		x	x	x
	10.5			x		x		x	x				x
	7.4			x		x		x	x				x
	4.4			x		x		x	x				x
	1.4	x		x		x		x	x				x
2.5	13.8	x		x		x		x	x		x	x	x
3.0	13.8	x		x		x		x	x		x	x	x
3.5	13.8	x		x		x		x	x		x	x	x
4.0	13.8	x		x		x		x	x		x	x	x
	10.5			x		x		x	x				x
	7.4			x		x		x	x				x
	4.4			x		x		x	x				x
	1.4			x		x		x	x				x
4.5	13.8	x		x	x	x	x	x	x	x	x	x	x

TABLE I (Concluded)
b. Phase 2

M_∞	$Re_\delta \times 10^{-6}$	N ₂ T ₅	N ₂ T ₆	N ₂ T ₇	N ₂ T ₈	N ₂ T ₉	N ₂ T ₁₀	N ₂ T _{10(N)}	N ₂ T ₁₁	N ₂ T ₁₂
0.3	8.3	X, P			x	X, P	X			
0.6	13.8	X, P			x	X, P	X			
0.8		X, P			x	X, P	X			
1.0		X, P			x	X, P	X			
1.1		X, P			x	X, P	X			
1.3		X, P			x	X, P	X			
2.0		X, P	x	X, P	X, P	X, P	X		x	
2.5					X, P	X, P	X		x	
3.5		X, P	X	X, P	X	X, P	X	x	x	x
4.5		X, P	X	X, P	X, P	X, P	X	x	x	x

(N) Indicates nozzle simulator on

P Indicates plume simulation data

TABLE II
TABULATED DATA ($\alpha = 0$)
a. Configuration N₂T₄

M_∞	$C_{N\alpha}/\text{deg}$	$C_{Y\beta}/\text{deg}$	$C_{m\alpha}/\text{deg}$	$C_{n\beta}/\text{deg}$	C_{mq}/rad	C_{nr}/rad	C_{Nq}/rad	C_{Yr}/rad	$\frac{\partial C_{mq}}{\partial (\Delta x_{cg})}/\text{ft-rad}$	C_{At}
0.3	0.1622	-0.1622	-0.9750	0.9750	-2045.6	-2045.6	194.9	194.9	-2507	0.3265
0.6	0.1493	-0.1493	-0.8832	0.8832	-1869.5	-1869.5	178.8	178.8	-2299	0.3195
0.8	0.1470	-0.1470	-0.8973	0.8973	-1844.9	-1844.9	176.2	176.2	-2267	0.3144
0.9	0.1537	-0.1537	-0.9546	0.9546	-1918.9	-1918.9	183.7	183.7	-2364	0.3036
1.0	0.1854	-0.1854	-1.2118	1.2118	-2306.3	-2306.3	221.2	221.2	-2845	0.2919
1.1	0.1779	-0.1779	-1.1614	1.1614	-2230.0	-2230.0	213.1	213.1	-2742	0.4824
1.3	0.172	-0.172	-1.04	1.04	-2370.0	-2370.0	220.0	220.0	-2686	0.5470

M_∞	$C_{N\alpha}/\text{deg}$	$C_{Y\beta}/\text{deg}$	$C_{m\alpha}/\text{deg}$	$C_{n\beta}/\text{deg}$	C_{mq}/rad	C_{nr}/rad	C_{Nq}/rad	C_{Yr}/rad	C_{At}	$\frac{\partial C_{mq}}{\partial (\Delta x_{cg})}/\text{ft-rad}$
1.5	0.1721	-0.1721	-1.0535	1.0535	-2166.4	-2166.4	206.6	206.6	0.4487	-2658
2.0	0.1378	-0.1378	-0.6537	0.6537	-1747.5	-1747.5	166.0	166.0	0.3870	-2136
2.5	0.1163	-0.1163	-0.3972	0.3972	-1489.9	-1489.9	140.8	140.8	0.3377	-1812
3.0	0.1063	-0.1063	-0.2809	0.2809	-1369.8	-1369.8	129.1	129.1	0.3044	-1662
3.5	0.1007	-0.1007	-0.1427	0.1427	-1310.6	-1310.6	122.9	122.9	0.2735	-1582
4.5	0.0942	-0.0942	-0.0453	0.0453	-1233.7	-1233.7	115.4	115.4	0.2322	-1485

TABLE II (Continued)
b. Configuration N₂T₂

M_∞	C_{N_α}/deg	C_{Y_β}/deg	C_{m_α}/deg	C_{n_β}/deg	C_{mq}/rad	C_{n_r}/rad	C_{N_q}/rad	C_{Y_r}/rad	C_{At}	$\frac{\partial C_{mq}}{\partial (\Delta x_{cg})}/\text{ft-rad}$
0.3	0.1810	-0.1810	-1.1012	1.1012	-2199.1	-2199.1	213.4	213.4	0.3449	-2741
0.6	0.1804	-0.1804	-1.1098	1.1098	-2165.1	-2165.1	211.4	211.4	0.3420	-2715
0.8	0.1788	-0.1788	-1.1272	1.1272	-2151.5	-2151.5	209.8	209.8	0.4270	-2694
0.9	0.1810	-0.1810	-1.1546	1.1546	-2179.4	-2179.4	213.1	213.1	0.3265	-2736
1.0	0.1881	-0.1881	-1.1952	1.1952	-2251.9	-2251.9	220.2	220.2	0.3220	-2827
1.1	0.200	-0.200	-1.33	1.33	-2536.3	-2536.3	247.4	247.4	0.4929	-3177
1.3	0.207	-0.207	-1.38	1.38	-2530.0	-2530.0	242.0	242.0	0.544	-3160
1.5	0.2070	-0.2070	-1.3367	1.3367	-2500.8	-2500.8	243.4	243.4	0.4914	-3126
2.0	0.1799	-0.1799	-1.0479	1.0479	-2184.2	-2184.2	212.0	212.0	0.4040	-2723
2.5	0.1497	-0.1497	-0.7187	0.7187	-1839.7	-1839.7	177.5	177.5	0.3641	-2280
3.0	0.1364	-0.1364	-0.5739	0.5739	-1687.4	-1687.4	162.5	162.5	0.3228	-2085
3.5	0.1222	-0.1222	-0.3727	0.3727	-1605.0	-1605.0	153.4	153.4	0.2844	-1972
4.0	0.1156	-0.1156	-0.2734	0.2734	-1457.6	-1457.6	138.8	138.8	0.2587	-1785
4.5	0.1143	-0.1143	-0.2337	0.2337	-1447.0	-1447.0	125.1	125.1	0.2429	-1769

TABLE II (Continued)
Tabulated Data ($\alpha = 0$)
c. Configuration N₂T₃ and all Phase 2 Fins

M_∞	$C_{N\alpha}/\text{deg}$	$C_{Y\beta}/\text{deg}$	$C_{m\alpha}/\text{deg}$	$C_{n\beta}/\text{deg}$	C_{mq}/rad	C_{nr}/rad	C_{Nq}/rad	C_{Yr}/rad	$\frac{\partial C_{mq}}{\partial (\Delta x_{cg})}/\text{ft-rad}$
0.3	0.1669	-0.1669	-1.0476	1.0476	-1987.6	-1987.6	194.3	194.3	-2494
0.6	0.1698	-0.1698	-1.0228	1.0228	-1999.4	-1999.4	197.1	197.1	-2530
0.8	0.1780	-0.1780	-1.1082	1.1082	-2116.1	-2116.1	208.6	208.6	-2677
0.9	0.1820	-0.1820	-1.1605	1.1605	-2141.3	-2141.3	211.8	211.8	-2718
1.0	0.1840	-0.1840	-1.1829	1.1829	-2186.5	-2186.5	216.1	216.1	-2774
1.1	0.1927	-0.1927	-1.22	1.22	-2277.6	-2277.6	224.1	224.1	-2876
1.3	0.195	-0.195	-1.23	1.23	-2380.0	-2380.0	230.0	230.0	-2961
1.5	0.2034	-0.2034	-1.2859	1.2859	-2409.2	-2409.2	236.8	236.8	-3040
2.0	0.1880	-0.1880	-1.0959	1.0959	-2232.9	-2232.9	219.1	219.1	-2814
2.5	0.1592	-0.1592	-0.8007	0.8007	-1914.6	-1914.6	186.7	186.7	-2398
3.0	0.1455	-0.1455	-0.6366	0.6366	-1762.5	-1762.5	171.3	171.3	-2200
3.5	0.1337	-0.1337	-0.4421	0.4421	-1643.9	-1643.9	158.5	158.5	-2037
4.0	0.1269	-0.1269	-0.3568	0.3568	-1566.0	-1566.0	150.7	150.7	-1937
4.5	0.1197	-0.1197	-0.2839	0.2839	-1489.9	-1489.9	142.8	142.8	-1836

TABLE II (Concluded)
d. Roll and Axial-Force Data

M_∞	N ₂ T ₅		N ₂ T ₈		N ₂ T ₉		N ₂ T ₁₀		N ₂ T ₃ (TAB B)	
	C _{A_t}	C _l	C _{A_t}	C _l	C _{A_t}	C _l	C _{A_t}	C _l	C _{A_t}	C _l
0.3	0.4215	0.0914	0.3830	0.0516	0.3804	0.0285	0.4170	0.3550	0.3737	-0.1517
0.6	0.3975	0.0970	0.3740	0.0519	0.3722	0.0288	0.4100	0.3620	0.3580	-0.1630
0.8	0.4140	0.1012	0.3830	0.0534	0.3838	0.0294	0.4160	0.3650	0.3561	-0.1686
0.9	---	---	---	---	---	---	---	---	0.3582	-0.1720
1.0	0.6480	0.1101	0.5350	0.0619	0.5408	0.0320	0.5570	0.3825	0.3779	-0.1730
1.1	0.7295	0.1129	0.6460	0.0650	0.6540	0.0309	0.6840	0.3751	0.5400	-0.1767
1.3	0.6966	0.1135	0.6170	0.0650	---	---	0.6480	0.3620	0.5960	-0.1790
1.5	---	---	---	---	---	---	---	---	0.5395	-0.1793
2.0	0.5030	0.0740	0.4580	0.0580	0.4665	0.030	0.5170	0.4020	0.4456	-0.1253
2.5	0.0423	0.0550	0.3800	0.0540	0.4520	0.0256	0.4330	0.3140	0.3694	-0.0901
3.0	---	---	---	---	---	---	---	---	0.3338	-0.0728
3.5	0.3080	0.0220	0.3030	0.0490	0.3113	0.0182	0.3280	0.1710	0.2968	-0.0617
4.0	---	---	---	---	---	---	---	---	0.2785	-0.0531
4.5	0.2730	0.0145	0.2600	0.0460	0.2600	0.0159	0.2675	0.1200	0.2496	-0.0506

For All Fins	
M_∞	C _{l_p}
0.3	-4.85
0.5	-5.15
1.0	-6.30
1.3	-6.60
1.5	-6.50
2.0	-6.40
3.0	-6.10
4.5	-5.75

UNCLASSIFIED

Security Classification

DOCUMENT CONTROL DATA - R & D

(Security classification of title, body of abstract and indexing annotation must be entered when the overall report is classified)

1. ORIGINATING ACTIVITY (Corporate author) Arnold Engineering Development Center ARO, Inc., Operating Contractor Arnold Air Force Station, Tennessee		2a. REPORT SECURITY CLASSIFICATION UNCLASSIFIED
		2b. GROUP N/A
3. REPORT TITLE RESULTS OF AN AIR FORCE ADVANCED TACTICAL ROCKET DEVELOPMENT PROGRAM		
4. DESCRIPTIVE NOTES (Type of report and inclusive dates) Final Report - April 17, 1970 to March 10, 1971		
5. AUTHOR(S) (First name, middle initial, last name) James C. Uselton, ARO, Inc. <i>Document has been approved for public release its distribution is unlimited. Rey TAB 74-16 JFC 2 August, 74.</i>		
6. REPORT DATE July 1971	7a. TOTAL NO. OF PAGES 111	7b. NO. OF REFS 17
8a. CONTRACT OR GRANT NO. F40600-72-C-0003	9a. ORIGINATOR'S REPORT NUMBER(S) AEDC-TR-71-141 AFATL-TR-71-73	
b. PROJECT NO c. Program Element 63716F	9b. OTHER REPORT NO(S) (Any other numbers that may be assigned this report) ARO-VKF-TR-71-71	
d. System 670A		
10. DISTRIBUTION STATEMENT <i>Distribution limited to U. S. Government agencies only; this report contains information on test and evaluation of military hardware; July 1971; other requests for this document must be referred to Armament Development and Test Center (DLDG), Eglin AFB, Florida 32542.</i>		
11. SUPPLEMENTARY NOTES Available in DDC	12. SPONSORING MILITARY ACTIVITY Armament Development and Test Center (DLDG), Eglin AFB, Florida 32542	
13. ABSTRACT <i>Currently the Air Force Armament Laboratory (AFATL) is developing an Advanced Tactical Rocket (ATR). The ATR aerodynamic configuration is being designed by the von Kármán Gas Dynamics Facility of the Arnold Engineering Development Center for AFATL. The details of the development of the aerodynamic configuration are presented in this report. It contains the results of wind-tunnel tests, a trajectory analysis, and a dispersion analysis. The wind-tunnel tests provided essential data necessary for the trajectory and dispersion investigations. Static-force and moment tests were conducted over a broad range of Mach numbers (0.3 to 4.5), Reynolds number (1.4×10^6 to 17.1×10^6), and angle of attack (-3 to 10 deg). These test data were used in a six-degree-of-freedom trajectory program to obtain the basic trajectory and dispersion results. Included in the dispersion study are the effects of thrust misalignment, fin misalignment, initial angular disturbances, and cross-winds. This study indicates that both a 2.5- and a 3.0-caliber tangent ogive nose are acceptable and that a 2.0-caliber tail fin with an 11-deg leading-edge sweep angle is most advantageous. The tail fin should either be canted to 0.5 deg or have 10-deg (0.36 sq in., area) roll tabs to provide the required roll characteristics. An initial spin rate of 500 rpm is necessary for low dispersion of the rocket.</i> <i>Distribution limited to U.S. Government agencies only; contains information on test and evaluation of military hardware; July 1971; other requests for this document must be referred to ADTC(DLDG), Eglin AFB, Florida 32542.</i>		

UNCLASSIFIED

Security Classification

14 KEY WORDS	LINK A		LINK B		LINK C	
	ROLE	WT	ROLE	WT	ROLE	WT
Advanced <u>tactical rocket</u> s						
missile models						
cylindrical body						
folding fins						
fin stabilization						
wind-tunnel testing						
roll						
angle of attack						
<i>2 Rockets -- Development</i>						